Applying MODFLOW and Artificial Neural Networks to Model the Formation of Mine

Pools in Underground Coal Mines

A thesis presented to

the faculty of

the College of Arts and Sciences of Ohio University

In partial fulfillment

of the requirements for the degree

Master of Science

Frederick Twumasi

August 2018

This thesis titled

Applying MODFLOW and Artificial Neutral Networks to Model the Formation of Mine

Pools in Underground Coal Mines

by

FREDERICK TWUMASI

has been approved for

the Department of Geological Sciences

and the College of Arts and Sciences by

Dina L. Lopez

Professor of Geological Sciences

Robert Frank

Dean, College of Arts and Sciences

ABSTRACT

TWUMASI FREDERICK, M.S., August 2018, Geological Sciences

Applying MODFLOW and Artificial Neutral Networks to Model the Formation of Mine

Pools in Underground Coal Mines

Director of Thesis: Dina L. Lopez

The development and release of acidic drainage and formation of mine pools in decommissioned coal mines is an environmental problem for government regulators, mining companies and the communities. AMD, characterized by acidic metalliferous conditions in water, is responsible for physical, chemical, and biological degradation of stream habitat. There is urgent need to be able to predict within some uncertainty the formation of mine pools in future mines before the permits are granted by the regulatory agencies. This research is part of a larger project that intends to produce a set of GIS based tools for regulators and mining companies to determine the probability of development of a mine pool. This thesis has two main purposes. The first purpose is to model the sensitivity of the Meigs Mine Complex (Ohio) parameters that determine the development of mine pools using a groundwater flow modeling program (MODFLOW). The second purpose is to determine the best possible regression equation that permits the prediction of potentiometric heads in the mine region from variables such as surface elevation, bottom of well elevation, overburden thickness, thickness of mined coal, thickness of shales, thickness of sandstones, thickness of limestone, accumulated coal volume, average precipitation, underground mine area and thickness of the coal seam mined using Artificial Neural Network (ANN). Data was collected for the second objective from the mine permits and quarterly mining reports that the mining companies

present to Ohio Department of Natural Resources (ODNR) and other government
institutions.

Results from the physical model of the Meigs mine show that the groundwater
flows in the direction of the Ohio River. The numerical model of the Meigs Mine
Complex was elaborated in three stages, the first model was a steady state model to
simulate water level in wells as reported in 1996, the second model simulated the water
withdraw and decrease of water levels in the shafts as it was measured in January 2004.
The third model was a transient model to simulate the recovery of the water levels in the
shafts after the mine was closed from January 2004 to December 2007.   These results of
these models show high hydraulic conductivities that are consistent with highly fractured
rocks and secondary permeability due to the exploitation of the coal, especially in the
rock layers closer to the void in the coal mine.

For the ANN simulations the Group Method of Data Handling (GMDH) of the
NeuroShell 2 program was used to obtain polynomial regressions using ANN. Two types
of simulations were done: one considering water withdraw and another without
considering water withdraw. Results from the artificial neural networks simulations show
that the average parameters without water withdraw regression equation was the best
possible equation that will aid in the prediction of the potentiometric heads. Correlation
of the average calculated potentiometric head at the bottom of the coal layer with the two
model equations, and the elevation of the top of the coal layers, suggest that all the mines
that have been considered in this study will develop mine pools if the hydrogeological
regime is allowed to recover without any other perturbation. This study suggests the need

to monitor more regularly wells during mine exploitation and to keep good records of the water extracted and locations of extraction points.

DEDICATION

This thesis is dedicated to God and Irene Opokuah Dapaah.

ACKNOWLEDGMENTS

I would like to thank Professor Dina L. Lopez for the opportunity, unwavering support, patience's, motivation, enthusiasm, guidance's and immense knowledge throughout this research project. I would also like to express my gratitude to the OSM team (Dr. Natalie Kruse Daniels, Professor Dina L. Lopez, Jen Bowman, Nora Sullivan, Lindsey Schafer, Rebecca Steinberg, and Matthews Zachary) for their immense support and guidance's.

I would also like to thank my thesis committee, Professor Dina L. Lopez, Dr. Natalie Kruse Daniels and Dr. Gregory Nadon and the staff of the Geological Sciences Department of Ohio University.

I would like to extend a very special thanks to the Ohio University Geological Science Alumni Group, Office of Surface Mining (OSM) and Geological society of America for funding and research assistantships.

TABLE OF CONTENTS

LIST OF TABLES

LIST OF FIGURES

CHAPTER 1: INTRODUCTION

1.1. Background

The development and release of drainage from mine pools in decommissioned coal mines is an environmental problem for government regulators, mining companies and communities. An area impacted by acid mine drainage will have physical, chemical, and biological degradation. Approximately 20,000 km of creeks and rivers in the United States are affected by acid mine drainage, and about 85% to 90% of these waterbodies receive acid mine drainages from older, abandoned surface and underground mines (Skousen et al., 2002). The study of the formation and hydrogeology of mine pools in underground coal mines is the focus of this thesis.

Acid mine drainage (AMD) is produced when sulfide minerals in rocks are subjected to oxidizing conditions. Large quantities of AMD may be released from coal mines rich in sulfides. The drainage character originating from mines is contingent on the acid (sulfides) and alkaline (carbonate) minerals present in the geologic strata in contact with the water. AMD is distinguished by low pH and high sulfate and iron concentrations. Chemical, biological and physical factors are important for determing the rate of acid generation (Akcil, 2004). Primary factors that determine the rate of acid generation includes pH, temperature, oxygen of the gas peroid, oxygen concentration in the water period, degree of water saturation, chemical action of Fe^{3+}, surface area of exposed sulfide and bacterial action (Akcil, 2004).

AMD associated with underground mines are deemed significant environmental hazard (Akcil, 2004).   More recently, AMD originating from open pit workings has become a problem. Little is known of the possible hazard created by these operations, as

many are still being worked or maintained. In this method of mining, large quantity of rock are initially subjected to an oxidizing environment (Akcil, 2004). The hazard of long-term run degeneration continually making current rock surfaces accessible for oxidization shows that considerable volumes of AMD could materialize following closure (Akcil, 2004).

According to (Currie, 1999), in 1993, the largest underground coal mine in Ohio at the time released contaminated acid mine water into Parker Run, a tributary of Leading Creek, at an approximate rate of 35,042 gallons per minute due to flooding of the workings and discharge from the resulting mine pool. Roughly one billion gallons of mine water were released into the stream (Ohio EPA, 2005). The contaminated discharge destroyed natural homes and killed fish along a fifteen-mile stretch of Parker Run, into Leading Creek (US Department of Justice, 1996).

One key factor that determines the impacts of AMD in the environment is the formation of mine pools and their potential discharge to the surface. Mine pool formation depends on factors such as recharge of water to the mine, thickness of the overburden and development of subsidence features above the mines that can generate quick flow recharge. Other factors include slope of the mine, elevation of water table, precipitation and infiltration, types of rock and connectivity of the mine with other neighboring mines. Prediction of formation of mine pools and location of possible discharge is a multivariable problem that is difficult to assess, however there is an urgent need for a set of empirical models that can allow applicants and regulators to predict within some certainty the possible formation and consequences of mine pools. According to the law in Ohio, if a mine could develop mine pool that may discharge to the surface, the

exploitation permit should either not be issued or the mine plan should be amended to avoid potential surface discharge. However, regulators and mining companies do not have a scientifically based methodology to determine if the mine will develop a mine pool or not. The research in this thesis aims to address this problem.

1.2. History of Mining in Ohio

Ohio is situated in the northern part of the Appalachian Coal Basin, which is one of the extensive coal areas in the United States. The coal-bearing region in Ohio covers thirty-two counties, and is located in the southern and eastern portions of the state (Crowell, 1997). Guernsey and Noble Counties were considered to host one of the best coal veins in the world (Crowell, 1995). It is estimated that Ohio has 11,265 million short tons of economically recoverable coal reserves (USEIA, 2002).

The first European settlers in Ohio recognized the presence of coal in natural outcrops in stream and watercourse banks within the state. Till the time of World War I, coal mining in Ohio was conducted virtually completely underground and mostly by hand extraction (ODNR, 2011). These underground mine workings gained access to coal seams either by vertical mine shafts up to two hundred feet deep, by horizontal mine entries (drift entries) in hillsides at the coal elevation, or by sloping tunnels oriented downward from the ground surface (ODNR, 2011). With the arrival of excavating machinery, new drilling techniques, and recently developed explosives within the mining business around World War II, massive earthmoving operations became feasible. Surface mining operations became an economic substitute to underground mining. In surface mining, all of the rock and soil (overburden) on top of the targeted coal seams are excavated, exposing the seam at the surface. The excavated rock and soil on top of the

coal is called "overburden," and it is placed in piles. The exposed coal is removed until mostly non-coal rock adjacent to the coal layer is left.

In Ohio, mines are regulated by Ohio Department of Natural Resources Division of Mineral Resource Management (ODNR-DMRM). ODNR-DMRM regulates the mining business in a process that strikes a balance between protection of society from the adverse effects of mining operations and providing for the country's requirement for coal as essential supply of energy. The duties of ODNR-DMRM include reviewing permit applications, amendments, and revisions, inspections of active mines and guaranteeing compliance with rules designed to guard population and therefore the environment from the potential impacts of mining (ODNR, 2011).

On August 3, 1977, the Surface Mining Control and Reclamation Act (SMCRA) was established by Congress. According to (ODNR, 2011) the Act established rigorous national regulations for coal mining and reclamation. Due to the diverse mining environment in the country, the government established the Federal Department of the Interior's Office of Surface Mining Reclamation and Enforcement. Congress planned that the states become the primary regulator, upon acceptances by the Secretary of Interior of a state's nominated law and order. In addition to the mining and reclamation laws, operators must comply with a number of alternative county, state, and federal laws and programs to maintain a permit to mine coal in Ohio (ODNR, 2011).

1.3. Mine Pools and AMD as Environmental Problem

Rock layers related to coal seam often contain iron sulfide minerals, with pyrite being the most common. Sulfur-bearing rocks exposed to the environment during mining react with oxygen and water to form sulfuric acid (ODNR, 2011). This contaminated

water (AMD), often flows from underground mines and surface mined areas. AMD is a notable environmental issue associated with abandoned mine land and is often challenging to control (ODNR, 2011).

Discharges from underground mines have had significant impact on surface waters (Kruse et al., 2013). When mining ceases and groundwater rebounds, there is the potential for a mine pool to form. If there is sufficient interconnection between groundwater and surface water or weak points in the geological strata, a mine pool may discharge into surface water. Mine water transports contaminants from the underground mine voids into surface water and groundwater, impacting aquatic chemistry and biological communities. Mine pools also have the potential to impact human health and safety when unexpected failures lead to large volume discharges.

There is a need for more accurate prediction of post-mining water level at the permit stage to mitigate future environmental impacts. This need is high because mine pools often develop after bond release, leaving no funding sources for remediation. The discharge of mine pools from closed coal mines is an liability for government regulators, mining companies and the communities. In Ohio alone, $28,877,746 has been spent on environmental cleanup of pre-SMCRA mines in five watersheds, totaling 61 projects from 2005 to 2014 (Bowman, 2015). Therefore the best management procedure is prevent mine discharges from occurring, hence the need for empirical models that can help in predicting the formation and discharges of a mine pool.

1.4. Office of Surface Mining (OSM) Project

As part of the mining permit process, there is not a science based set of tools used to model the possibility of underground mine pool development. The current method of

predicting the post mining water level is by using the elevation of the top of mining or the top of coal, but that is not science based so we are developing an empirical predictable relationships between topography, soil types, coal thickness, overburden thickness, types of overlaying rocks, neighboring mines, precipitation and the difference between pre- and post-mining water level. This empirical model will help in the determination of the development of mine pools. Often the mining permit process is sufficient to protect water resources; however, some abandoned mines develop pool and produce mine discharges. These discharges are in some cases after the bond has been released and the coal mining company is no longer responsible. Other times the coal mining company is still under bond, creating an expensive and long-term problem for both mine operators and regulators.

This research is part of a larger project that intends to produce a set of GIS based tools for regulators and mining companies to estimate the post-mining water level and to identify potential areas where there is a risk of surface discharge. The larger project covers four objectives: 1) gathering of the data, 2) statistical analysis, 3) modeling of the data using Artificial Neural Network (ANN), and 4) creation of the GIS tool. This thesis deals with the first and third objective. In addition, the groundwater flow modeling of one well studied mine pool, the Meigs Mine Complex in Ohio, was done.

1.5. Objectives

This thesis work tried to achieve this goal in two ways: studying and modeling carefully the hydrogeology of a mine with pool development (the Meigs Mine Complex, location in Figure. 2.3) and modeling the hydraulic head dependent variable with respect to data collected from recent exploited coal mines of Ohio with artificial neural networks.

They cover the last 35 years and include mines that have mining permits starting with the letter D and corresponding to the most recent legislature that came into effect 1982. The objectives for the study of the Meigs Mine Complex were:

1) To investigate the flow regime of the mine and the response of the water levels in the mine after the mine closed.

2) To determine the impact of hydraulic variables such as hydraulic conductivity, specific yield, specific storage, and recharge on the water level response.

A groundwater flow modeling program (MODFLOW) was used to model the sensitivity of the Meigs Mine Complex parameters that determine the development of mine pools. For the modeling of all the data collected for wells in the recent coal mines of Ohio, I had the following objectives:

1) To determine the best possible regression equation that permits the prediction of potentiometric heads in the mine region from variables such as surface elevation, bottom of well elevation, overburden thickness, thickness of mined coal, thickness of shales, thickness of sandstones, thickness of limestone, accumulated coal volume, average precipitation, underground mine area and thickness of the coal seam mined.

2) To use the regression equation to determine the potentiometric head at the elevation of the bottom of the coal layer to determine if the water level will be higher than the top of the coal layer or the ground surface.

CHAPTER 2: GEOLOGICAL SETTING

2.1. Site Location

The Meigs Mine Complex is located in Meigs, Vinton, and a small section in northern Gallia counties of southeastern Ohio near the town of Wilkesville as seen in Figure 2.1. The site is bounded to the southeast by Ohio River and Campaign Creek and to the east by Leading Creek. Meigs County has approximately 23,345 residents and per capita income of $21,317 as cited by the (U.S Census Bureau, 2016). The site has a moderate relief with rolling and precipitous hills and narrow mature valleys (Moody and Associates, Inc., 2006).

Land surface elevations range from 640 to 1029 feet above mean sea level (m.s.l.) with a maximum relief of 400 feet at the southern part of the site and at the northern part, the topographic elevations range from 590 to 870 feet mean sea level with a maximum relief of 280 feet (Moody and Associates, Inc., 2006). Meigs County drains to the Ohio River by way of the Shade River, Leading Creek, Raccoon Creek, and smaller direct tributaries to the Ohio River (USDA, 1991). A very small area in the northeastern part of the county drains into the Hocking River, a tributary to the Ohio River. The Ohio River forms the entire eastern boundary and about half of the southern boundary between Meigs County and Jackson, Mason, and Wood Counties in West Virginia (USDA, 1991). The Ohio River front stretches about 57 miles in Meigs County (USDA, 1991). The site has a low to moderate stream slope and land uses are primarily hardwood forests and pasture (Moody and Associates, Inc., 2006).

2.2. Geology

2.2.1. Regional Geology

The coal-bearing lithologies of Ohio were emplaced during the Pennsylvanian and Permian periods (Figure 2.1), approximately 320 to 245 million years ago (Wickstrom, 2005). Lithologies of this geologic system are well exposed throughout a large, mostly unglaciated area of eastern Ohio. The Pennsylvanian system in Ohio is distinguished by beds of economically essential bituminous coal. The coal beds are deep and broad in some part of Ohio and slender and discontinuous in other parts. (Crowell, 1995). The coal beds in Ohio were formed in broad coastal marsh which grew lush vegetation with the coal-forming coastal marsh developing rapidly in warm, moist climate near the paleoequator (Crowell, 1995).

Pennsylvanian rocks in Ohio consist of four divisions which are, in ascending (oldest to youngest) order: Pottsville, Allegheny, Conemaugh, and Monongahela. Each of these groups consists of repeating sequences of sandstones, siltstones, mudstones, freshwater limestones, shales, clays and coals that in most cases are comparatively thin and laterally discontinuous (Crowell, 1995) The lithology of the Pennsylvanian system shows varying depositional environments that appears to have been repeated cyclically throughout the duration of the time period (Walker, 1975). Ohio has been exposed to extensive uplift, erosion, and weathering during the Mesozoic era and the tertiary period of the Cenozoic era (Wickstrom, 2005). Approximately 60 separate seams of coal have been identified in Ohio (Crowell, 1995).

Pennsylvanian lithologies in eastern Ohio have long been the most essential economically to the state. Early settlers discovered large deposits of bituminous coal,

low-grade iron ores, limestone, clay, shale, and sandstone (Crowell, 1995).The presence

of these lithologies spurred industrialization of the state (see Figure. 2.2 for coal mines in

Ohio). In 2008, revenue from coal produced in the state is estimated at more than $600

million annually and is mined by both surface and underground methods

(Wickstrom,2005).
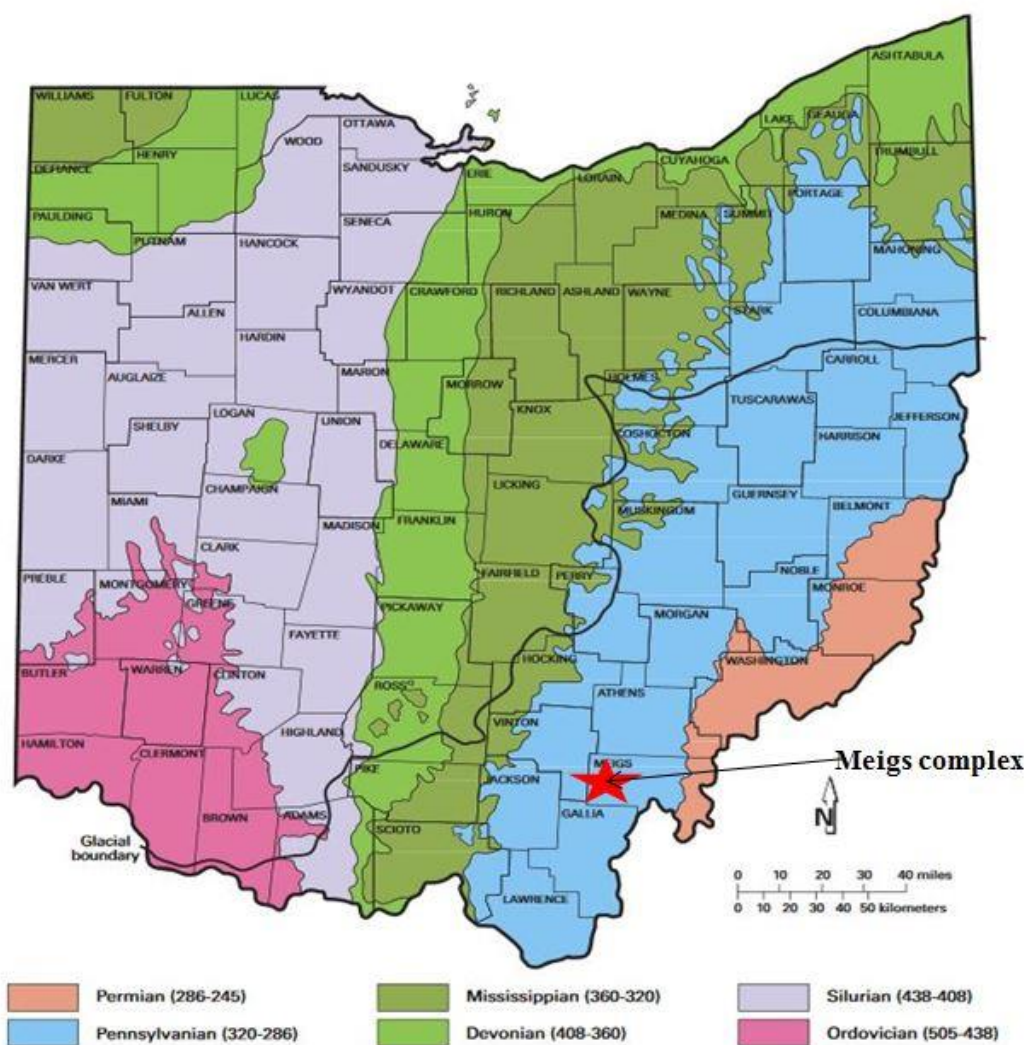
Figure 2.1. Bedrock geologic map of Ohio. Scale 1:2,000,000 (after Ohio Division of Geological Survey, 2006).
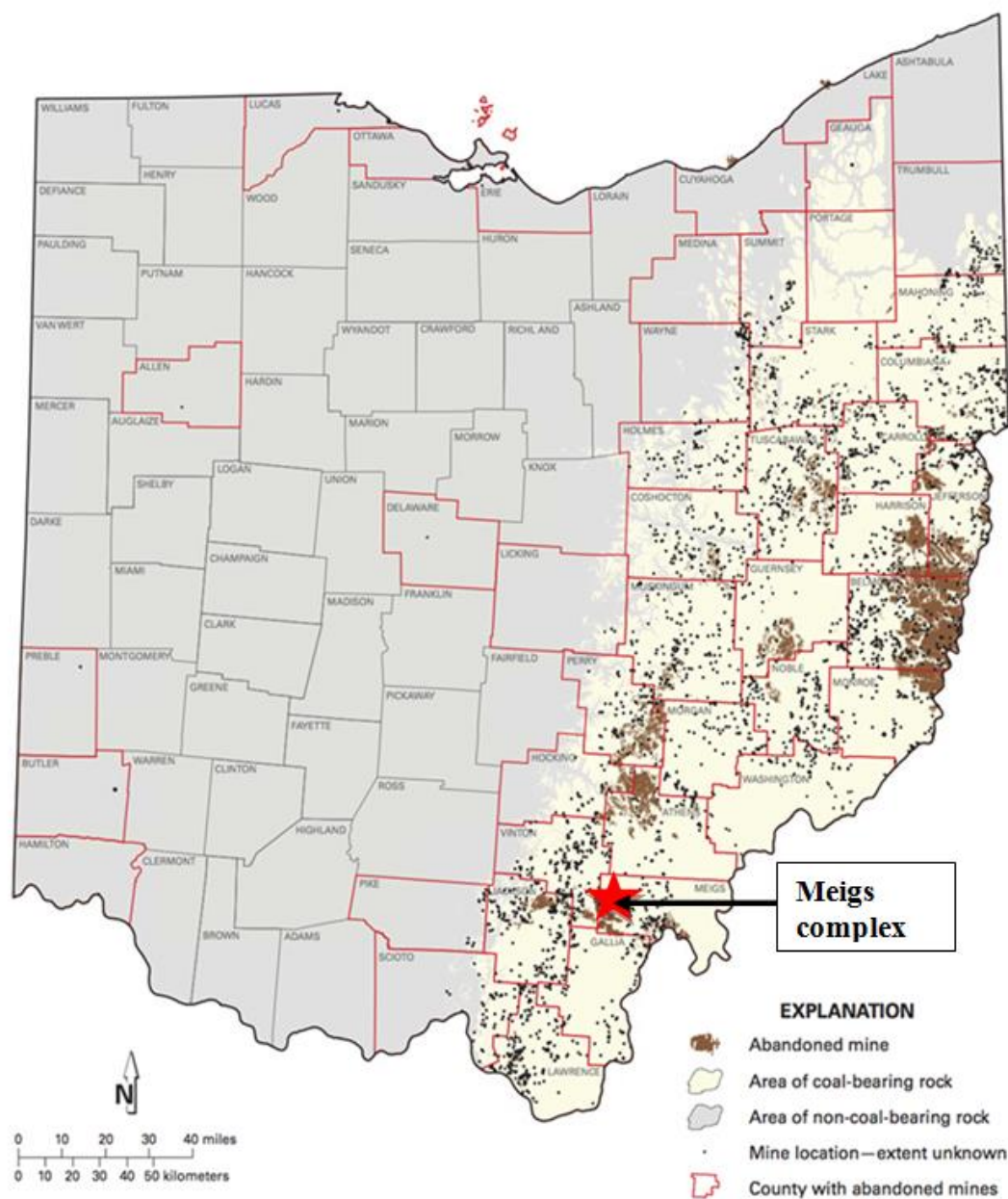
Figure.2.2. Abandoned coal mines in Ohio. Scale 1:2,000,000 (after Ohio Division of Geological Survey, 2012).

2.2.2. Local Geology

Meigs County is located in the unglaciated Western Allegheny Plateau region of the Appalachian highlands (Austin, 1965). Most of the soils are underlain by sedimentary rocks of the Conemaugh and Monongahela Formations of the Pennsylvanian System and

the Dunkard Group of the Permian System (USDA, 1991). The rocks generally consist of siltstone, shale, sandstone and coal with thin layers of limestones in some areas (USDA, 1991). Most areas of the bedrock have a northeast-southwest strike, with an average dip of 30 feet per mile toward the southeast (Sturgeon et al 1958). The western part of the county is underlain by rocks of the Conemaugh Formation, the central part by rocks of the Monongahela Formation, and the eastern part by rocks of the Permian System (USDA, 1991).

The Meigs Mine Complex comprises the Meigs 31, Meigs 2, and Raccoon mines (Figure 2.3). The footprint of the entire mine complex is 23,500 acres (Borch, 2008). The Meigs 31 and Raccoon mines are openly connected, whereas Meigs 2 is separated from them by a solid coal barrier, 1,350 feet wide at its narrowest point (Borch, 2008). The Meigs Mine Complex exploited the Clarion No. 4 coal seam. The elevation of the Clarion coal ranges from 611 feet m.s.l. (m.s.l. = feet above mean sea level), according to nomenclature used by miners) at the western edge of the mine declining to 250 feet m.s.l. on the eastern side (Borch, 2008). The coal thickness ranges from 4.5 – 6.5 feet and the overburden thickness ranges from 190 to 640 feet over Meigs 31 and 115 to 400 feet m.s.l. over Meigs 2 (Borch, 2008). Above the complex, the lowest topography is at approximately 600 m.s.l. The complex used both room and pillar and longwall methods of mining.
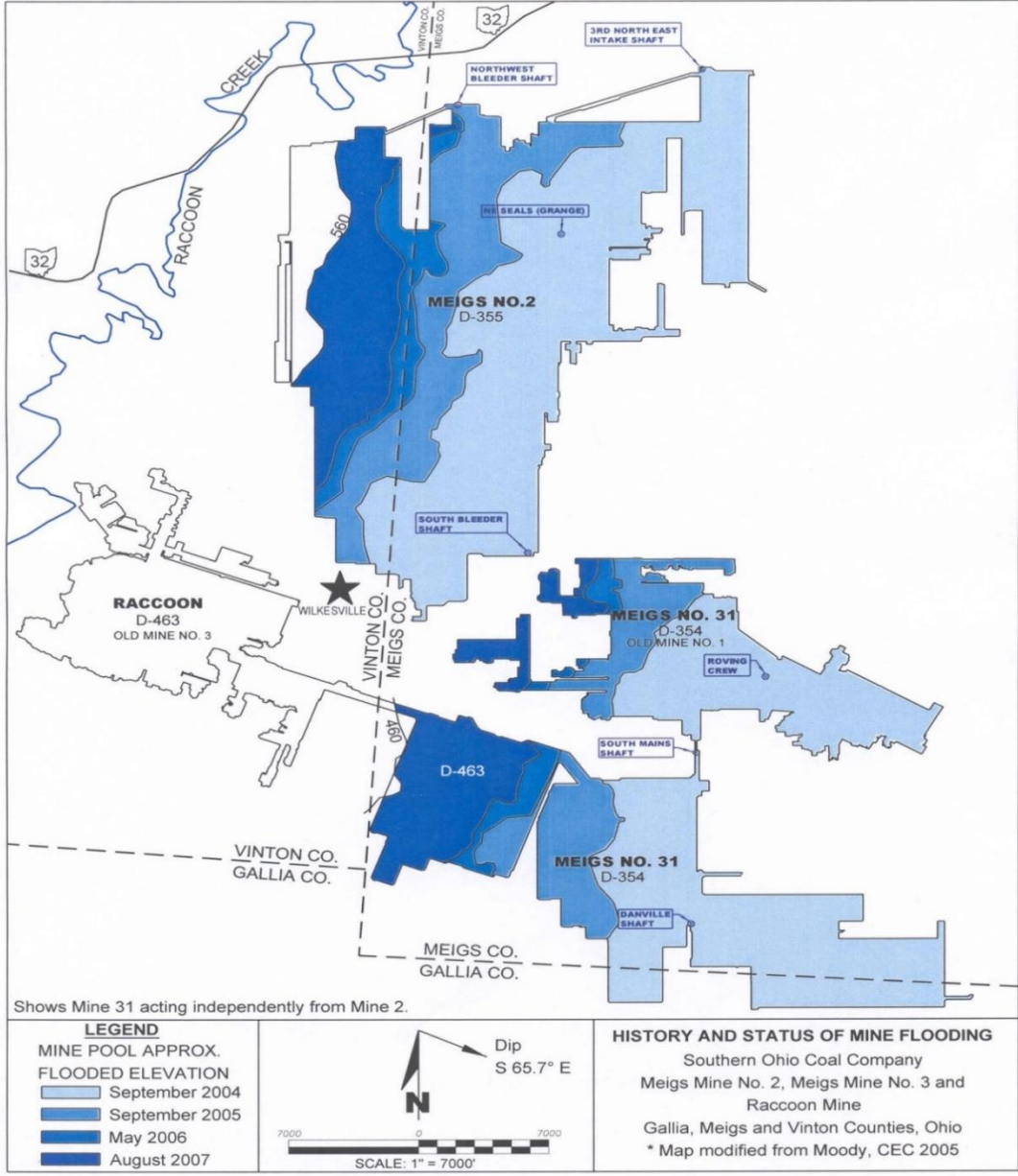
Figure. 2.3: Map of the status of mine flooding in the Meigs complexes, (Meigs Mine No.2, Meigs Mine No.3 and Raccoon Mine) as presented in Borch (2008) and modified from CEC (2005). The mine area is contained within the Gallia, Meigs and Vinton Counties, Ohio.

2.2.3. Soils

The Meigs Mine Complex catchment area is underlain by four different soils with different hydraulic properties that define four different recharge areas. They are the

Upshur-Gilpin, Gilpin-Rarden-Aaron, Upshur-Steinsburg-Gilpin and Upshur-Gilpin-Pinegrove soils (USDA, 1991).
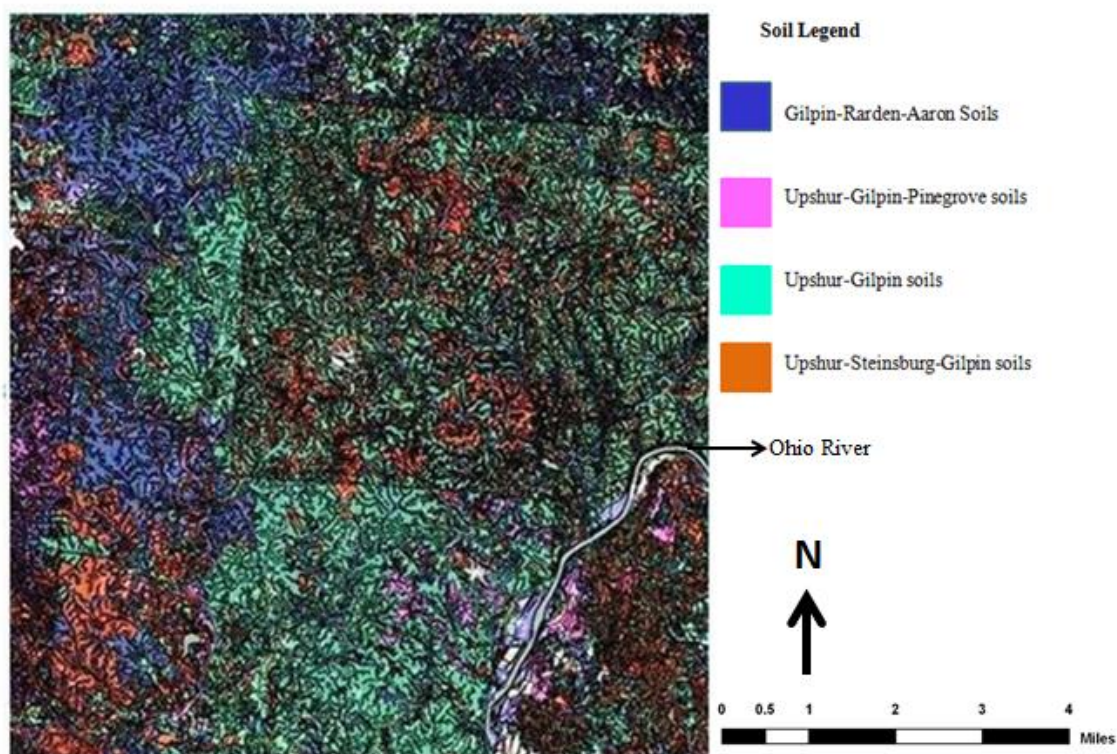
Figure. 2.4: Recharge zone boundary (retrieved from https://websoilsurvey.sc.egov.usda.gov).

The Upshur-Gilpin soils makes up about 67 percent of the Meigs County (USDA, 1991). The soil association consists of about 55 percent Upshur soils, 35 percent Gilpin soils, and 10 percent soils of minor extent (USDA, 1991). The soils are formed in residuum generated from siltstone, sandstone, and shale. The Upshur-Gilpin soils have a high shrink-swell potential, low permeability and mostly found on hillsides and ridgetops. Some of the minor soils associated with the Upshur-Gilpin are the well-drained Chagrin, poorly drained Newark, Moshannon, Keene, Vandalia and Nolin soils (USDA, 1991).

Gilpin-Rarden-Aaron soils consist of 45 percent Gilpin soils, 25 percent Rarden soils, 10 percent Aaron soils, and 20 percent soils of minor extent (USDA, 1991). The

soils are formed in residuum derived from siltstone, sandstone, and shale. The soils have a moderate permeability, are well-drained, and are mostly found on steep hillsides and ridgetops (USDA, 1991). Minor soils associated with Gilpin-Rarden-Aaron are the well-drained Chagrin, Nolin and Vandalia soils.

Upshur-Steinsburg-Gilpin soils consist of 40 percent Upshur soils, 40 percent Steinsburg soils, 5 percent Gilpin soils, and 15 percent soils of minor extent (USDA, 1991). The very deep, well drained Upshur-Steinsburg-Gilpin soils are on strongly sloping to very steep hillsides and ridgetops with a slow to moderate permeability (USDA, 1991). Well-drained Chagrin, poorly drained Orrville, poorly drained Kyger, and the well-drained Nolin soils are the minor soils associated with these groups (USDA, 1991).

Upshur-Gilpin-Pinegrove soils consist of 30 percent Upshur soils, 25 percent Gilpin soils, 20 percent Pinegrove soils, and 25 percent soils of minor extent (USDA, 1991). The very deep, well drained Upshur-Gilpin-Pinegrove soils are on strongly sloping to very steep hillsides and have a moderate permeability (USDA, 1991). The very deep, well drained Pinegrove soils have a rapid Permeability (USDA, 1991).

According to the information in the (USDA, 1991) literature, the order of permeability or infiltration of the soils in this area includes from lowest to highest Upshur-Gilpin soils, Gilpin-Rarden-Aaron soils, Upshur-Steinsburg-Gilpin soils and Upshur-Gilpin-Pinegrove soils.

2.2.4. Climate

Precipitation is uniformly distributed throughout the year with winter snow and rains providing a good accumulation of soil moisture by spring (USDA, 1991). Normal

annual precipitation is adequate for all crops that are suited to the temperature and length of growing season in the area. 23 inches of precipitation out of the total annual precipitation (40 inches) usually falls in April through September the growing season for most crops (USDA, 1991). In winter, the average temperature is 32 degrees Fahrenheit and the average seasonal snowfall is about 21 inches (USDA, 1991). In summer, the average temperature is 71 Fahrenheit degrees and the average daily maximum temperature is 84 degrees (USDA, 1991). The average relative humidity in midafternoon is about 60 percent and at dawn the average is 80 percent (USDA, 1991). Humidity is higher at night. The average wind speed is 11 miles per hour in Spring from the south (USDA, 1991).

2.2.5. Hydrogeology

The Meigs Mine Complex is entirely below drainage with the exception of the western edge of the Raccoon Mine where the coal seam is just at or near Raccoon Creek (Borch, 2008). No significant quantities of water were encountered during drilling operations at Meigs Mine Complex. However, much water was encountered during mining of low cover areas, especially in the west sides of the mine (Borch, 2008). The primary water producing zone is 77 to 148 feet below the surface which is at 764 feet m.s.l. The hydraulic conductivity which indicates the amount of water able to travel through an area per unit time under the influence of a hydraulic gradient in this zone ranged from impermeable to a high of 5.67×10^{-5} cm/sec (Borch, 2008) or 0.16 feet/day. The controlling factor in water flow is due to secondary permeability that exists as joint systems, bedding planes, and natural fractures.

Groundwater flow is solely restricted to the interaction between near vertical fractures and bedding planes separations, which is to be expected due to the low primary permeability of the strata (Borch, 2008). In Appalachian valleys, groundwater flow occurs as vertical infiltration along valley walls via stress-relief fractures and lateral movement along bedding planes fractures (Wyrick and Borchers, 1981). Permeability in this region is thought to decrease with depth by an order of magnitude for each 100 feet (Siplivy, 2004).

CHAPTER 3: PREVIOUS WORK AT MEIGS MINE COMPLEX

Borch (2008) presented a paper about the flooding conditions in the Meigs Mine Complex with the purpose of establishing background and hydrologic information regarding the Meigs Mine Complex pool. The report also talked about mine pool development, water quality and water quantity. Data presented in this report was used throughout this research.

Mining began in 1972, 1973, and 1974 in the Meigs 2, Meigs 31 and Raccoon No. 2 respectively and closed in 2002 (Borch, 2008). During mining, the workings were dewatered by pumping water to the surface for treatment. With the completion of the mine, the potential exists for mine pool water to surface and contaminate various tributaries of Leading Creek and Raccoon Creek. This potential discharge would occur in the low-lying stream valleys where vertical fractures from stress relief or from subsidence may provide a conduit to the surface (Borch, 2008).

According to (Borch, 2008) pumping of mine water from Meigs 2 into Meigs 31 began in January 2008 and, in September of 2008, Meigs 31 began pumping into Parker Run at approximately 5000 gpm.

3.1. Effect of Longwall Mining on the Permeability of the Strata.

The longwall method of underground mining includes the excavation of large rectangular coal blocks called panels that can produce subsidence. Total subsidence movement is to a large extent influenced by overburden thickness and lithology (Borch, 2008). Kendorski (1993) provides a model that describes types of fracturing above longwall mines, from the mine roof to the ground surface as shown in Figure 3.1.

SURFACE FRACTURE TO 50t

SURFACE DISTURBENCES MAY CLOSE OR FILL IN 2 YEARS OR LESS

TENSION — COMPRESSION — TENSION

SURFACE WATER DRAINS INTO SURFACE DISTURBENCE ZONE

CONSTRAINED ZONE

WATER BELOW SURFACE DISTURBENCE ZONE IS UNAFFECTED

AQUIFER

DILATED ZONE 24t to 30t to 60t

WATER IN THIS ZONE GOES INTO STORAGE IN DILATED ROCK MASS

TEMPORARY DROP RECOVERS AS STORAGE IS FILLED OR DILATION CLOSES AS MINE PASSES THROUGH AND BEYOND

TEMPORARILY INTERMITENT

AQUIFER

FRACTURED ZONE 6t to 10t

FRACTURES

WATER IN THIS ZONE DRAINS TO THE MINE

CAVED ZONE ROOF TO 6t to 10t

CAVED ZONE

WATER INTRUSION

MINED COAL SEAM

t = AVG. COAL THICKNESS

MODIFIED FROM KENDORSKI - 1993

Figure 3.1 Longwall mining subsidence fracture model (as presented by Borch, 2008, and modified from Kendorski, 1993).

According to Borch (2008) aquifer dewatering is enhanced by enlargement of existing fractures or opening of new fractures above the zone of caving during a subsidence event representing both an increase in permeability and porosity that could result in dewatering aquifers or streams. Dewatering of the aquifer is usually limited to active mining areas. As the strata settles and becomes re-compressed, groundwater levels may rebound as flow paths to the mine become more restricted and less direct. These fractures may heal themselves with time if sufficient amount of clay and shale material are in the strata (Borch, 2008). On the other hand, if the strata are friable sandstone units with little silts and clays, the ability of the fractures to heal is diminished.

At Meigs Mine Complex, near surface aquifers were dewatered by surface tension- induced fractures, according to Borch (2008) water infiltration into the mines was direct in areas of low cover where vertical subsidence-induced fractures intersect with surface tension fractures and natural stress-relief fractures. Wyrick and Borchers (1981) and Ferguson (1974) describe stress relief fractures in the Appalachians that extend to a depth of approximately 150 feet in valley bottoms and sides.
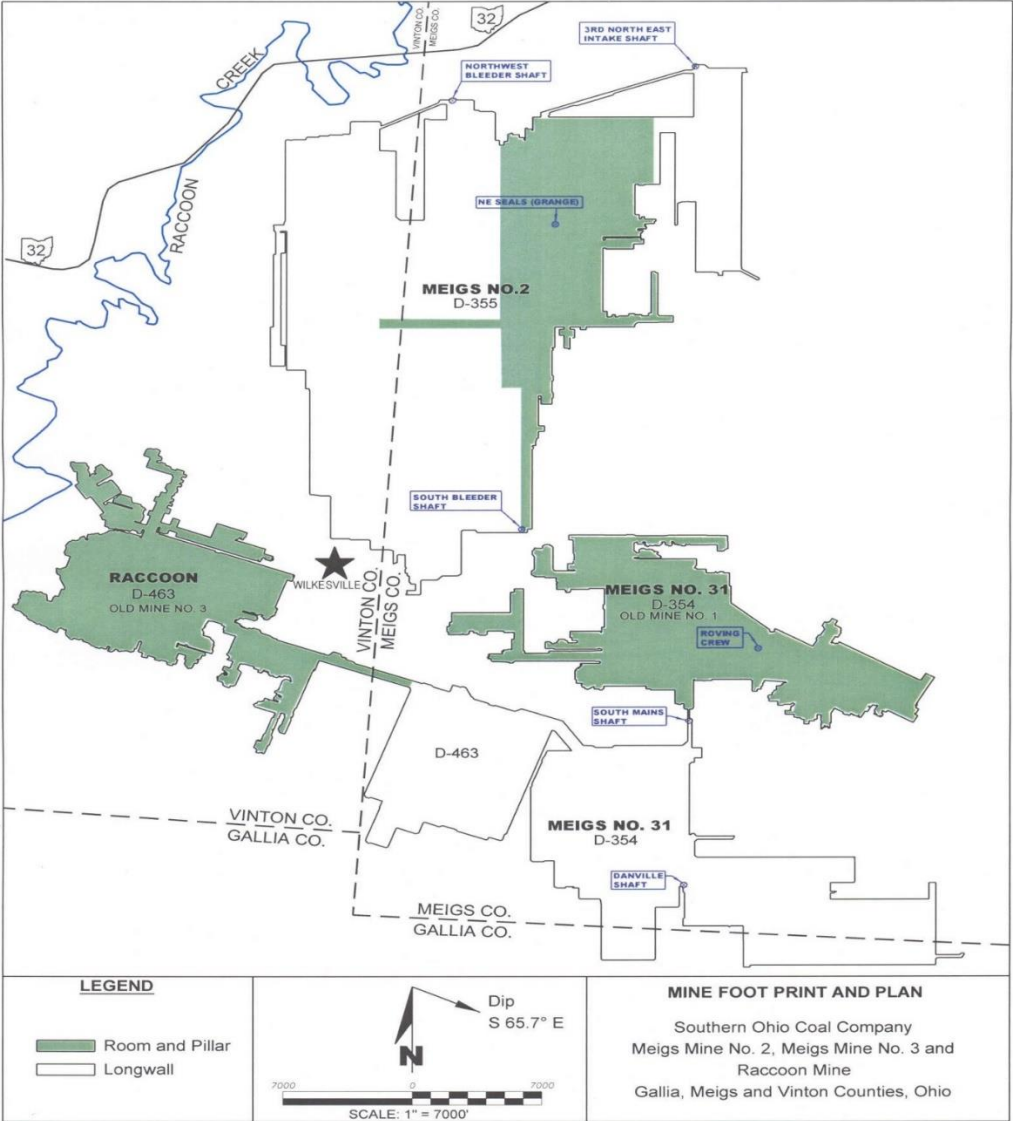
Figure 3.2. Areas showing longwall and room and pillar methods of mining. (Meigs Mine No. 2, Meigs Mine No. 3 and Raccoon Mine), Gallia, Meigs and Vinton Counties, Ohio (Map presented by Borch, 2008 as modified from Moody, CEC 2005).

3.2. Meigs Complex Mine Pool.

3.2.1. Mine Pool Characteristics

According to Borch (2008) Meigs Mine Complex was recharged by vertical infiltration, lateral inflow from adjacent flooded mines and from ground water in the coal itself. The Meigs Complex has 7 mineshafts which are accessible for pool level monitoring (Figure. 3.2). Recharge into the mines reflects the seasonal climatic precipitation as shown in Figure 3.3 and 3.4. The graphs show a long-term trend of seasonal changes in mine water entering the mine pool. Due to the 1,350 foot barrier separating Meigs 2 from the Meigs 31 and Raccoon Mine complex, the Meigs 2 mine pool acts independently from the Raccoon and Meigs 31 mine pool (Borch, 2008). The Raccoon and Meigs 31 mines are hydrologically connected and therefore act in concert.

The Meigs Mine Complex has undergone several stages from pre-mining conditions, active mining and post-mining condition. Water elevation data for the pre-mining period was unavailable but data for domestic wells that were drilled during active mining were available for modeling. Exploitation and dewatering was active during the active mining period. Data for the rate of water extraction during the mining period was also unavailable. The post-mining stage consists of two stages, the free recovery of the water levels from the time of mine completion to January 2008, and pumping of the water for treatment from January 2008 to December 2014. Water elevation data from January 2004 to December 2007 was available for the period of free recovery and from January 2008 to October 2016 for pumping of water for treatment.

Prior to pumping out of Meigs 2, the average monthly rate of change of water elevation within the mine from January 2006 through January 2008 was 1.44 feet/month

and Meigs 31 also had an average monthly rate of change in water elevation of 1.4

feet/month prior to pumping out (Borch, 2008).
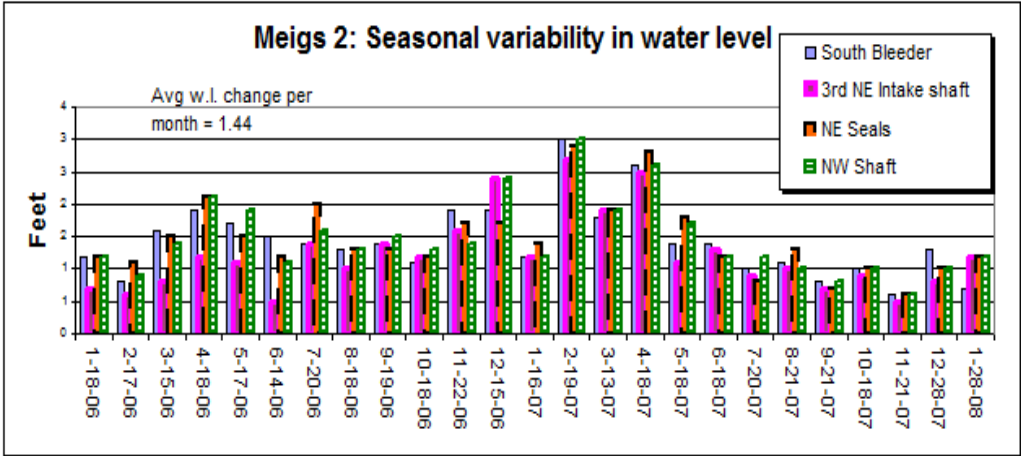
Figure.3.3. Rate of mine pool flooding and seasonal variability in Meigs 2.The location of shafts in Meigs 2 can be seen in Figure 3.2 (Borch, 2008).
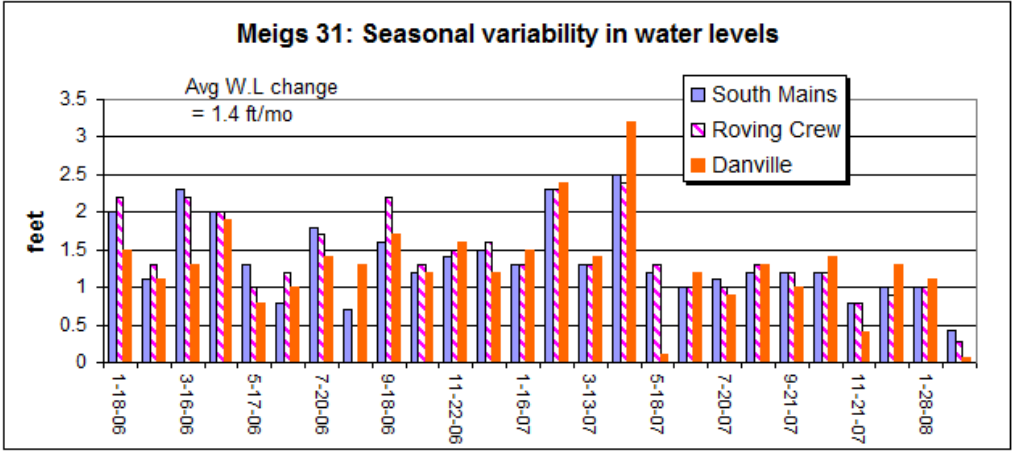
Figure.3.4. Rate of mine pool flooding and seasonal variability in Meigs 31.The location of shafts in Meigs 31 can be seen in Figure 3.2 (Borch, 2008).

3.2.2. Recharge rate calculations.

Different sections of the mine commonly have distinctly different recharge rates.

Siplivy (2004) identified eight recharge areas on the western side of the mine complex,

primarily at Meigs 2. These discrete inflow zones are defined as areas of the mine

beneath a stream valley, areas with prominent lineaments, and areas with shallow cover

ranging from 115 feet to 220 feet.

Recharge rates were determined volumetrically for the Meigs 2 and for Meigs 31 sections (Siplivy, 2004). Siplivy based recharge rates on mine pool inflow volumes over a 322-day time period. After mining ceased, water levels were monitored in the mine pools. Volume and inflow rate were calculated using mine geometry parameters, in-mine elevations, type of mining, and areas of inundation. For Meigs 2, with a volume of 1,097,645,880 gallons, the inflow rate was estimated at 2367 gpm (455,647.50 ft^3/d) over 11,900 acres (518,364,000 ft^2) with a 75% coal recovery rate. This value corresponds to a recharge of 3.85 inches/year. For Meigs 31, with a volume of 837,197,255 gallons, inflow rate was estimated at 1811 gpm (348,617.50 ft^3/d) over 11,600 acres (505,296,000 ft^2) with a 55% coal recovery rate. This value corresponds to a recharge of 3.02 inches/year. Note that this recharge rates assume that recharge is only occurring from the overlying rocks and surface, not from lateral movement of water.

3.2.3. Meigs 2 Flooding Conditions.

Figures 3.5 and 3.6 shows pool elevation through time representing distinct segments of the mine. The NE Shaft and the NW shaft merged with the South Bleeder shaft by early 2005 (Borch, 2008). These two sections now act as one pool evidenced by the identical water levels.

According to Borch (2008) the pool monitored from the 3rd NE Intake shaft remained completely isolated from the rest of the flooded sections on Meigs 2 until August 2004, when the pool elevation rose to a coal elevation of 530 feet m.s.l. which is a topographic high point. Upon reaching the coal elevation the water then spilled over into the rest of Meigs 2 through the entry west of the 3rd NE intake shaft. The water levels appeared to be converging until about October 2006 after which time the elevation

trends appear to be parallel. The 3rd NE Intake shaft shows water rising at a rate equal to or slightly slower than the rest of Meigs 2 although the elevation of the pool is higher.

Figure 3.6 shows that the 3rd NE section has not converged with the rest of the mine pool. This section of the mine pool maintains a consistent hydrologic head signaling that it may be hydrologically separate from the rest of Meigs 2. However, when Meigs 2 began pumping water from the South Bleeder shaft into Meigs 31 on January 28, 2008, an immediate response was observed at rates of 3000 gpm (Borch, 2008). The South Bleeder shaft is a little less than six miles from the 3rd NE shaft thus indicating permeable conditions in the rocks connecting the two mine pools and between the mine pool and the 3rd NE shaft (Borch, 2008).
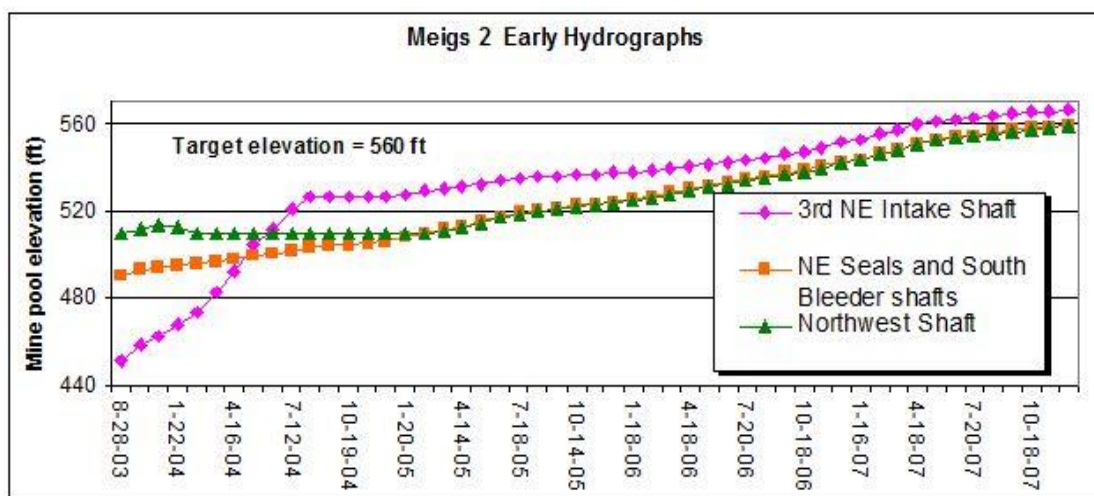
Figure.3.5. Graph showing early flooding conditions in Meigs 2 (Borch, 2008).

Borch (2008) explained that Meigs 2 mine pool had exceeded its control elevation in the NE section of the mine and was affecting near surface aquifers. Most resident's water supplies were replaced with centralized piped water systems after the longwall mining impacted private water wells. The NE section of the mine, while still elevated above the rest of the mine pool did exhibit an immediate response to the pumping of the

mine pool. As stated earlier, pumping occurs at the most southern part of the Meigs 2 pool from the South Bleeder Shaft.

Borch (2008) estimated that the monthly infiltration rate increased from an average 1.4 feet per month to an average 2.9 feet per month. At this rate, a trend analysis indicates the mine pool would reach inundation (600 feet m.s.l.) by the end of 2012 if it were not pumped. In January 2008, pumping from Meigs 2 to Meigs 31 started and the water level in Meigs 2 stabilized. However, our interest is in looking at the response of the mine pool under non-stressed conditions and free recovery. For that reason, this last period of time of the Meigs Mine Complex will not be modeled.

CHAPTER 4: MODELING TOOLS

A groundwater flow model was created for Meigs Mine Complex with the purpose of understanding the effect of the different hydraulic parameters and geology of the area in the formation of mine pool, especially the water level recovery after the mine was closed. For that objective Visual MODFLOW was used to create the groundwater flow model. In addition, different coal mines of Ohio that have been included in the OSM project were studied for this thesis. Collection of these data is explained in Chapter 5. An Artificial Neutral Network program called NeuroShell 2 was used to build empirical models for the mines in the OSM project.

4.1. Ground Water Flow Modeling: Visual MODFLOW

According to Frank and Guiguer (1990) Visual MODFLOW is a windows based program used in creating input files interactively, linking, running the flow, solute transport programs and displaying the program results. Visual MODFLOW is the proven standard for professional 3D groundwater flow and contaminant transport modeling. Visual MODFLOW combines the most powerful and intuitive interface available with the latest versions of MODFLOW, MODPATH, Zone Budget and MT3D (Khadri, 2016). MODFLOW models the solution of the groundwater flow equations, MODPATH is a particle tracking program that models the movement of particles (e.g. contaminants) in an advective flow regime system (its uses solutions of fresh water head obtained with MODFLOW), and MT3D is a program that solves the solute transport equation considering advection, diffusion, and dispersion processes as well as some chemical reactions between the solute and the porous media (e.g. sorption, first order decay, etc.). Visual MODFLOW is used for evaluating groundwater remediation systems, delineating

well capture zones, simulating natural attenuation of contaminated groundwater,

determining contaminant fate and exposure pathways for risk assessment, designing and

optimizing pumping well locations for dewatering projects, etc. (Khadri, 2016).

MODFLOW is a block centered model, which means that head values are

calculated for the center of each cell node making up the model grid. The finite

differences of the model means the same head value calculated at the center of the cell is

representative of the head value located within the entire cell. Visual MODFLOW

integrates the numerical parameters of all the hydrogeological properties making up the

field of consideration in order to answer the ground water flow equation in three

dimensions (Anderson and Woessner, 1992).

Visual MODFLOW has been designed to enlarge modeling efficiency and

decrease the complication typically related to creating three-dimensional groundwater

flow models (Khadri, 2016). The system is divided into three separate modules, the input

module, the run module, and the output module. The input system permits the user to

graphically allocate all of the essential input parameters for creating a three-dimensional

groundwater flow model. It contains the fundamental model building blocks for gathering

a data set for MODFLOW. The system tours the modeler through the process necessary

to design a groundwater flow model. The run module allows the user to modify the

MODFLOW parameters and options which are run-specific. These involves selecting

initial head values, setting solvers for the matrix equations (the program has options for

several matrix solver approaches), activating the re-wetting package, specifying the

output controls, etc. Each of these system selections has default settings, which are able

to running most simulations. The output system enables the user to show all of the

modeling and calibration results for MODFLOW and the other programs. The output menu enables the user to select, customize, and overlay the various options for presenting the modeling results.

According to (Khadri, 2016) MODFLOW model calibration consists of changing values of model input parameters in an attempt to match field conditions within some acceptable criteria. Lack of proper site characterization may result in a model that is calibrated to a set of conditions which are not representative of actual field conditions. The calibration procedure involves calibrating to steady-state and transient situation. With steady-state simulations, there are no observed changes in hydraulic head with time for the field conditions being modeled. Transient simulations involve the change in hydraulic head with time. These simulations are needed to narrow the range of variability in model input data since there are numerous choices of model input data values which may result in similar steady-state simulations (Khadri, 2016).

4.2. Artificial Neutral Network

Artificial neural networks are computational method formed by individual cells that perform computational calculations similar to the way the human brain works, learning from training data (Sanchez-Mesa et al., 2002). Artificial neural network base the predictive power in the large number of interconnections between each of the different neurons that comprise the neural systems (input neurons, intermediate neurons or output neurons). Each of these neurons is connected to the neurons of the preceding layer and subsequent layer throughout an algorithm that enables network learning based on the training cases.

Artificial neural networks have been used for environmental prediction and forecasting in hydraulics and hydrology (Schaap et al., 1998, Kisi, 2004), water quality (Recknagel et al., 1997, Maier and Dandy, 2000), in engineering, for example to study the solar energy potential in Turkey (Sozen et al., 2005), or to predict the fracture parameters of concrete (Ince, 2004), in computer science for estimating the effort required for developing an information system (Heiat, 2002), in hydrology for predicting the river flow forecast in reservoir management (Baratti et al., 2003), in medicine for gene expression data analysis (Tan and Pan 2005) and in daily life for bus arrival time prediction at bus stop with multiple routes (Yu et al., 2011).

In general all artificial neural network models present better results than other kinds of models like linear regressions. An artificial neural network can model complex and non-linear processes through different layers (input layer, intermediate layers and output layer) trained by back propagation algorithm to relate input variables to output variables (Aznarte et al., 2007). The learning process of neural networks is based on the relationship change between the different neurons in neural network. The parameters that define this relationship or importance value are called weight. The weight together with the bias associated to each neuron, changes throughout the training process to adjust the outputs of the neural network to the value of the training cases, allowing the neural network learning during the operations in the training phase (Venkatasubramanian et al., 2003). For reliability of the predictive model a number of data points are reserved for a validation of the results obtained in the training phase.

The training of the neutral network starts with the introduction of the data in the first layer of the neutral network (input layers formed by input neutrons). The data,

constituted by the training cases, is entered as a vector $(X_1, X_2, X_3 .... X_n)$ and it is

propagated to the first intermediate layer by the propagation equation as seen in Figure

4.2. According to (Gopalsamy, 2004) The input values from input neurons (M) is

processed with the weight (Wmn) of the connection linking the intermediate neuron (n)

with the previous neuron (m) from which the data comes. Bn is the bias associated with

the intermediate neuron (n) as seen in Figure 4.2. According to (Gopalsamy, 2004) the

propagation equation changes all data to a single signal and activate the signal with the

activation function to provide an output neuron signal (Y_n). This process is repeated for

all neutrons in intermediate and output layer to create a final predicted value in the output

layer.

Group Method of Data Handling (GMDH) is a very powerful architecture in

NeuroShell 2 that is used in creating polynomial model where predicted value of the

output would be as close as possible to the actual value of the output. The most common

approach to solving such models is to use regression analysis. Regression models in

NeuroShell 2 can be used to obtain regression equations that can be applied to any

unknown sample, also NeuroShell 2 can be used without identifying a particular

regression equation and it gives results for the dependent variable that are obtained from

the information obtained in the training process and then applied to test or unknown

samples. In this case, you need to have the artificial neural network program NeuroShell

2 with the training data to obtain the value of the unknown Y. However, if the GMDH

method is used, an equation that can be imported into EXCEL or other worksheet and

used to find the unknown Ys without having to have NeuroShell 2. The algorithm in

NeuroShell 2 determines values of the regression coefficients by minimizing the squared sum (over all samples) of differences between sample outputs and model predictions.
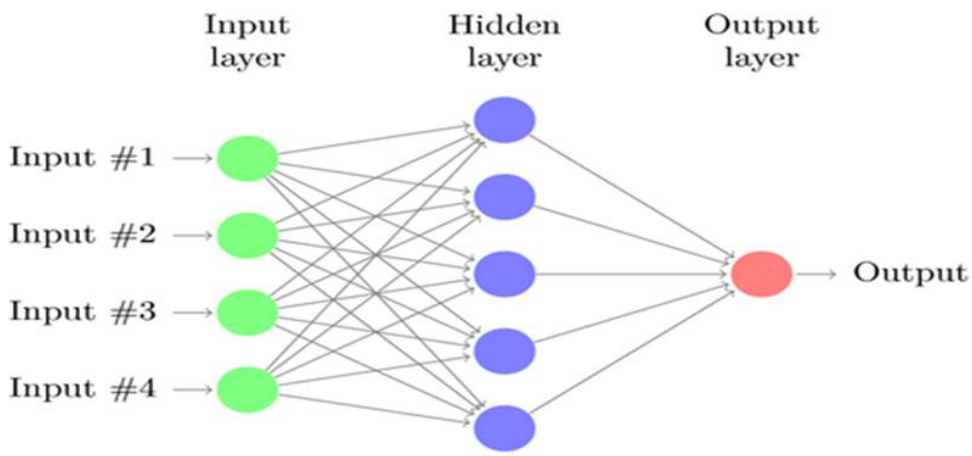
Figure 4.1 Neural network topology (Astray et al., 2016).
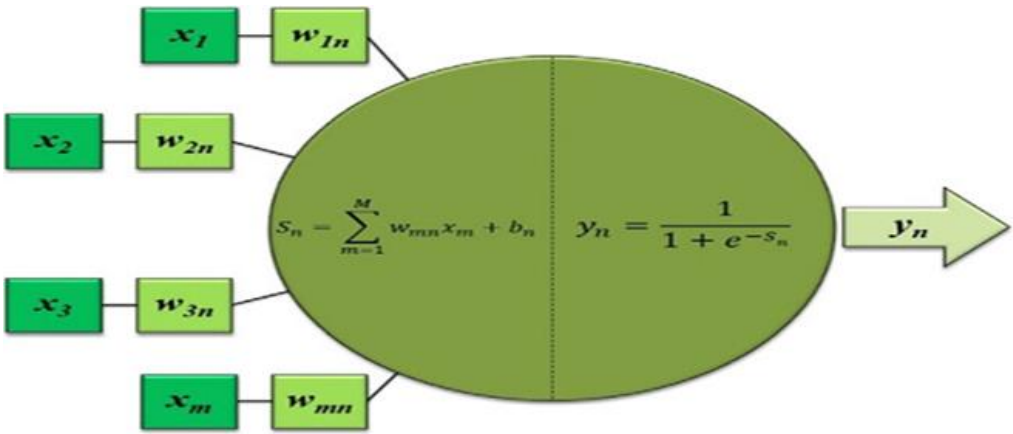
Figure 4.2 Neural network Structures and rules in the first intermediate layer (Astray et al., 2016).

CHAPTER 5: METHODOLOGY

The two objectives of this thesis will be achieved with the following two tasks: the modeling of the groundwater flow in the Meigs Mine Complex and the application of artificial neural networks to the large data set compiled by the members of the OSM project team for all the recent mines of Ohio that have adequate data. The methodology presented here is then divided in three sections: data collection, modeling of the Meigs Mine Complex, and artificial neural networks.

5.1. Data Collection

5.1.1. Data for the modeling of the Meigs Mine Complex

The initial stage of my thesis dealt with the extraction of data from mine permits of mines commissioned during the last 35 years by ODNR as well as monitoring reports after mines were closed. Well identification, coordinates, dates, surface elevations, depth of well below land surface, static water levels and aquifer types were extracted for the pre-mining, mining and post-mining from the well logs in the permits and quarterly monitoring reports (QMRs). Actual pre-mining data are often not available because multiple mines are often in close proximity of each other, so pre-mining periods are obscured by the interaction between mines. For the Meigs Mine Complex, some well information reported in the permit was incomplete with many wells lacking coordinates and having only the owner name. With the information about the owner name, the approximated coordinates of the wells were extracted from the Meigs County property database (Meigs County Auditor, 2017). Aquifers reached by those wells were identified according to the elevation of the well bottom. Monitoring shaft data used for the modeling were also extracted from Borch (2008).

5.1.2 Data for artificial neural network modeling of all mines included in this study

For all the wells and boreholes of the recent mines studied in the OSM project, the information in drill holes for each mine was also extracted from the mine permits: drill hole identification, co-ordinates, surface elevations, dates, overburden thickness, depth from surface, thickness of different layers in the borehole (shales and clays, sandstone, limestone, and other coal layers), kind of strata above coal, kind of strata below coal, and thickness of coal seam mined were extracted from the permits for the boreholes.

I participated in the data collection process for the mines studied in the OSM project, a total of 28 mines were analyzed for this project, but only 11 mines are sealed and contained adequate information for the project. A total of 381 wells are represented in the data set. Figure 5.1 shows the location of mines that were considered in this project; however, a complete explanation of the way these data was extracted and its corresponding statistical analysis is presented in a thesis developed by another student (Schafer, 2018). She developed statistical models of the data using the program Unscramble X and determine the best regression equations for the data using multivariate linear regression, principal component analysis, principal component regression, and partial least squares regression. The purpose of applying artificial neural networks to this data was to compare results and decide which is the best equation for the geographic information system tool that will be developed later. After the completion of Schafer's and my thesis, the OSM team will work in the selection of the best equation for this implementation.
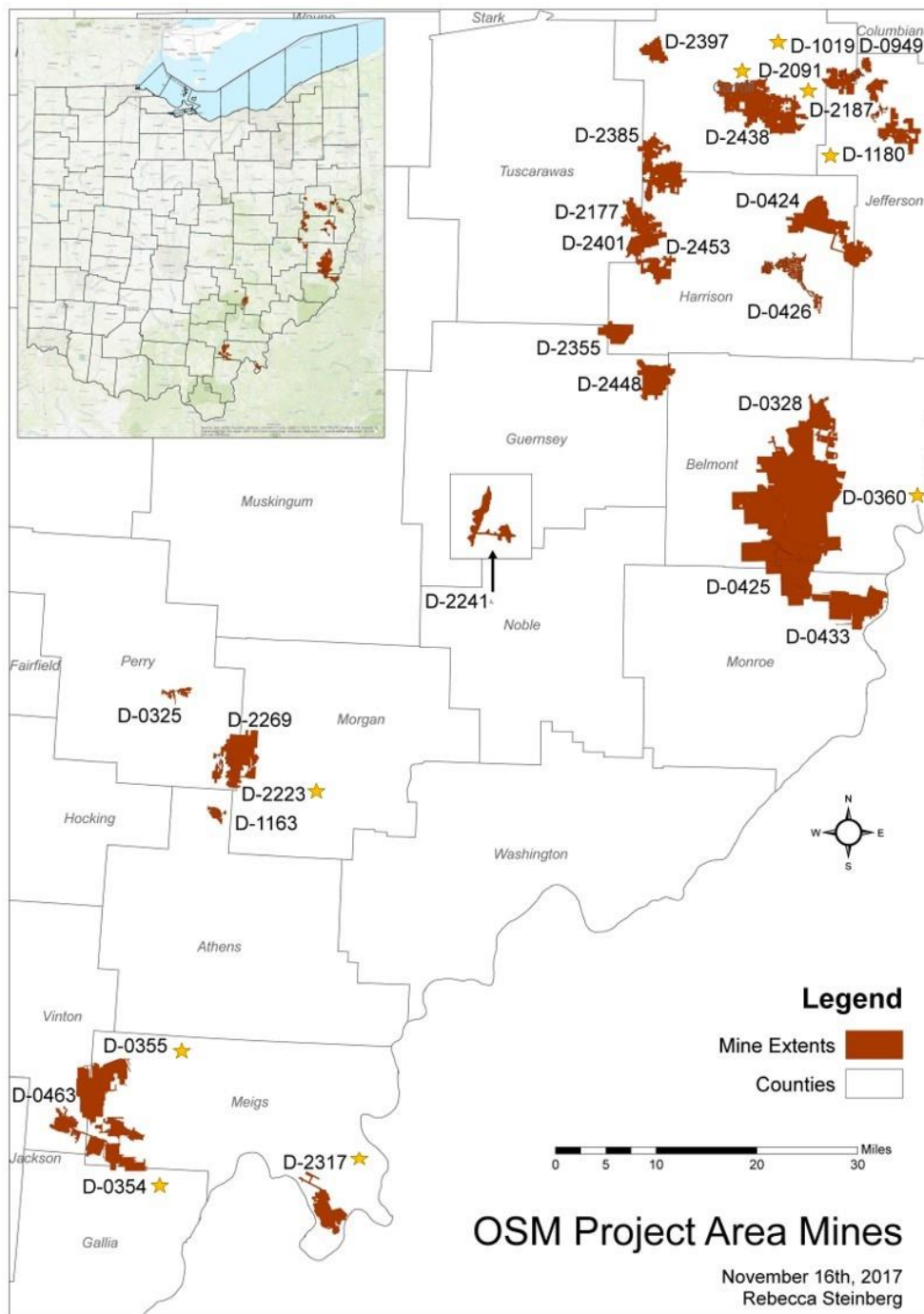
Figure 5.1. Mines with D permits that were issued mining permits during the last 35 years. Only the mines with a star had the data needed for this project and were considered for the artificial neural networks modeling (map elaborated by Rebecca Steinberg for the OSM project).

5.2. Modeling of the Meigs Mine Complex

5.2.1 Conceptual Model

According to Anderson and Woessner (1992) a conceptual model is a pictorial image of the area to be modeled. Establishing the flow regime and determining hydrostratigraphic units of the modeled area defines the conceptual model. Potentiometric maps are used in establishing flow regimes in the model area and they are constructed by plotting surface water elevation within the wells with their respective well coordinates. In this thesis work, the kriging option in Surfer 12.0 has been used to produces the flow direction of groundwater and pinpoint hydrologic boundaries. Hydrostratigraphic units are used in building the model and they are determined from the examination of boreholes, geologic maps and cross sections.

The physical model of Meigs Mine Complex also used hydrogeological parameters (e.g. specific storage, hydraulic conductivity, etc.), hydrostratigraphy, topography, and watershed boundaries for the active and post-mining condition. The modeled area was selected based on the hydrological boundaries of the surrounding watershed to the mine as identified on the topographic watershed map. No-flow and river boundaries were assigned to the Meigs mine base map. The hydrostratigraphic units of the Meigs complex were determined by constructing cross-sections correlating lithologies of boreholes.

Thirty boreholes evenly distributed within the mines concessions were selected for Meigs Mine model building. The stratigraphic data for each borehole was recorded. Variables included surface elevation, coal elevation, and depth from surface and strata thickness for every significant rock layer reported in the Meigs Mine permit. In this way,

the elevation of every contact was calculated (see Table 5.1). Eight Contacts maps were generated out of these thirty boreholes and imported into MODFLOW for model building. These contact maps were generated by plotting the various lithological contact elevations against their respective coordinates using the kriging options in Surfer 12.0.

With well information (surface elevation, static water level, coordinates, aquifer identification, well names, and depth of well below land surface) from the Meigs Mine permit and the county property database, maps of potentiometric elevation were constructed. The wells used in this modeling are for simulating mining conditions during mining because data was not available prior to mining. Maps of potentiometric elevation in the wells of each aquifer were constructed to determine the flow regime of the area. These maps were generated by plotting the surface water elevation within the well with their respective well coordinates using the kriging option in Surfer 12.0.

5.2.2. Numerical Model.

A numerical model of Meigs Mine Complex was created using the established physical Meigs model and Visual MODFLOW. The catchment area for the Meigs complex was gridded 0.5 miles by 0.5 miles and areas beyond the boundaries were deactivated.

Layer boundaries were determined by plotting surface elevations of the contacts between different lithologies of the thirty boreholes with their respective coordinates using the kriging option in Surfer 12.0 and then imported in MODFLOW. The eight contact maps constructed were imported into MODFLOW for numerical model building. Boundaries for the watershed where Meigs Mine Complex is located were identified in the topographic map and served as river boundaries of the groundwater flow model as

well as no-flow boundaries for the model. Six streams identified in the catchment area were used as river boundaries during modeling, individual cells making up the river boundary were allocated values of river conductance, river bottom elevation and river stage elevation. Areas beyond the boundaries were deactivated in MODFLOW. Constant head boundary conditions were assigned to the western and eastern margin of the three aquifers in the model based on head elevations obtained from the water potentiometric maps for each aquifer.

Visual MODFLOW incorporates the numerical values typical of all the hydrogeologic characteristics making up the catchment area such as porosity, hydraulic conductivity, specific yield, specific storage, etc., in order to solve the ground water flow equation in three dimensions. During the calibration procedure of the potentiometric heads using MODFLOW, input parameters for the model are systematically changed until a good match between observed and simulated heads in observation wells is obtained. The model is calibrated by systematically examining the possible scope of values for each input parameter (e.g. hydraulic conductivity and recharge) against constant conditions of all other input parameters included in the model. Only one parameter is changed at a time. The procedure is iterative until the minimum error is obtained in the calibration.

As it was discussed earlier, the Meigs Mine Complex has experienced several stages from pre-mining conditions, active mining, and post-mining conditions. This last stage includes two periods: free recovery of the water levels and pumping of the water for treatment. In our work, we are interested especially in the free recovery period. Unfortunately, we could not find water elevation data for the pre-mining period or data

for the rate of water extraction during the mining period. We only had data for domestic wells that were drilled during April 1996 to May 1996; however, at that time the mine was under exploitation and was probably being dewatered. We also have data from November 2003 to October 2016 for the elevation of water in the shafts, with data from January 2004 to December 2007 for the period of free recovery and from January 2008 to October 2016 for pumping of water for treatment. In order to know the hydraulic conductivities and other parameters of the mine after closure, the free recovery period should be modeled. The heads measured in the shafts starting at the end of 2003 and ending in December 2007 could be used for this purpose. The initial elevation of water in the Mine Complex with only the elevation of water in shafts could not be reproduced. For that reason, it was decided to work a steady state model to reproduce the water levels in the wells during April 1996 assuming no pumping. This calibrated model was later used as the initial condition to simulate a second model pumping water out of the shafts to reproduce the elevation of water in the shafts in January 2004. Once this second model was calibrated, it was the initial starting model for the third transient model to simulate the recovery of the water levels during the period of free recovery. This last model and period is the most interesting for this work. In this way, the hydraulic conductivites, specific yield, and specific storage of each the layers, as well as the recharge was calibrated for the free recovery of the water levels in the post-mining period.

For the steady-state models and the transient model, they were calibrated until the lowest error values based on calculated heads and observed heads was obtained. This process was repeated for the hydraulic conductivity of the layers and four recharge areas in the model until they supported the lowest error values calculated by the model. A

sensitivity analysis was performed in order to establish the confidence of each of the calibrated recharge and hydraulic conductivity parameters and to determine the parameters that affect more the results of the model. A sensitivity analysis was conducted by systematically altering the value of each independent calibrated parameter and observing the change in model error results with respect to the calibrated model parameters. All the other parameters were kept at the value of the calibrated model.

After the sensitivity analysis had been performed in the steady-state calibrated second model, transient simulations were conducted to establish the changes in groundwater flow conditions throughout the modeled area with respect to time (third model). The transient model was then run for a total of 4 years (January 2004 to December 2007) to simulate the evolution of the potentiometric head in that period of time. The transient model was calibrated until the lowest error values based on calculated heads and observed heads was obtained. Here all the heads measured during that period of time every month were considered. This process was repeated for the hydraulic conductivity of the layers, specific storage of the layers, specific yield of the layers and four recharge areas in the model until they supported the lowest error values calculated by the model. A sensitivity analysis was performed for the transient calibrated input parameters.

5.3. Artificial Neural Networks applied to potentiometric heads in wells at coal mines in Ohio

The final stage of my thesis involves building empirical models for mine pools using artificial neural networks. This prediction method was selected due to the complexity of the data, nonlinearity of the variables and the variety of the variables

involved. Statistically identified variables of the mines obtained by Schafer (2018) in her

thesis project were used as inputs parameters to this model. The parameter that was more

difficult to obtain for the data set was the withdraw of water during the time the heads

were measured in the different wells. The data for the wells include all the mines that

have been active during recent years and have a D permit. Two data sets were available

for all the wells of the mines, one with water withdraw obtained from the National

Pollutant Discharge Elimination System (NPDES) permit from the Environmental

Protection Agency and another data set that was larger and contained no data for water

withdraws. However, the accumulated coal extracted for each mine at the time the well

was monitored was calculated by Schafer (2018) using data retrieved from Mine Safety

and Health Administration (2018). The water extracted at the time the mine was under

operation should be a function of the cavity that has to be dewatered or the accumulated

coal extracted. For that reason, these two variables should be related and even with the

lack of water withdraw data, it is expected that it is possible to obtain a good regression.

For reliability of the predictive model the statistically identified variables with water

withdraw and variables without water withdraw were divided into training and validation

data and imported into Neuroshell 2 for model building. Ninety per cent of the data was

selected randomly for training purpose and 10% of the data was selected randomly for

use as the validation data set. The same randomly selected calibration and validation data

sets used by Schafer (2018) for the multivariate analysis in Unscramble were used here

for a better comparison later.

The model was developed based on the training data and the produced models

were validated for prediction capacity using the validation data. The data extraction tool

in NeuroShell 2 was used to separate the two data sets prior to treatment. After that, the Design tool in NeuroShell 2 was used to apply the regression options. These variables were calibrated in NeuroShell 2 using the Group Method of Data Handling, which works by building successive layers with links that are simple polynomial terms. The layers are created by computing regressions of the input variables and then choosing the best ones called survivors. The design module create a great deal of flexibility in the configuration of the variables that are required for the training of the network. The maximum, average, and minimum potentiometric heads of the mines served as the dependent variables and the independent variables were overburden thickness, surface elevation, bottom of well, thickness of mined coal seam, accumulative coal volume extracted, water withdraw, underground mine area, and the average annual precipitation. In addition, the following independent parameters were also considered: total coal thickness, thickness of sandstone, thickness of limestone, and thickness of shale. These parameters were extracted from the closest borehole to each well. The best model was selected based on the estimation of errors between the observed and the calculated heads.

CHAPTER 6: GROUNDWATER FLOW MODELING RESULTS

6.1. Modeled Area

A catchment area map was created to determine the location of the Meigs Mine Complex. Figure 6.1 shows the area of the Meigs Mine Complex with the various River boundaries and No flow boundaries. The Meigs Mine Complex has an area of 23,500 acres. Raccoon Creek flows from the north to meet the No flow boundary at the south of the Meigs Mine Complex. Little Raccoon Creek flows from the north into the Raccoon Creek at the north western part of the Meigs Mine Complex. Little Leading Creek flows into Leading Creek at the eastern part of the Meigs Mine Complex which further flows into the Ohio River at the south. Campaign Creek flows into the Ohio River at the southern part of the Meigs Mine Complex. No flow boundary can be found at the western and eastern margin of the Meigs Mine Complex.
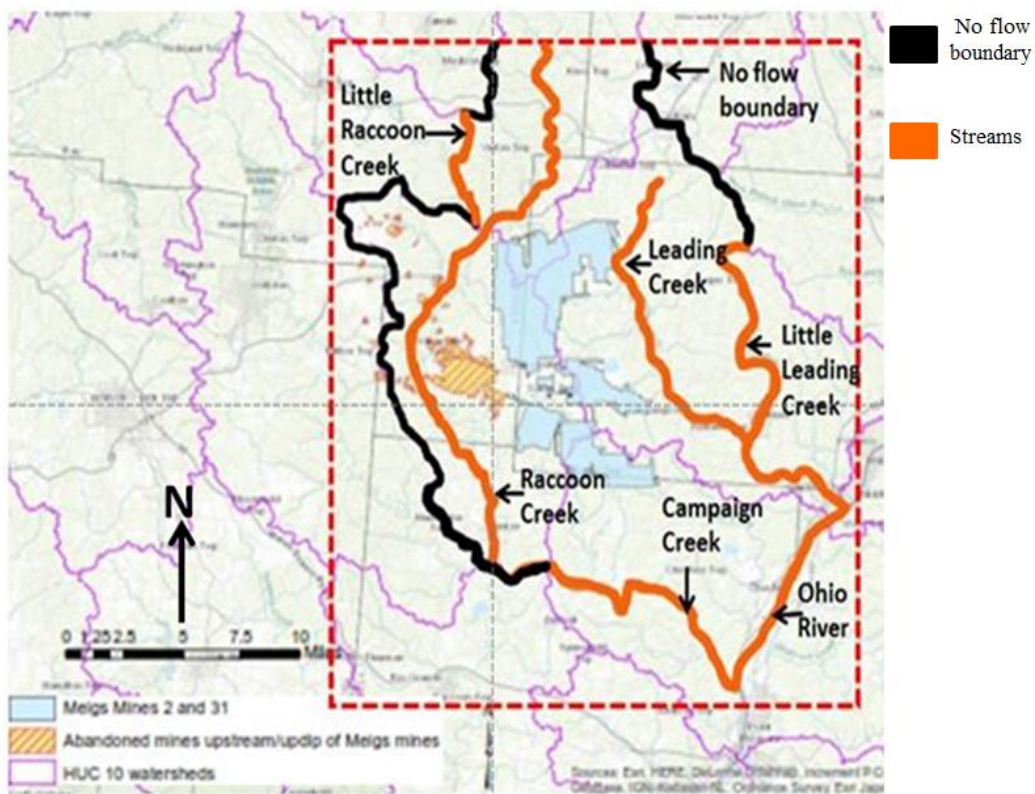
Figure 6.1 Boundary conditions of the modeled area.
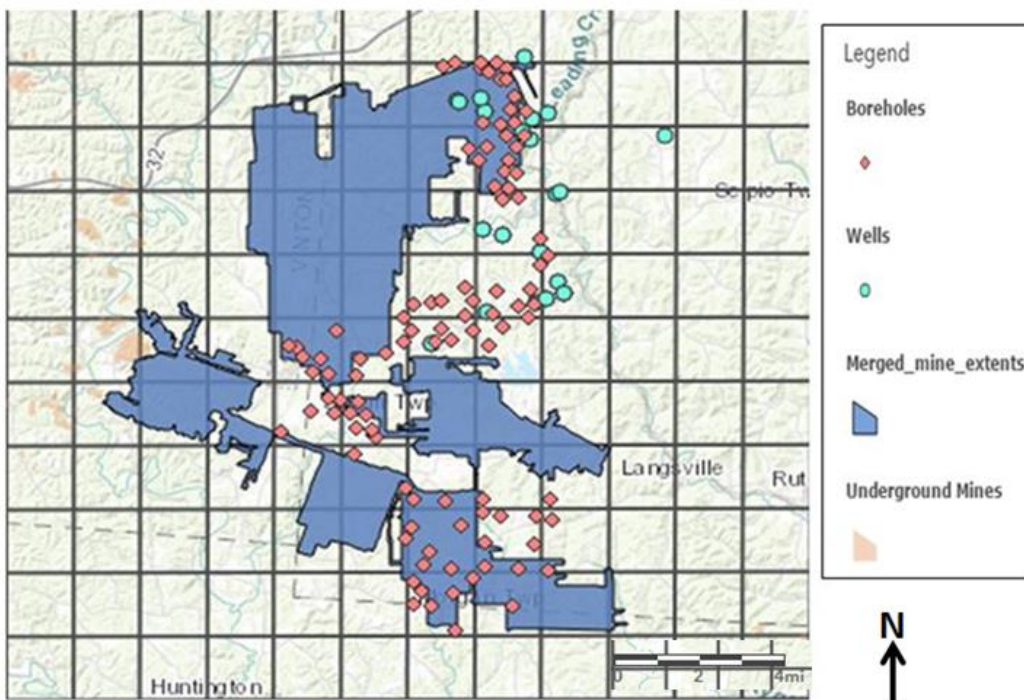
Figure 6.2 Modeled area showing locations of boreholes, wells, and mine extents.

6.2. Contact Maps

The extracted data for thirty boreholes (drill hole ids, co-ordinates, surface elevations, depth from surface and lithologies) from ODNR mine permits were used in the determination of the various contact elevations for the lithologies as seen in table 6.1

Table 6.1 shows the lithological contact elevations in the Meigs Mine Complex catchment area, whiles Table A.1 shows the various lithological contact elevations for the 30 boreholes. These boreholes were correlated together to establish the major lithologies within Meigs catchment area. Shale, sandstone and coal were the dominant hydrostratigraphic units determined. Eight lithological contacts were established among the sandstones, shales, and coal which can be seen in Table A.1 in Appendix A. The lithologies were in repeating sequences with layer 1 being shale 1, layer 2 being sandstone 1, layer 3 being shale 2, layer 4 being sandstone 2, layer 5 being shale 3, layer 6 being sandstone 3, layer 7 being shale, layer 8 being coal and layer 9 being shale.

Figure 6.3 below and Figures A.1, A.2, A.3, A.4, A.5, A.6, and A.7 in Appendix A show the contact maps generated out of the various calculated contact elevation of the boreholes. Elevation increases from southwest to northeast of the map for Figures 6.3, A.1 and A.2. For Figures A.3 and A.4 in Appendix A elevations increases from west to east of the map. For Figures A.5, A.6 and A.7 elevation increases from northwest to southeast of the maps.

Table 6.1. Different lithologies reported in the boreholes drilled by the mining company in the Meigs Mine Complex their average thickness of the strata, depth from surface of the upper contact and higher elevation of the upper contact. Red and light brown, represent rocks with low and high hydraulic conductivity, respectively. Black represents coal and blue limestone.

ID Name	Surface Elevation	Lithology	Strata Thickness (ft)	Depth from Surface (ft)	Higher contact ft depth	higher contact elevation ft	Colour type
787	722.98	casing	18	18			
		shale	11	29	18	704.98	red
		limestone	4	33	29	693.98	blue
		shale	16	49	33	689.98	red
		sandstone	49.4	98.4	49	673.98	black
		claystone	14.8	113.2	98.4	624.58	red
		sandstone	6	119.2	113.2	609.78	black
		shale	45.11	164.31	119.2	603.78	red
		sandstone	10.2	174.51	164.31	558.67	black
		shale	3.9	178.41	174.51	548.47	red
		coal	1	179.41	178.41	544.57	grey
		shale	3.9	183.31	179.41	543.57	red
		coal	1	184.31	183.31	539.67	grey
		shale	74.2	258.51	184.31	538.67	red
		claystone	6.5	265.01	258.51	464.47	red
		shale	9.1	274.11	265.01	457.97	red
		coal	1.1	275.21	274.11	448.87	grey
		claystone	6	281.21	275.21	447.77	red
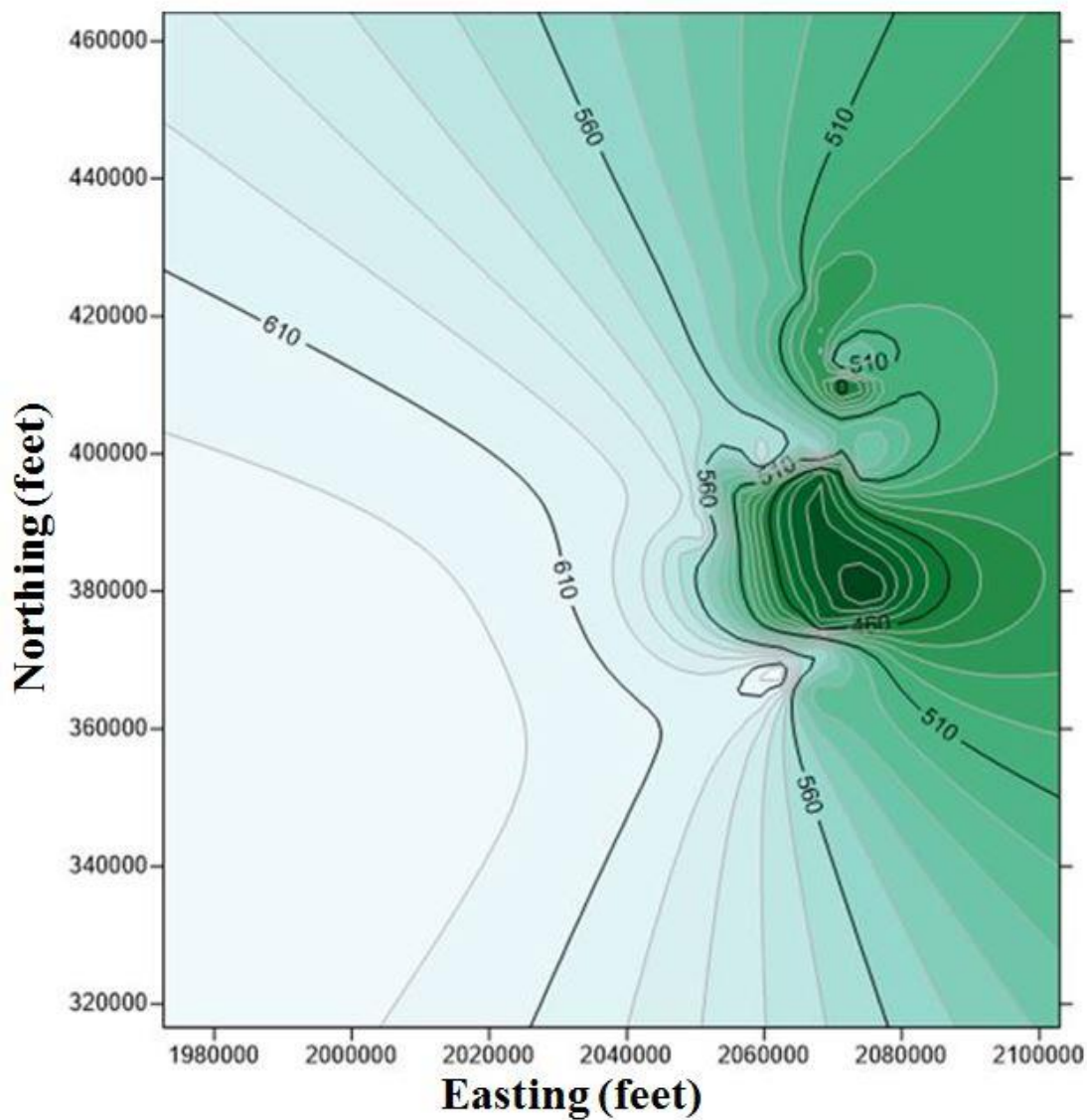
Figure 6.3. Upper contact map of aquifer C with a contour interval of 10 feet.

6.3. Potentiometric Maps.

Wells located in three aquifers were reported in the Meigs Mine Complex permits. With the information from the mine permit and the wells found in the Meigs county property database, maps of the potentiometric elevation in the wells of each aquifer were constructed. These maps were generated by plotting their surface water

elevation within the well with their respective well coordinates using Surfer software. The sandstone aquifers were identified as zone A, zone B and zone C.

Figure 6.4 shows the potentiometric heads for the shallowest aquifer (zone A). This Figure shows higher potentiometric heads at the eastern margin of the map and indicates general flow direction towards the western part of the map. Figure 6.5 (for aquifer zone B) shows higher potentiometric heads at the northeastern margin of the map and indicates general flow direction towards the southwest. Figure 6.6 which is the deepest aquifer (zone C) shows higher potentiometric heads at the northern margin of the map and indicates general flow direction towards the southern part of the map

Table 6.2 Wells from ODNR permits and Meigs property database. The blue colored wells were extracted from mine permits and the white colored wells were extracted from the Meigs County property database. Static water level (SWL) was reported for all the wells. Dates were not reported for the wells extracted from the county database.

Well	X	Y	Surface Elevation for Sampling Station (msl)	Depth of Well below Land Surface (ft)	SWL (ft)	Surface Water Elevation	Aquifer Identification	Date
MC-FR30-502 (DW)	2066321	420410	810	20	18	792	A	4/26/1996
DW-1VWC-4-110	2047650	392544	710	19.8	15.4	694.6	A	
DW-1MS-12-402A	2074893	372067	860	37.4	29	831	A	
DW-1MS-F31-26	2095675	369743	745	26.8	5.4	739.6	A	
MS-FR23-503 (DW1)	2063665	395197	690	15	3.50	686.50	B	4/8/1996
MC-FR1-501 (DW4)	2072712	417141	760	14	2.50	757.50	B	4/25/1996
MC-FR36-503 (DW)	2068902	419440	710	18	5.00	705.00	B	5/7/1996
DW-1,MS-F1-47	2069586	384553	650	13.5	3	647	B	
MS-11-501 (W)	2074025	399540	640	85	12.00	628.00	C	
MS-12-507 (WL)	2076100	401705	700	157	101.00	599.00	C	4/24/1996
MS-12-509 (W)	2076790	400505	620	67	8.50	611.50	C	5/2/1996
MC-8-506 (W)	2076390	410990	610	50	7.62	602.38	C	4/22/1996
MC-13-503 (W)	2070755	406640	720	190	109.00	611.00	C	4/25/1996
MC-16-505 (WL)	2072880	424940	760	160	30.00	730.00	C	4/22/1996
MC-FR2-503 (W)	2075252	419220	800	180	126.00	674.00	C	4/23/1996
W-1 MS-F13-61	2069352	380662	690	143	38	652	C	
W-1 VWC-4-68	2014459	399307	725	135	90	635	C	
W-1 MS-24-375	2062947	370137	755	220	91.6	663.4	C	
W-1 MS-18-384	2069811	370347	720	195	95	625	C	
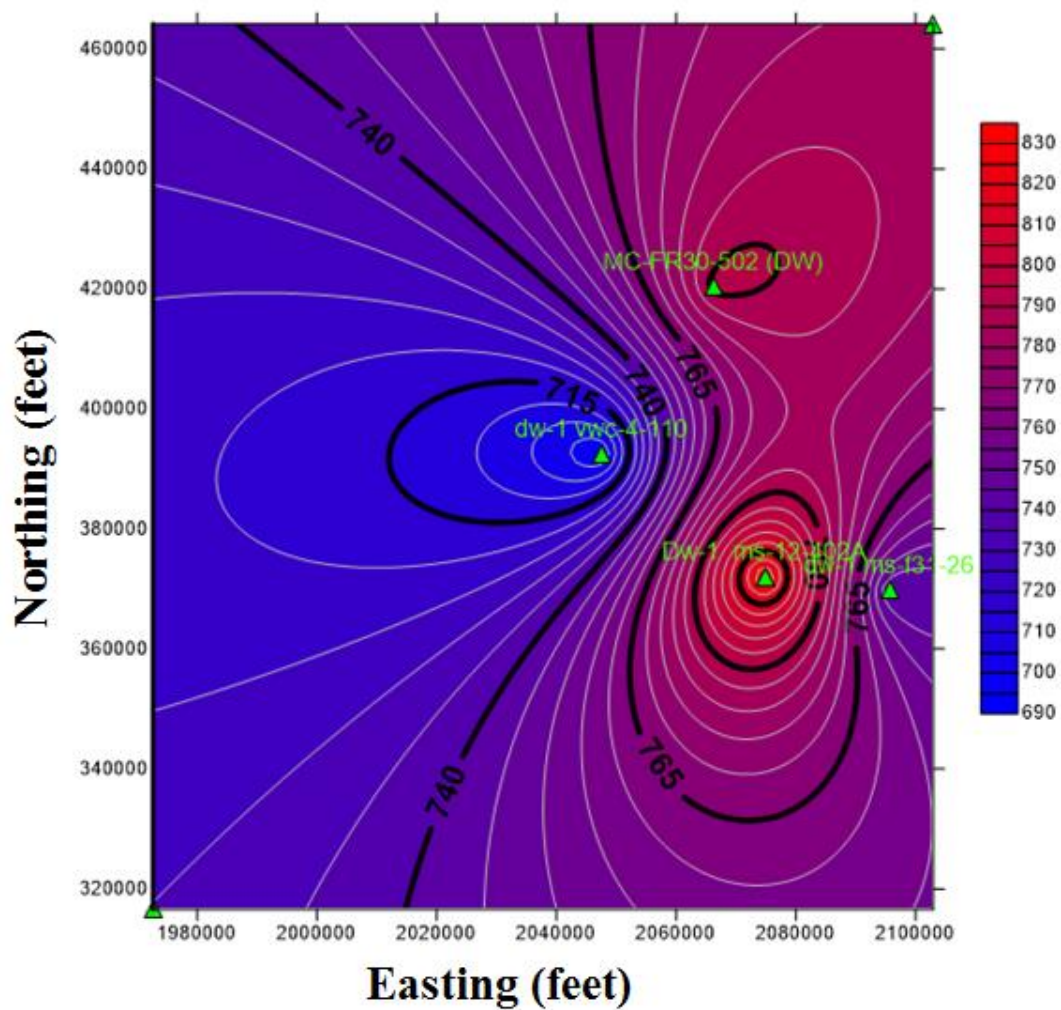
Figure 6.4. Potentiometric head map for aquifer A with a contour interval of 5 feet.
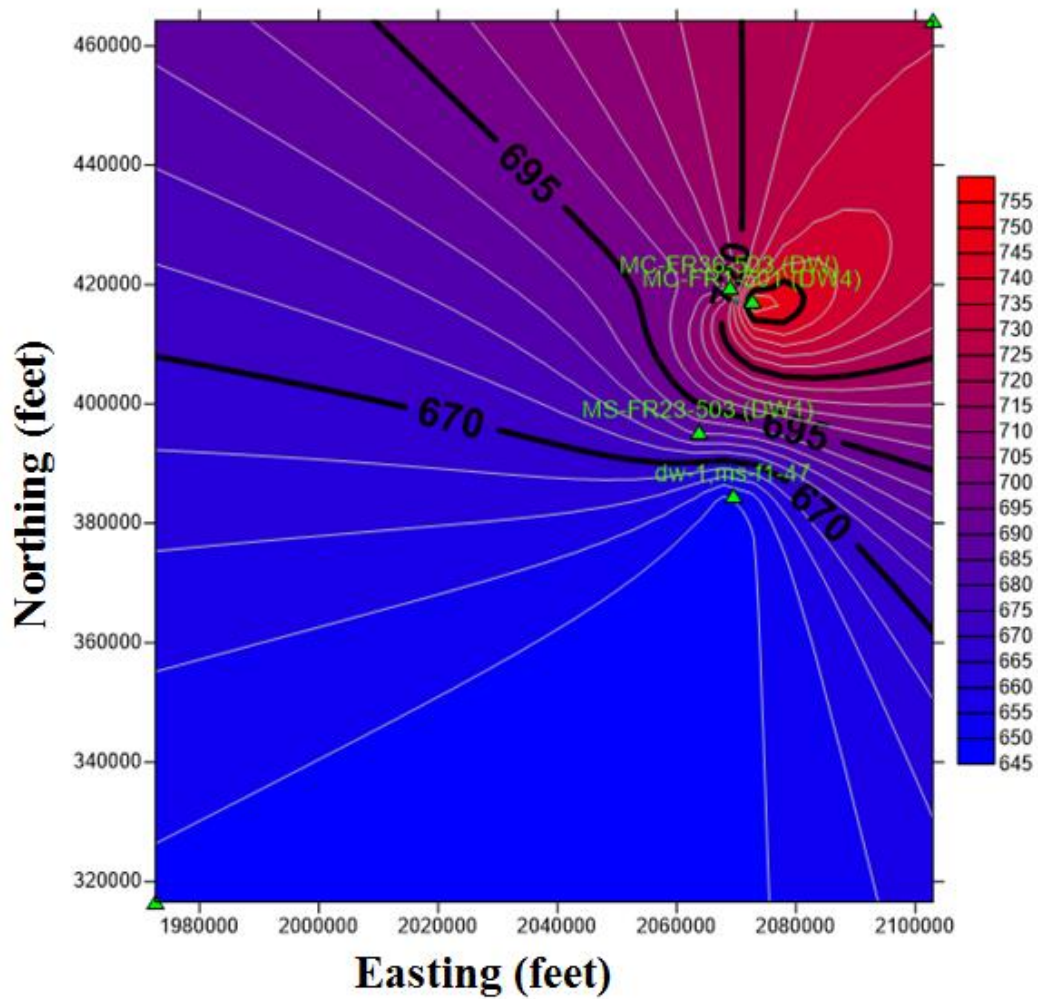
Figure 6.5. Potentiometric head map for aquifer B showing well locations with a contour interval of 5 feet.
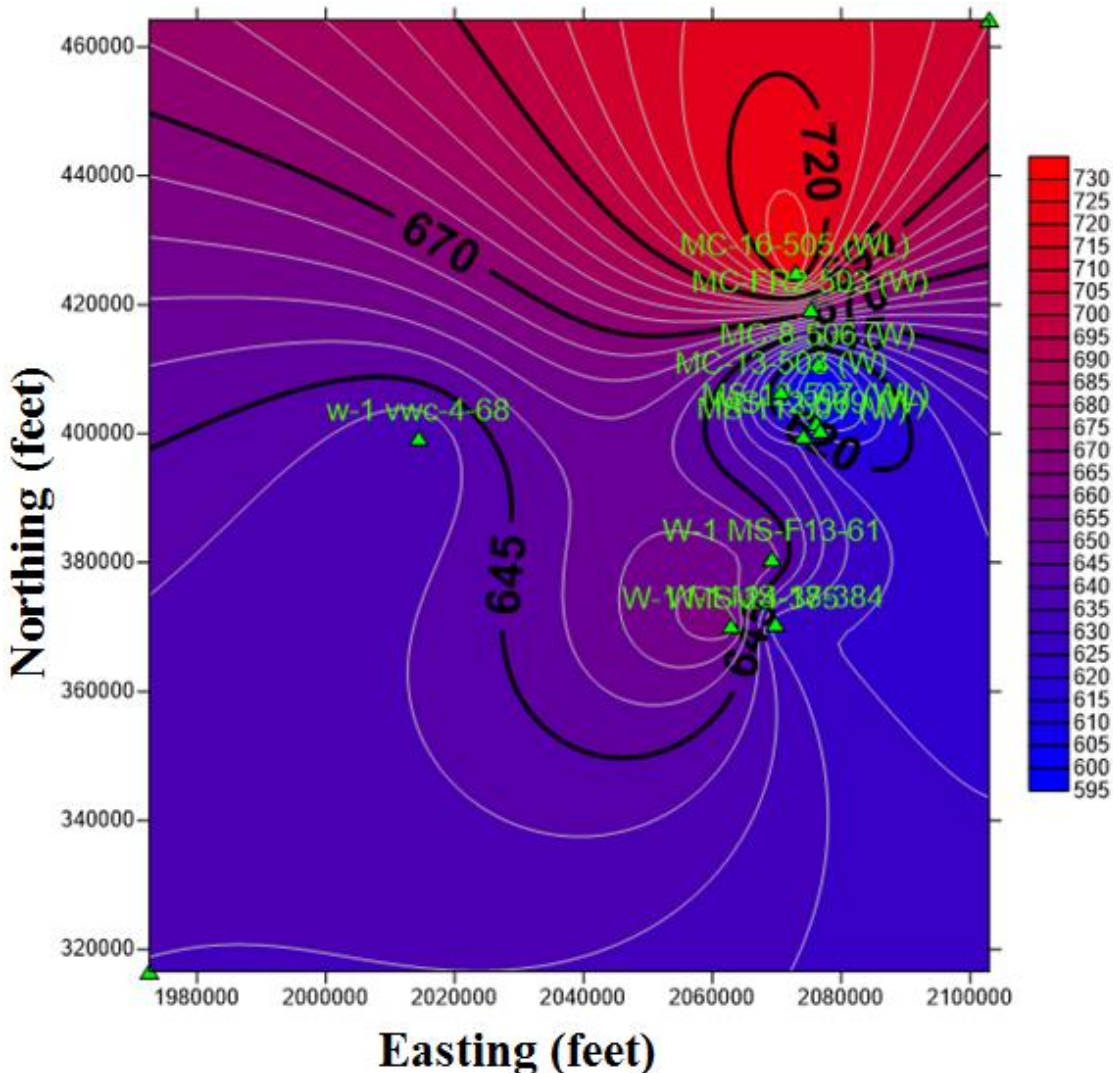
Figures 6.6 Potentiometric head map for aquifer C showing well locations with a contour interval of 5 feet.

6.4. Transient Data Analysis of water elevation recovery in shafts

Increasing heads with time was observed in the data for the head recovery period in Table B.1 in Appendix B. It was suspected that this increase in head could be correlated with precipitation because infiltration and recharge should be a function of precipitation. Figure 6.7 shows a strong positive correlation between accumulated precipitation and pool elevation in the Grange Seal monitoring shaft. This behavior is similar for the data of all the other shafts. Data for precipitation during the period of time

for the monitoring of free water level recovery for this shaft is presented in Table B.1 of

Appendix B. Cross-correlograms of precipitation and water level were done using the

program PAST (Hammer et al., 2001) to determine the lag time of precipitation and water

level. In a cross-correlogram, one variable is shifted in time with respect to the other

variable and the correlation coefficient between the variables is found. A maximum or

minimum in the correlation coefficient represent the lag time between the two variables.

Figure 6.8 shows a maximum in cross correlation coefficient between accumulated

precipitation and pool elevation in the Grange Seal shaft with head responding to

precipitation after 4 months. The other maximum at around 16 months is obviously due

to annual variation. Figure 6.9 shows an overburden thickness of 290 feet. With a lag

time of 4 months and overburden thickness of 290 feet for the Grange Seal shaft a flow

velocity of 2.4 feet/day was calculated. This is an unusually high water flow velocity and

can only be explained by a high hydraulic conductivity in the rocks overlying the coal

mine due to fractures produced by the coal exploitation.
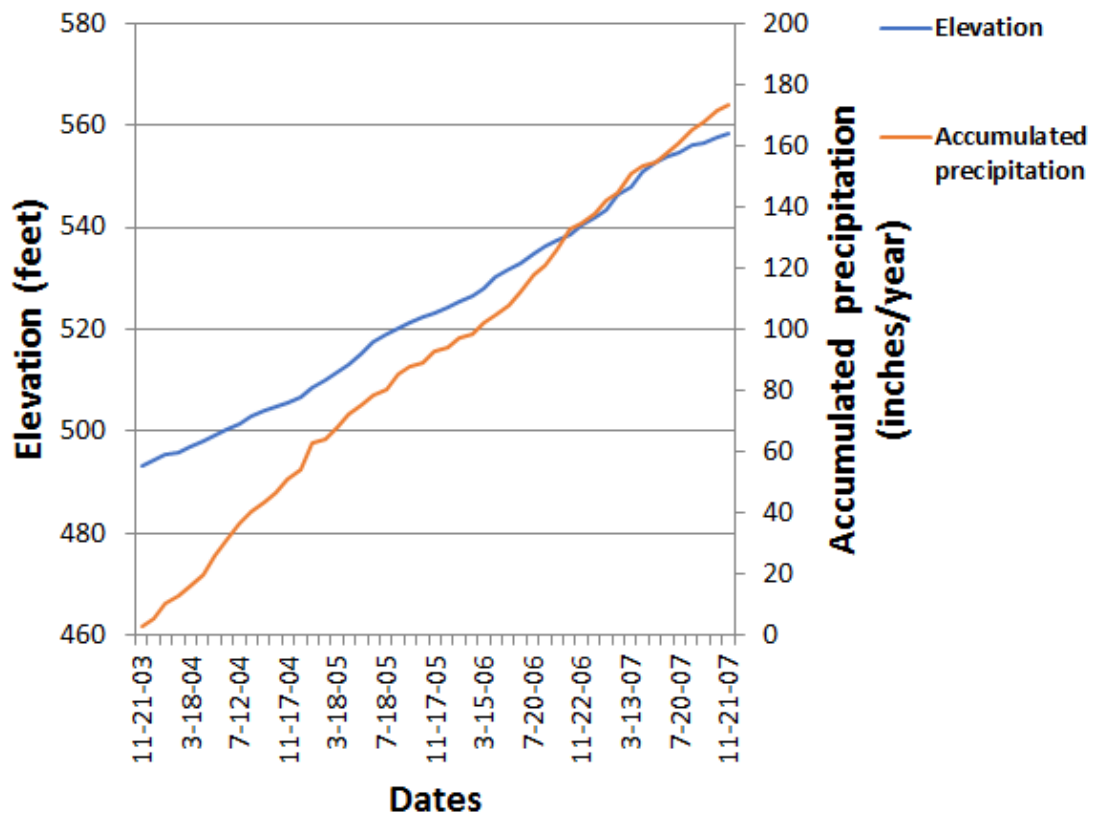
Figure.6.7. Response of post mining water elevation to precipitation in the Grange seal shaft showing a strong positive correlation between the accumulated precipitation and the mine pool elevation.
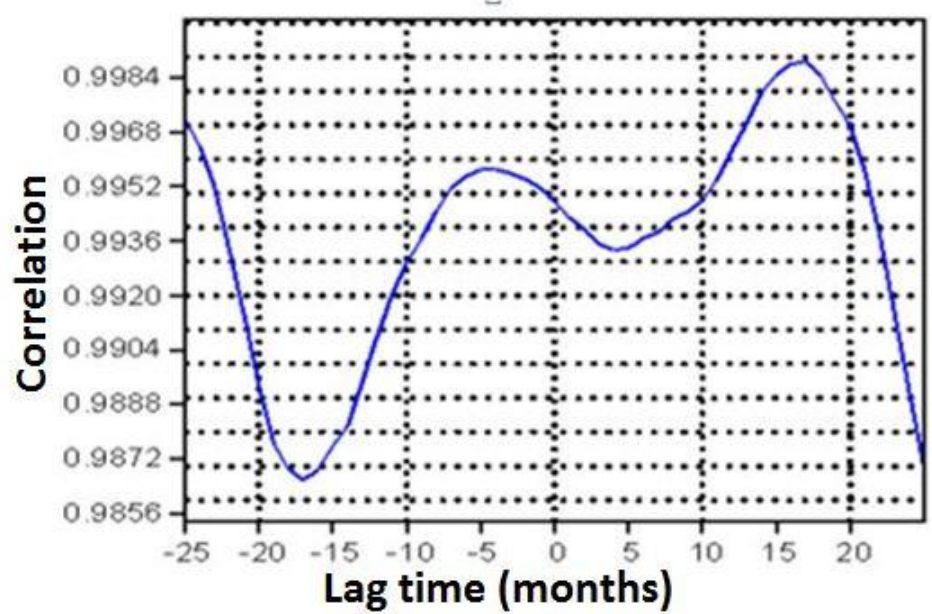
Figure 6.8. Cross correlation between accumulated precipitation and pool elevation elevation in the Grange Seal shaft with head responding to precipitation after 4 months.
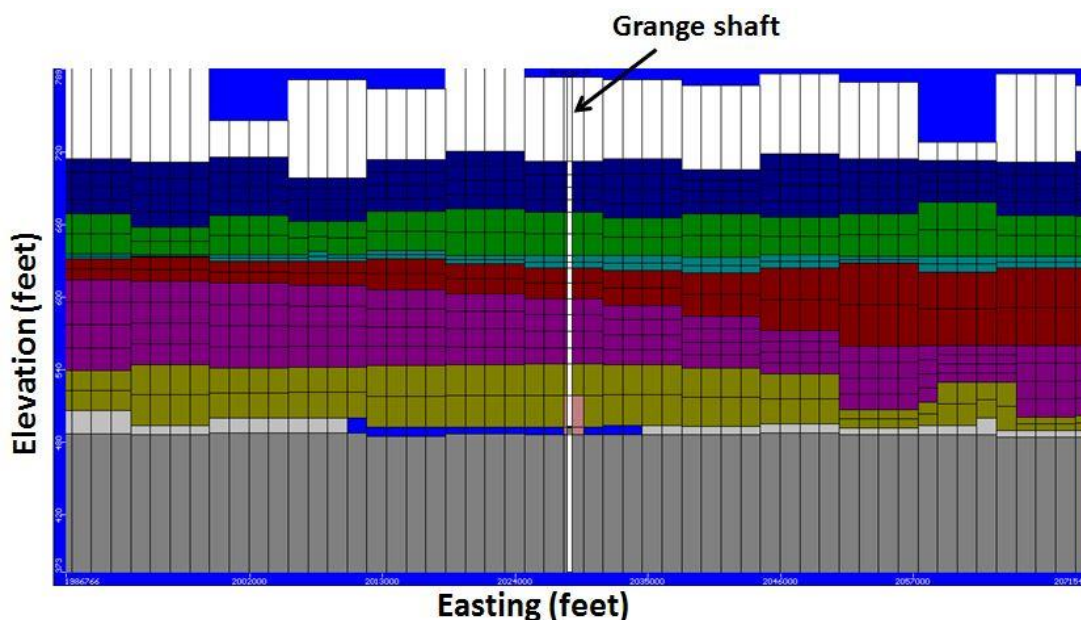
Figure 6.9 Location and overburden thickness of the Grange monitoring shaft. Different colors represent different hydrostratigraphic units in the model.

6.5. Summary of physical model

The transient analysis work of the response of water elevation within the mines to precipitation supports the relative fast movement of water in the lithologies. A flow velocity of 2.4 feet/day is consistent with highly fractured rocks and secondary permeability.

Correlation of the water potentiometric maps for each aquifer was compared with the elevation of the upper contact of the formation hosting the aquifer. For example, Figure 6.3 was correlated with Figure 6.6 and it was observed that the maps seem inversely correlated. Areas of the aquifer that have the higher contact elevation have the lower potentiometric head and the areas with lower contact elevation have higher potentiometric heads. This indicates that groundwater flows toward the southern part of the model (Ohio River) as it is illustrated in Figure 6.10.
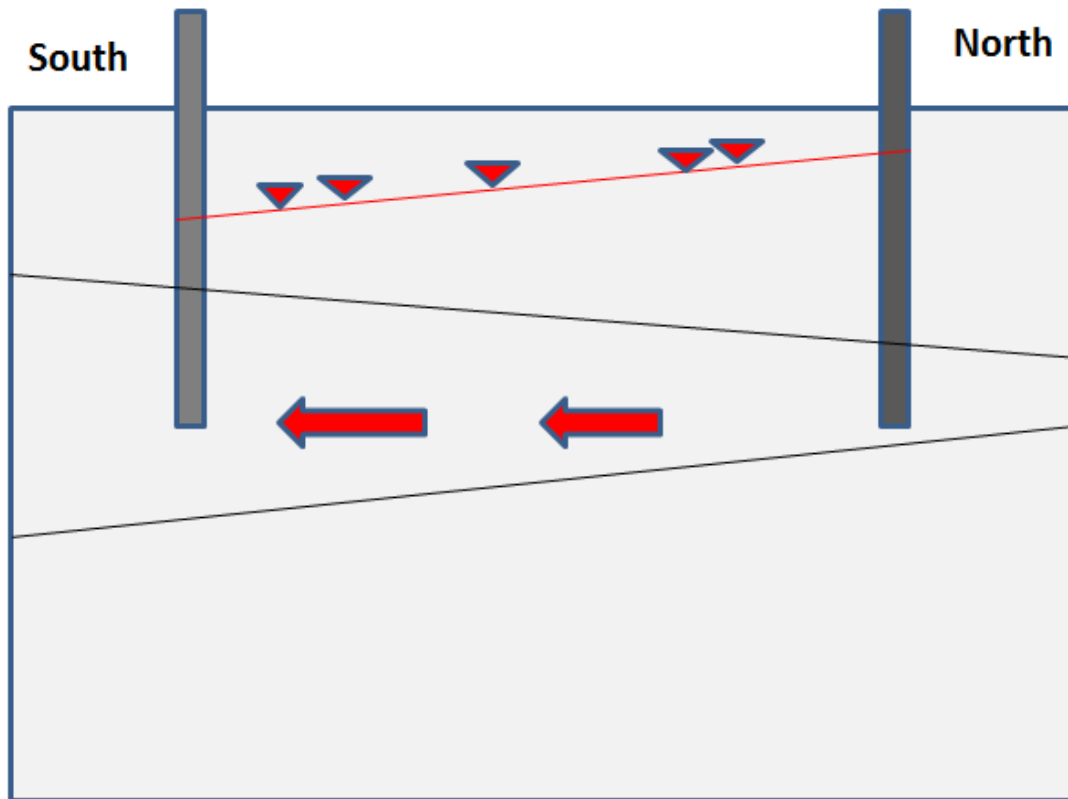
Figure 6.10 Schematic diagram showing the relationships between potentiometric head and lithological contact with groundwater flowing to the Ohio River in the south. The two lines represent the contact between aquifer C and the neighboring rocks.

CHAPTER 7: FLOW MODELING RESULTS

7.1. First Steady State Model

The development of a groundwater flow model begins with the transformation of the physical model dimension into a grid design. MODFLOW was used in creating the model in a steady-state condition. Visual MODFLOW calculates head values for the center of each cell node making up the model grid and the fact that the model is finite difference means that the same head value calculated at the center of the cell is representative of the head value located within the entire cell (Hunt, 1999).

Topographic elevation grid, bottom layer and the eight contacts map of the extracted boreholes were imported into MODFLOW for model building. Elevation grids were imported into the groundwater flow model. The model was the divided into nine strata based on the nine lithological layers and further refined by adding extra layers to each unit. The final groundwater flow model grid system consisted of 80 columns, 79 rows, and 9 layers, which created a total of 6,320 nodal points throughout the model. Figure 7.1 shows the horizontal dimensions of the model grid.

After the model was gridded, the area was activated based on the hydrological boundaries of the surrounding watershed to the mine and boundary conditions such as constant head, no flow, and river boundaries were added to the model. Constant head boundary conditions were assigned to the western and eastern margin of the aquifers of the model in accordance with the head elevations outlined by the potentiometric map in Figure 6.4, Figure 6.5, and Figure 6.6.
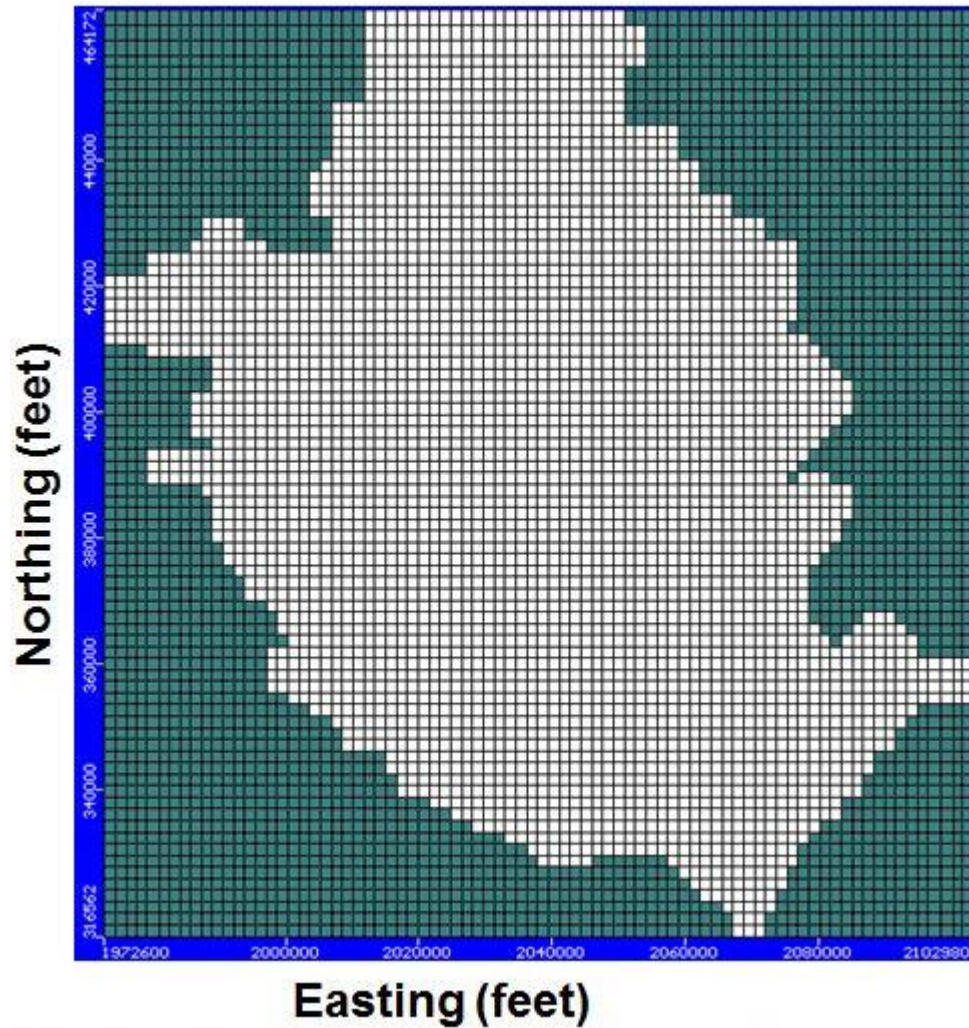
Figure 7.1. Horizontal dimension of the model grid for the Meigs Mine Complex.

Constant head elevation values ranged from 785-725 feet, 720-650 feet, 720-630 feet for aquifer A, aquifer B and aquifer C, respectively. Fig 7.2 shows the constant head boundary conditions for aquifer A. Similar constant head boundary conditions were assigned to aquifer B and C with the values corresponding to the potentiometric maps for each aquifer. The potentiometric map was overlaid on top of the grid to determine the values of the head at each boundary in each aquifer.

Figure 7.2. Constant head boundary conditions (brown cells) for aquifer A.

Six streams were identified in the modeled area causing river boundaries to be added to the groundwater flow model as shown in blue in Figure 7.3. Raccoon Creek, Little Raccoon Creek, Leading Creek, Little Leading Creek, Campaign Creek, and the Ohio River were stimulated within the model through MODFLOW river package. Within the river package individual nodes making up the river boundary were assigned values of the river stage elevation, river bottom elevation, and river conductance.

Figure 7.3. River boundaries (blue cells) of the modeled area.

River stage elevations and river bottom elevations for the streams were taken from www.watersheddata.com and USGS topographic maps. River conductance values were calculated for each cell by multiplying the length and width of each respective cell. River sediment conductance was calculated in units of (ft^2/day). Mcdonald and Harbaug (1998) explain that the MODFLOW river package uses the streambed conductance equation (CRIV) to account for the length (L) and width (W) of the river channel in the cell, the thickness of the riverbed sediments (M) and their hydraulic conductivity (K_r).

Vertical hydraulic conductivity values used for the bottom sediments (K_r) ranges from

(2.83 to 0.0283) ft/day and was taken from (Fetter, 2001). No-flow boundary conditions

were assumed in the groundwater model in accordance with the location of the watershed

boundaries. Areas with no constant head or river boundaries were no-flow boundaries.

$$CRIV = \frac{Kr \, L \, W}{M}$$

Table 7.1. Values used for River Package in MODFLOW.

Stream	Position of Stream	River Stage Elevation (ft)	River Bottom Elevation (ft)	Streambed Thickness (ft)	Conductance of streambed sediment (ft2/day)
Ohio River	Beginning	530	522	8	103662.9
	End	522	514	8	103662.9
Little Raccoon Creek	Beginning	640	638	2	1047.1
	End	638	636	2	1047.1
Leading Creek	Beginning	785	782	3	1396.13
	End	782	779	3	1396.13
Little Leading Creek	Beginning	780	778	2	1047.1
	End	778	776	2	1047.1
Raccoon Creek	Beginning	650	646	4	1963.31
	End	626	622	4	1963.31
Campaign Creek	Beginning	680	677	3	1396.13
	End	677	674	3	1396.13

Values for hydraulic conductivity, porosity, specific yield, and specific storage

values were taken from Freeze and Cherry (1979) for the groundwater flow model prior

to calibration as shown in Table 7.2. Different lithologies were assigned different

hydraulic conductivity values due to the intrinsic properties of the lithologies.

Table 7.2 Input parameters for the model prior to calibration.

Lithology	Hydraulic Conductivity (ft/day)	Porosity	Specific Storage (1/ft)	Specific Yield
Shales	0.00283	0.1	0.00001	0.12
Sandstones	2.83	0.25	0.0001	0.27
Coal	0.0283	0.1	0.00003	0.12

Figure 7.4 shows the cross sections of the lithological layers in the model. Figure 7.5 shows the Meigs Mine Complex extent within the coal layer of the model, the blue area represents Meigs 2 and Meigs 31 whiles the green area represent Raccoon No. 2 (abandoned mine). Figure 7.6 shows the location of the cross sectional views of the model in the N-S and E-W directions as presented in Figure 7.7 and Figure 7.8, respectively.
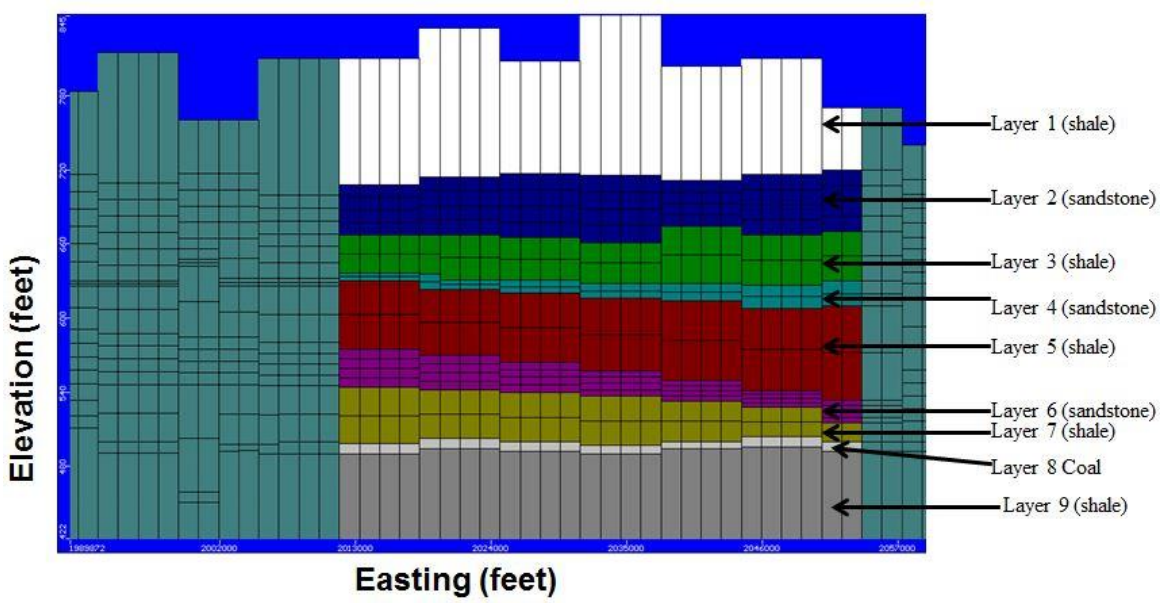
Figure 7.4. Cross section of the lithological layers in the model.
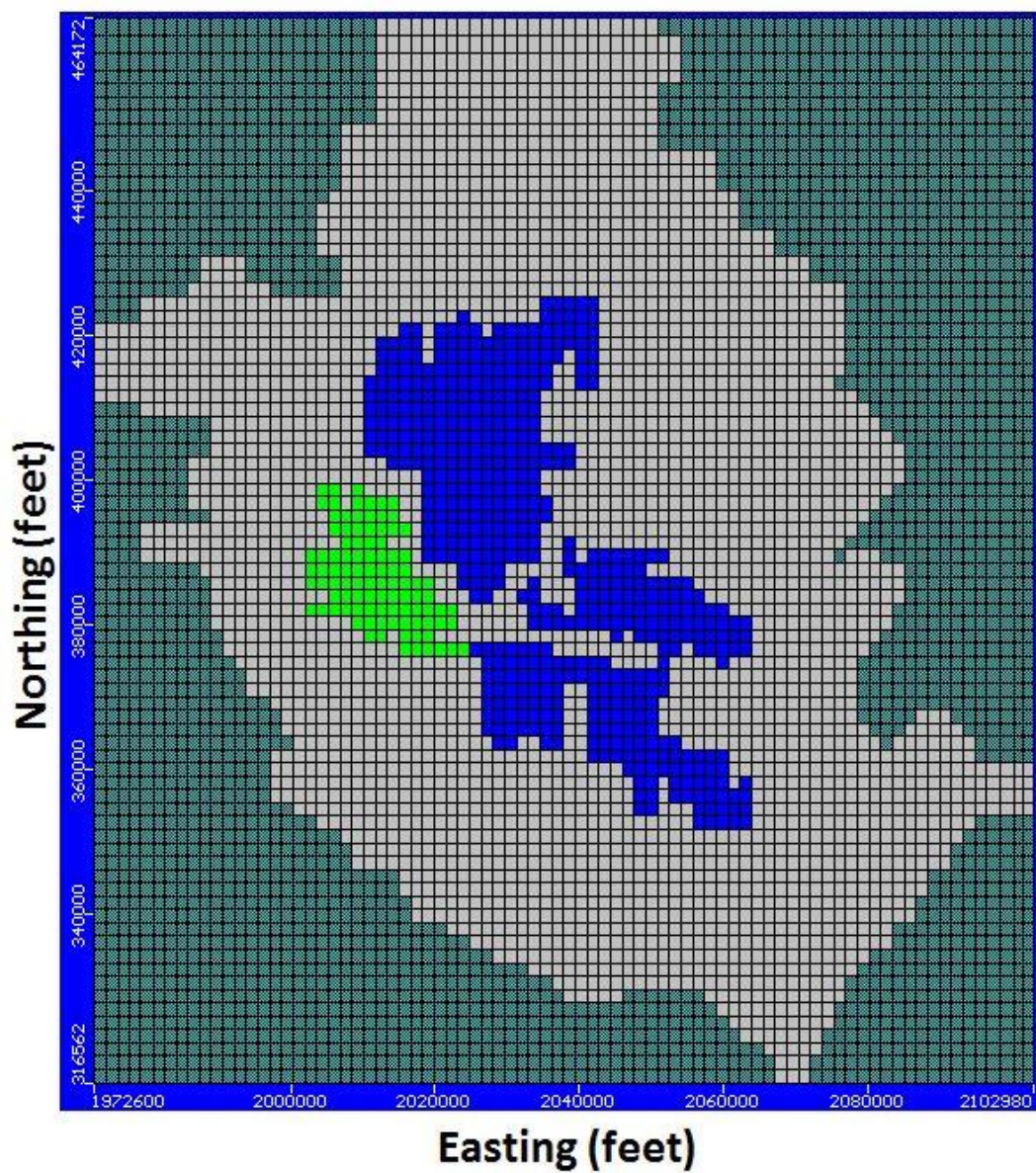
Figure 7.5. Coal layer showing the mine extent of Meigs 2, Meigs 31 (blue) and Raccoon No 2 (green, abandoned mine) in a layer view.
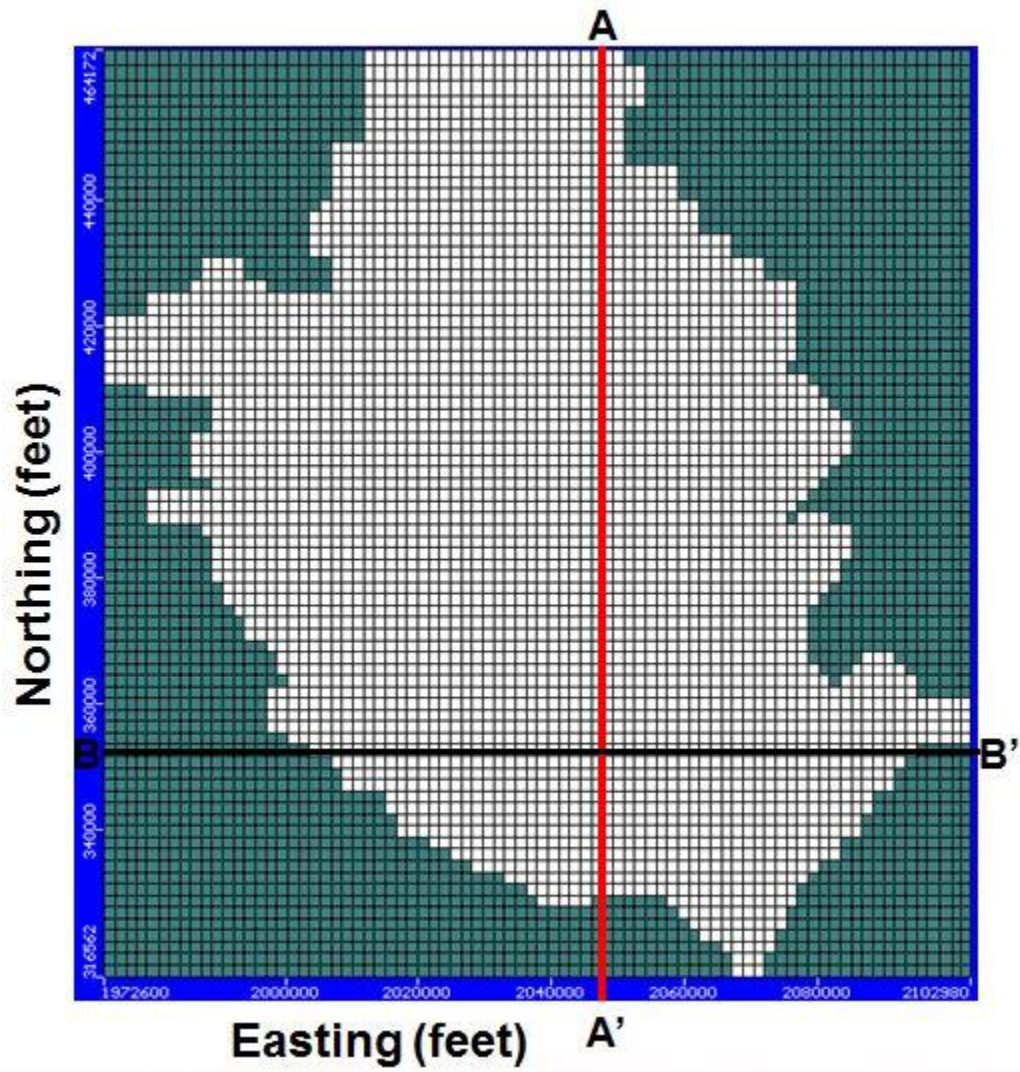
Figure 7.6. Locational view of the model in the N-S (AA') and E-W (BB') directions.
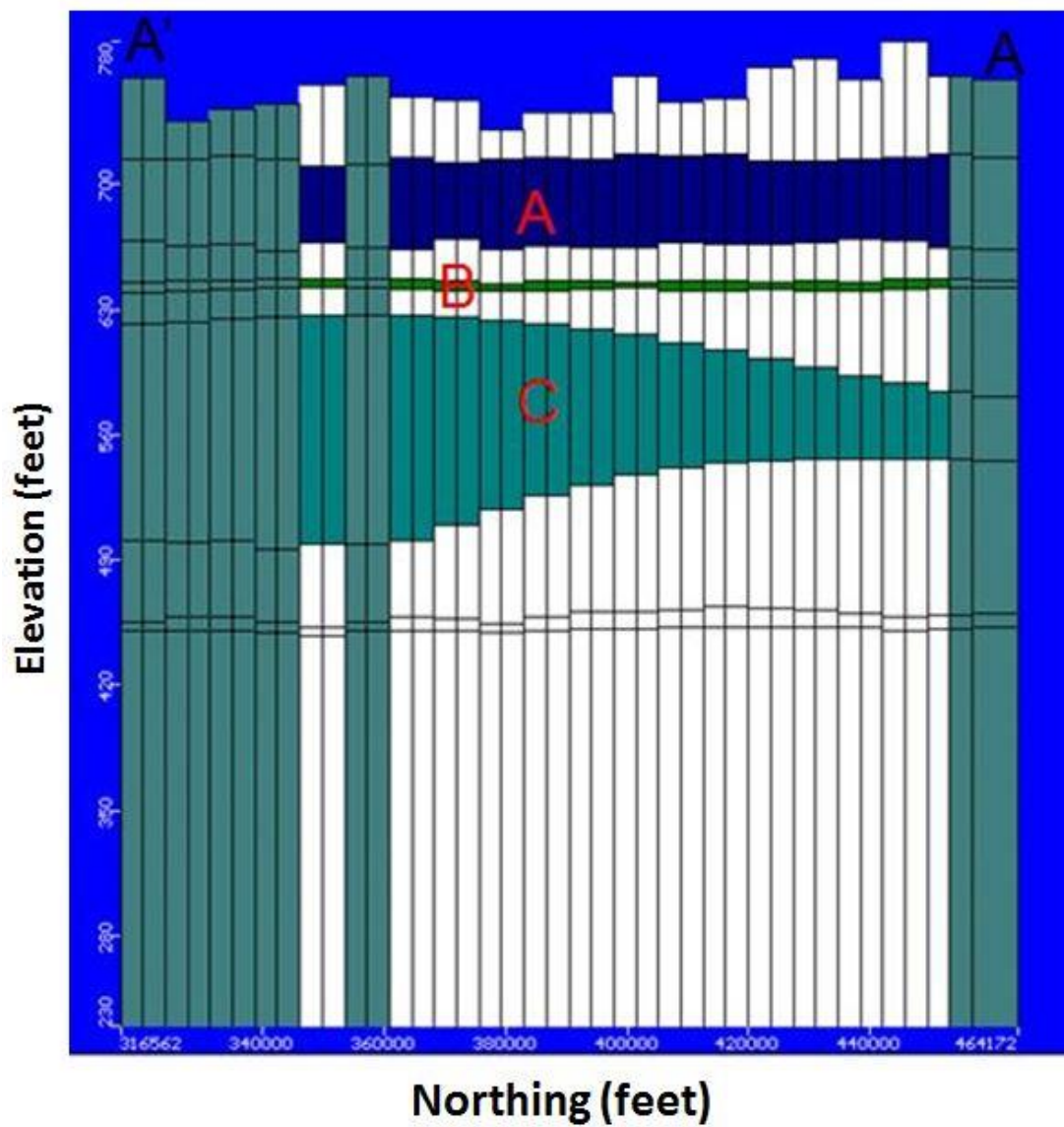
Figure 7.7. Cross sectional area map of the layers showing the aquifers (A, B, and C) in a south-north direction (AA' in Figure 7.6).
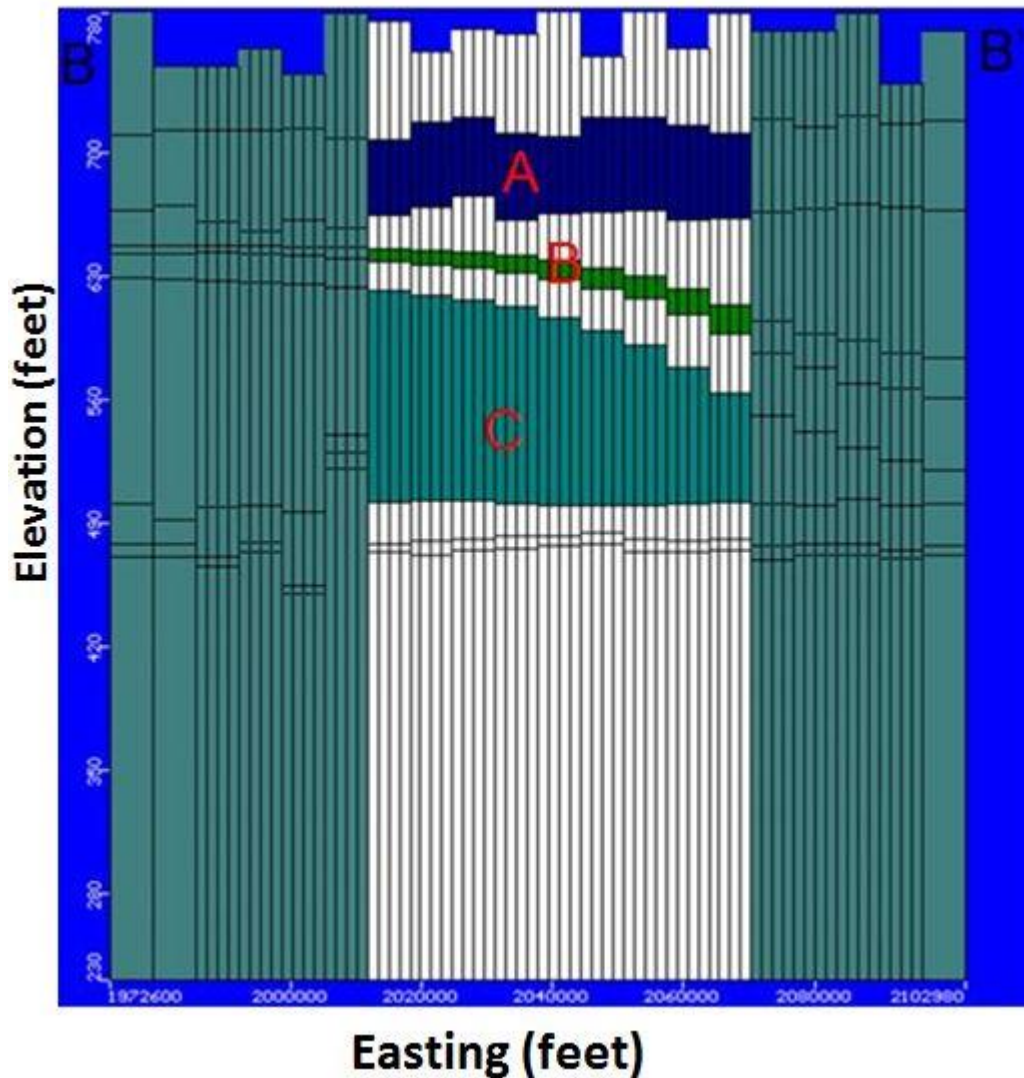
Figure 7.8 Cross sectional area map of the layers showing the aquifers (A, B, and C) in an east-west direction BB' in Figure 7.6.

Figure 7.9 shows the recharge boundary of the modeled area. These boundary conditions were added based on the different soil types and their infiltration rates found in the watershed area as seen in Figure 2.4. The blue area represents Gilpin-Rarden-Aaron soils (Figure 2.4) which are moderately deep and well drained with a moderate permeability (USDA, 1991). The white area represents Upshur-Gilpin soils which are moderately well drained with a low permeability (USDA, 1991). The brown area represents Upshur-Steinsburg-Gilpin soils which are deep, well drained and has low

permeability (USDA, 1991). The green area represents Upshur-Gilpin-Pinegrove soils which are along the Ohio River and have a very rapid permeability and are well-drained and deep soils (USDA, 1991).

The blue and green areas have moderate to high infiltration rates hence a different recharge rate was given to those areas. The white and brown areas had low infiltration rates so low recharges rates were assigned to them. The initial recharge rates assigned to the blue and green areas were 4 inches/year and 5 inches/year, respectively. The initial recharge rate assigned to the white and brown areas were 2.5 inches/year and 2 inches/year, respectively. These recharge values were changed for calibration purposes until the appropriate calibrated heads were reproduced.
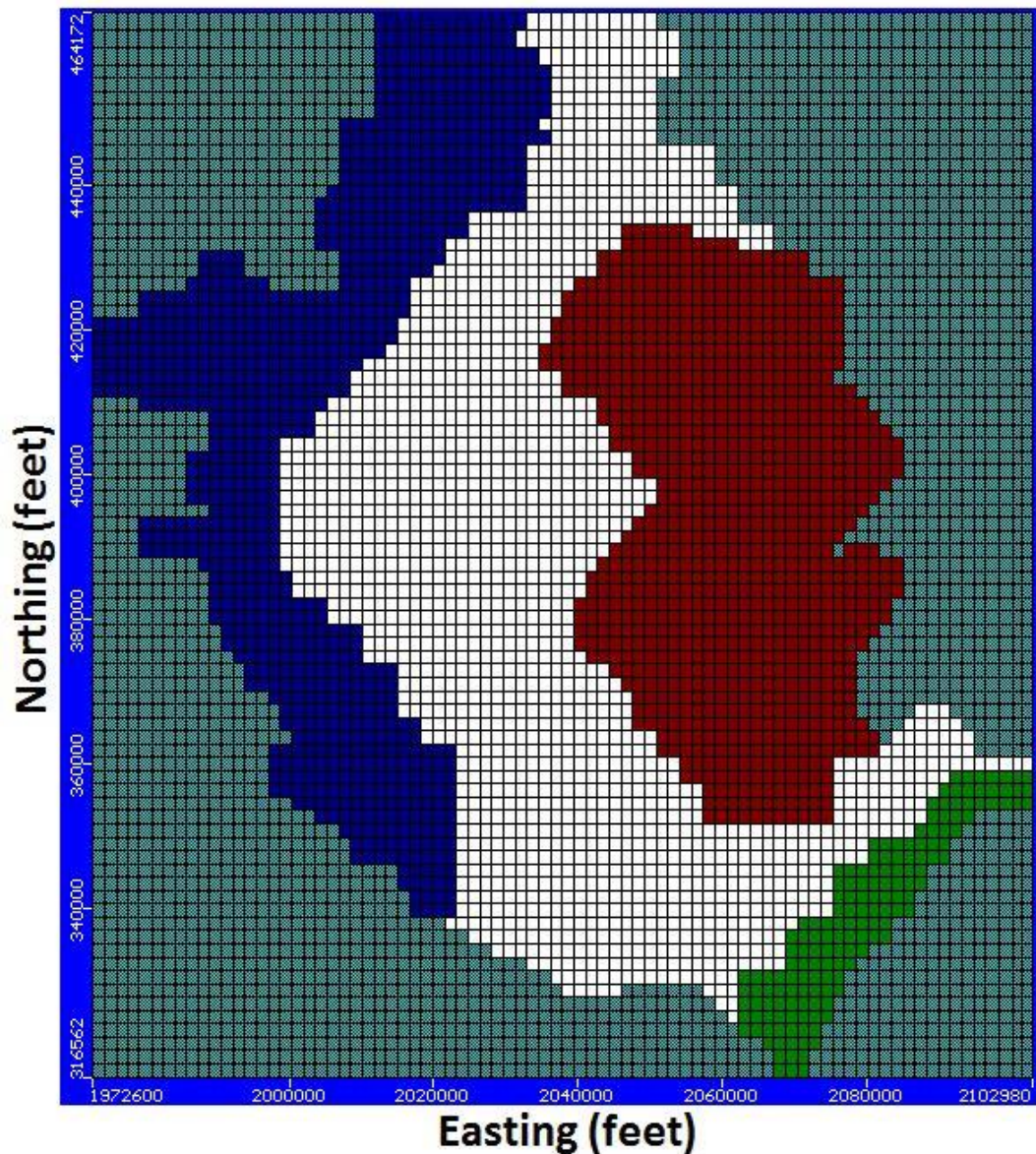
Figure 7.9. Recharge boundaries of the modeled area.

In the first model, the groundwater flow model was numerical simulated assuming a steady-state condition after all the input parameters (hydraulic conductivity, recharge rates, specific yield, specific storage, porosity, etc.) were assigned to the model in MODFLOW. The steady state condition assumes that the model flow conditions are not changing with respect to time. The input parameters were changed until the model converged. The model was then calibrated based on the hydraulic conductivity for the

nine lithological layers and the recharge values for the four recharge areas in the model. The numerical model was calibrated until the lowest error values based on calculated heads and observed heads was obtained.

Initial groundwater modeling simulations determined that the values of porosity, specific yield and specific storage had no effect on the model under steady state conditions. Also, manipulating the river conductance (calibrating for the vertical hydraulic conductivity of the bottom sediments of the streambeds) did not affect the head elevations of the output in MODFLOW; therefore, the river conductance was not calibrated in the model and the initial values were used.

Table 7.3 shows the hydraulic conductivity calibrated values for each lithological layer. Table 7.4 shows the calibrated recharge values for the four recharge areas. Figure 7.10 shows the calculated heads versus the observed heads graph for the steady state simulation given by MODFLOW and the corresponding error values obtained in this calibration.

Table 7.3. Calibrated hydraulic conductivity values for the first steady-state model.

Lithological Units	Hydraulic Conductivity Values (ft/day)		
	Kx	Ky	Kz
Layer 1 (Shale)	1.1	1.1	1.1
Layer 2 (Sandstone)	20	20	20
Layer 3 (Shale)	10	10	10
Layer 4 (Sandstone)	27	27	27
Layer 5 (Shale)	1	1	1
Layer 6 (Sandstone)	60	60	60
Layer 7 (Shale)	12	12	12
Layer 8 (Coal)	0.1	0.1	0.1
Layer 9 (Shale)	22	22	22

Table 7.4. Calibrated recharge values for the steady-state model.

Property	Color	Recharge (Inches/year)
R1		1.2
R2		1.3
R3		1.4
R4		1.2
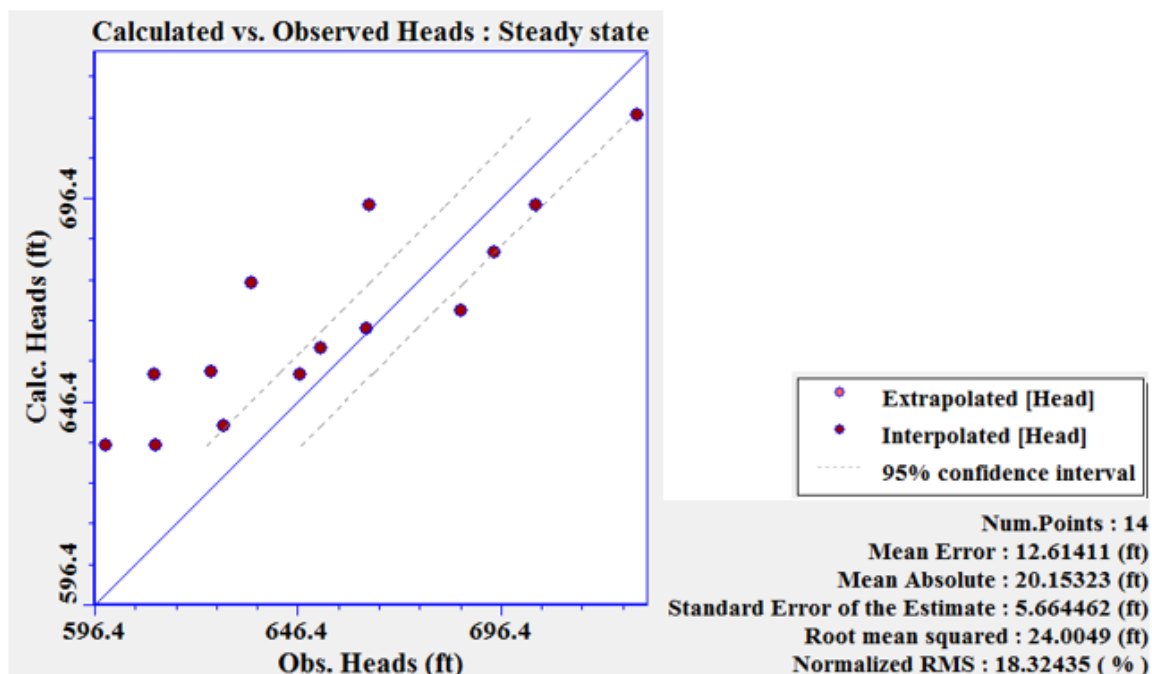
Figure 7.10. First steady state model. Graph showing the calculated heads versus the observed heads for the steady state simulation. Obtained errors are high because pumping of water was not simulated during the first steady state modeling.

Lithological units in the model have very high hydraulic conductivities, higher than those expected for the sandstones, shales, and coals. These results are consistent with highly fractured rocks and secondary permeability due to the exploitation of the coal. A network of fractures that rapidly transport groundwater could probably be present even when the matrix rocks have low permeabilities. The obtained errors are high as well as the hydraulic conductivities. One possible reason for this situation is the fact that in 1996 the mine was in exploitation and some pumping of water should have taken place. The fact that water pumping was not simulated probably produces inaccurate flow rates due to additional negative pressure applied by the pumping process. The hydraulic conductivities obtained in these simulations are not the final values for the post-mining period but they reflect the fact that water can flow at higher rates due to pumping and the additional fractures generated by the mining exploitation.

Figure 7.11, Figure 7.12 and Figure 7.13 show the output of the calibrated steady state model. Figure 7.11 presents the shallowest aquifer (aquifer A), Figure 6.12 presents aquifer B and Figure 6.13 presents the deepest aquifer (aquifer C). The contour intervals for the three Figures are 20 ft. The olive colored areas within the model constitute areas of unsaturation whiles the white colored areas constitute areas of saturation. Observation wells are represented with the white and green squares within the model.

Figures 7.11, 7.12 and 7.13 have the same flow pattern. Groundwater flows towards the Raccoon Creek, Little Raccoon Creek, Leading Creek, and Little Leading Creek. Groundwater diverges from the Ohio River feeding water to the groundwater system, and to the other three modeled rivers.
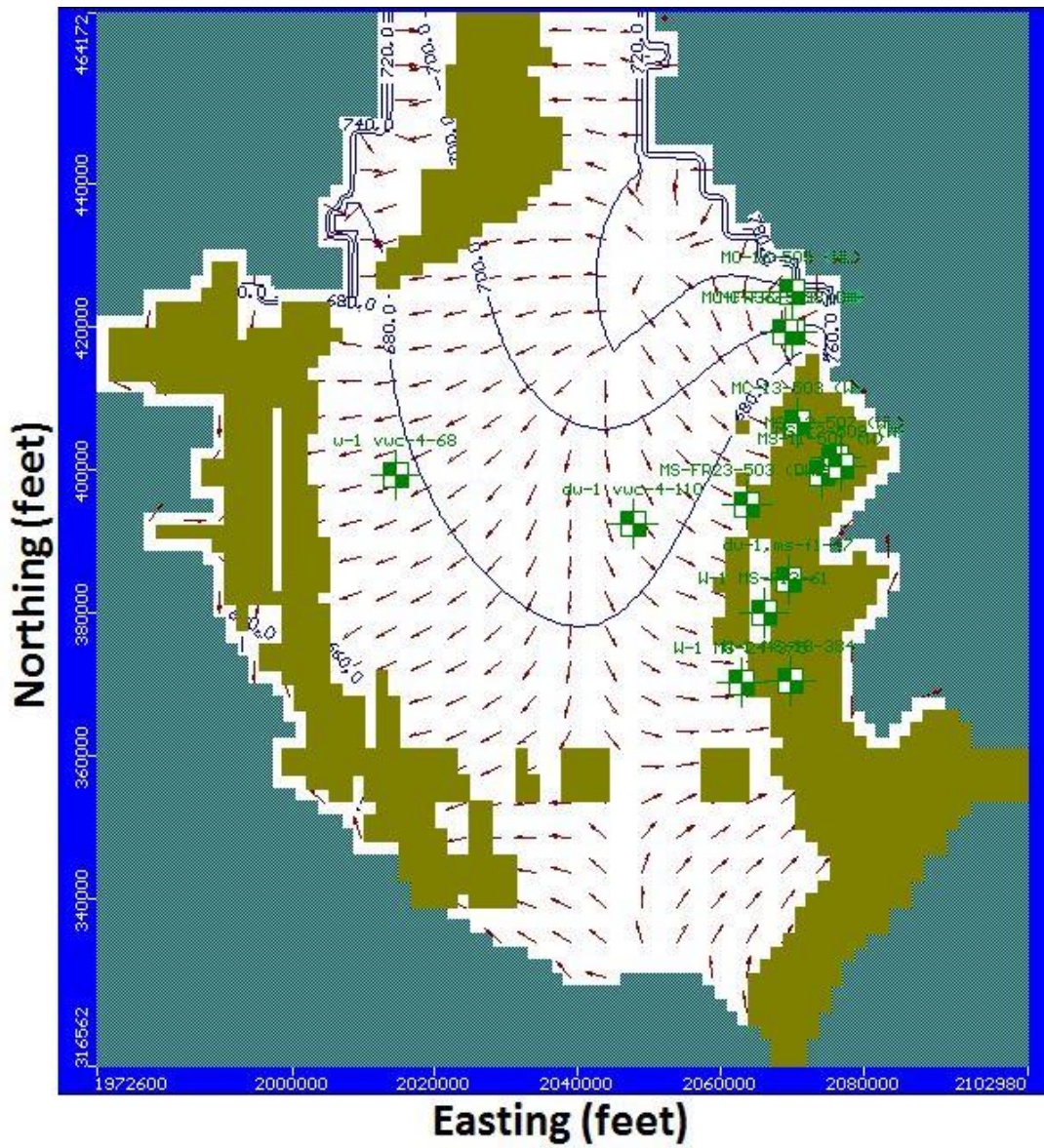
Figure 7.11. First steady state model. Aquifer A water table elevation showing equipotential contours at an interval of 20ft. Olive areas constitute areas of unsaturation whiles white areas constitute areas of saturation. Observation wells are represented with the white and green squares within the model.
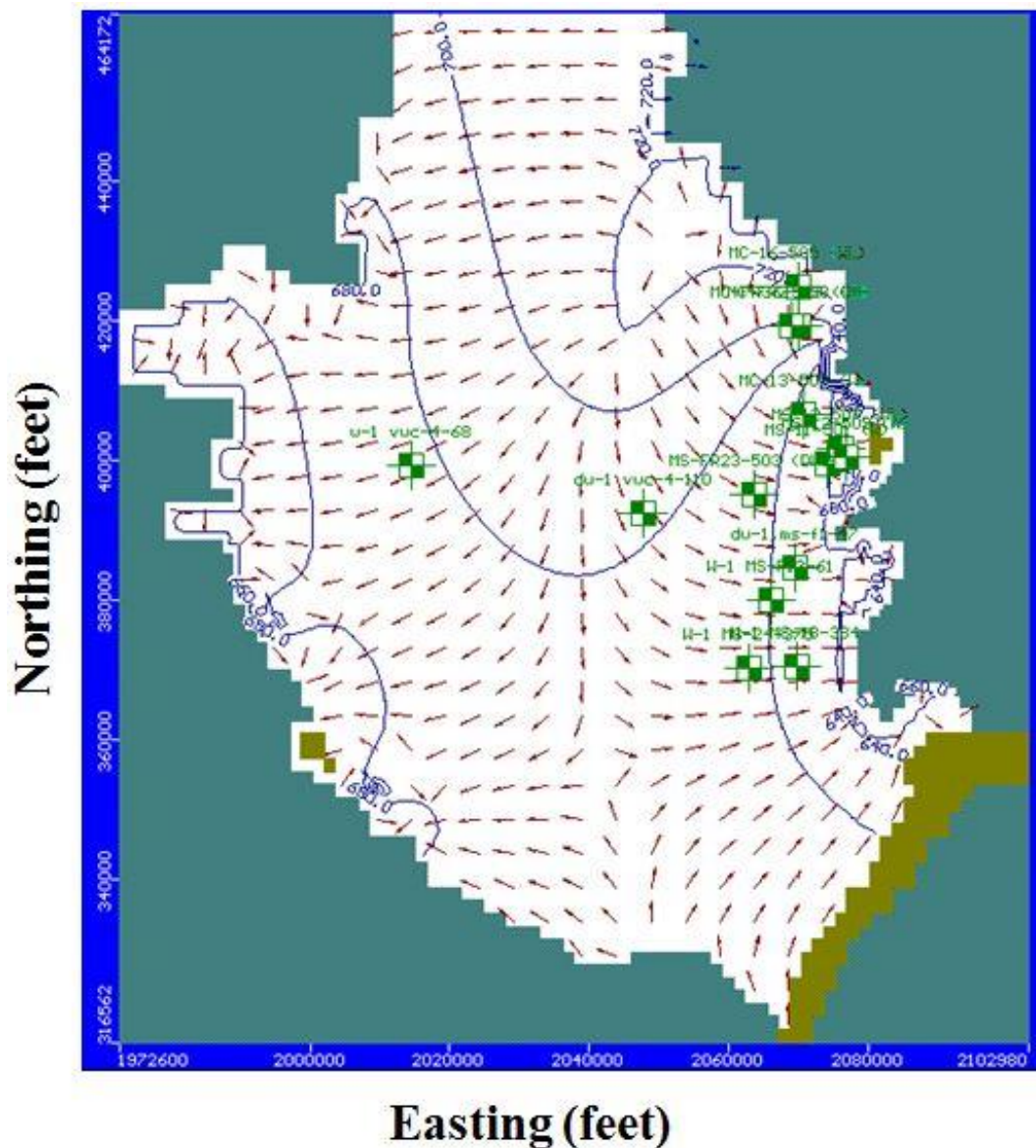
Figure 7.12. First steady state model. Aquifer B water table elevation showing equipotential contours at intervals of 20ft. Olive areas constitute areas of unsaturation whiles white areas constitute areas of saturation. Observation wells are represented with the white and green squares within the model.

Figure 7.13. First steady state model. Aquifer C water table elevation showing equipotential contours at intervals of 20ft. white areas constitutes areas of saturation. Observation wells are represented with the white and green squares within the model.

A sensitivity analysis was conducted on the calibrated groundwater flow model input parameters of recharge, hydraulic conductivity of the shales and hydraulic conductivity of the sandstones.

According to Zheng and Bennett (1995) a sensitivity analysis following optimum model calibration is important to quantify the sensitivity of the model results with respect to model input parameters. According to Anderson and Woessner (2002) a sensitivity

analysis determines how sensitive a model is when a certain parameter is changed while all other parameters remain constant. Zheng and Bennett (1995) also explain that a parameter found to be highly sensitive to the changes of the model input parameters should be given less confidence in final modeling predictions than those input parameters that shows little to no sensitivity towards changes in modeling conditions.

The calibrated input parameters of the recharges (R1, R2, R3, and R4), hydraulic conductivity of shale layers, and hydraulic conductivity of the sandstones were each evaluated separately. The evaluation of each input parameter was conducted by holding all other input parameters at constant calibrated values and altering the value under investigation in increments. The percentage change in the hydraulic conductivity $(calibrated\ hydraulic\ conductivity - altered\ hydraulic\ conductivity)/$ $(calibrated\ hydraulic\ conductivity)$ was then plotted on the x- axis with the associated mean error plotted on the y-axis for a graphical representation of the sensitivity. Values for the parameters are presented in Appendix C.

Figure 7.14 shows hydraulic conductivity sensitivity analysis for the shales in the model. Shale1 and shale 3 were very less sensitive to a decrease and increase in the hydraulic conductivity of the model. Shale 2 was very sensitive to an initial decrease in the hydraulic conductivity of the model and was sensitive as well to an increase in the hydraulic conductivity of the model. An initial decrease in hydraulic conductivity of shale 4 had a lower effect, but became very sensitive to the model when the hydraulic conductivity was increased. Shale 5 was very sensitive to both an increase and decrease in the hydraulic conductivity of the model. Shale 4 and 5 are the closest to the mined coal. Values for the parameters are presented in Appendix C.
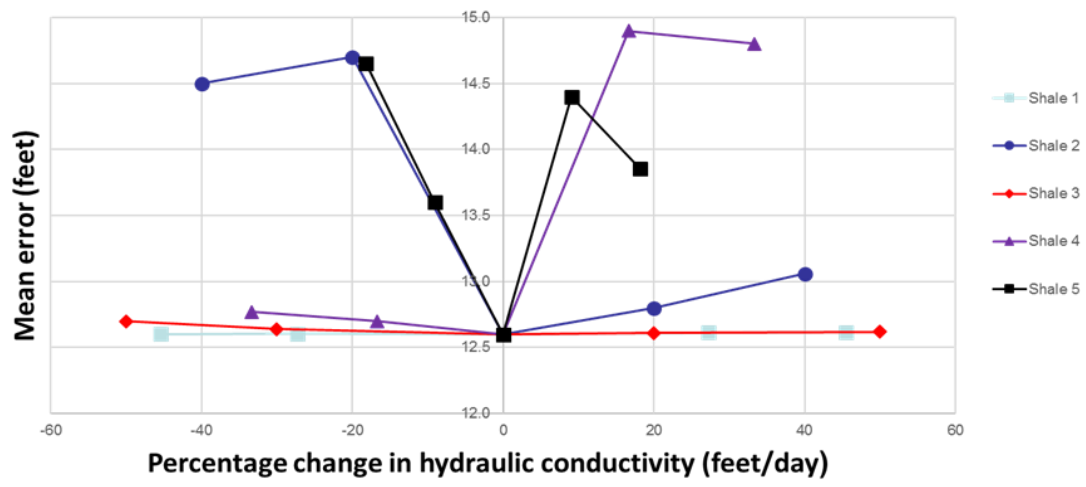
Figure 7.14. First steady state model. Hydraulic conductivity sensitivity analysis. Note that the shales closer to the exploited coal are the most sensitive.

For the hydraulic conductivity in the three aquifers, the model was very sensitive to a decrease in the hydraulic conductivity of aquifer A and aquifer B and slightly sensitive to an increase in their hydraulic conductivity. Aquifer C was very sensitive to the model for an increase in the hydraulic conductivity and less sensitive for a decrease in the hydraulic conductivity.
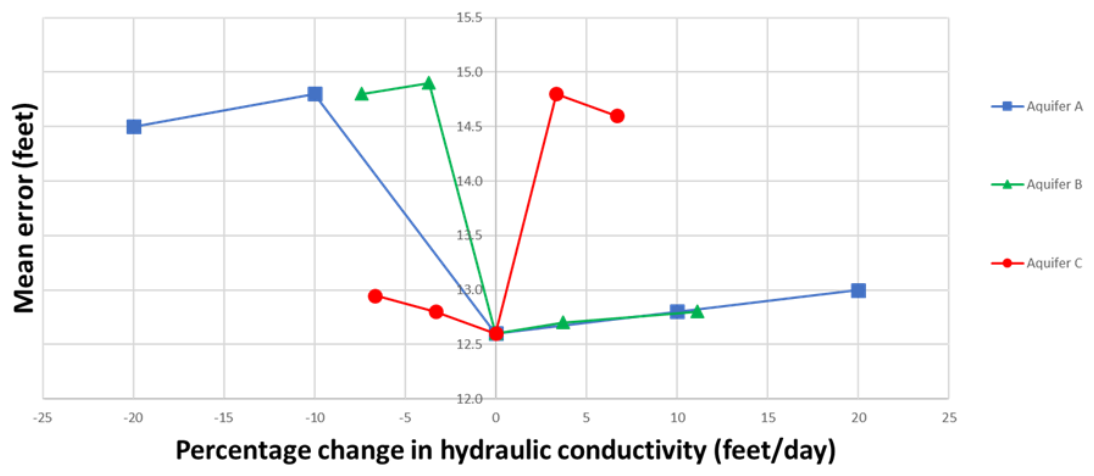
Figure 7.15. First steady state model. Hydraulic conductivity sensitivity analysis for sandstones in the model.

Figure 7.16 shows the hydraulic conductivity sensitivity analysis for coal in the model. The model was very sensitive to both an increase and decrease in the hydraulic conductivity of the coal. Figure 7.17 shows the sensitivity analysis of the recharge values for the four areas. The model was very sensitive to both increase and decrease in R1 and R4 (low recharges) and more sensitive to a decrease in R2 and R4 (high recharges). The model was less sensitive to an increase in R2 and R4.
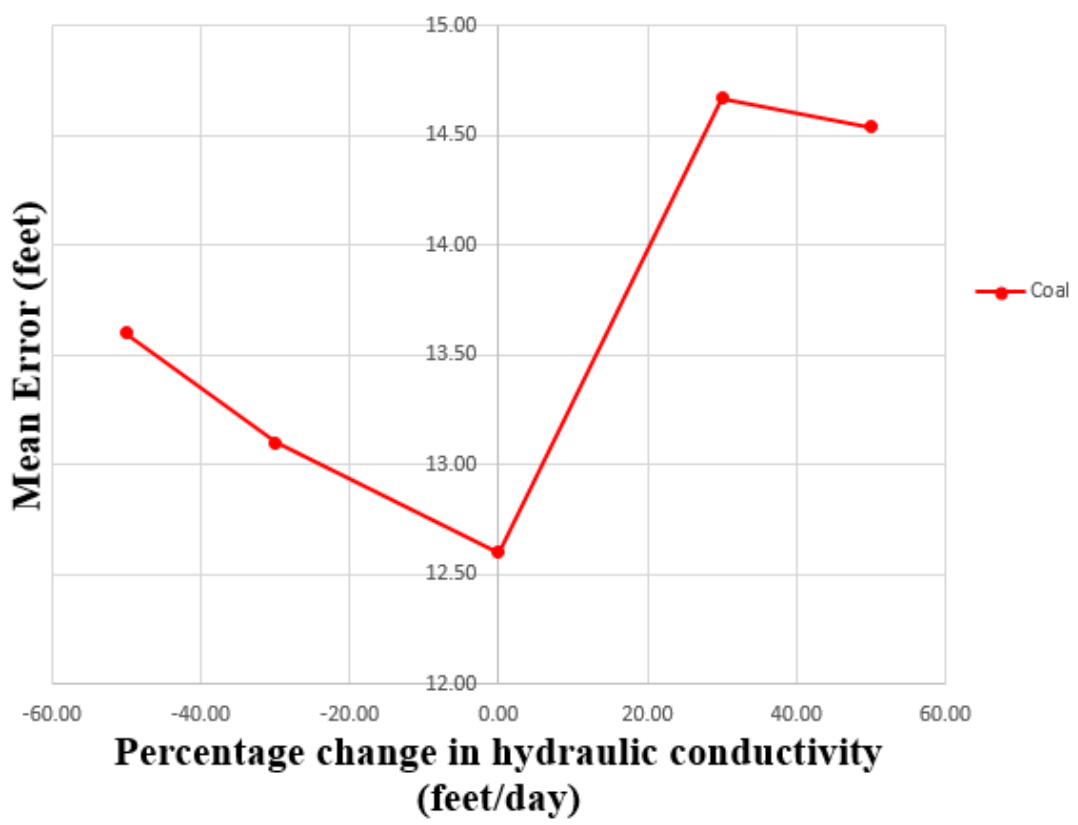
Figure 7.16. Sensitivity analysis for the hydraulic conductivity of coal in the first steady state model. The model was sensitive to an increase and decrease in the hydraulic conductivity of the coal.
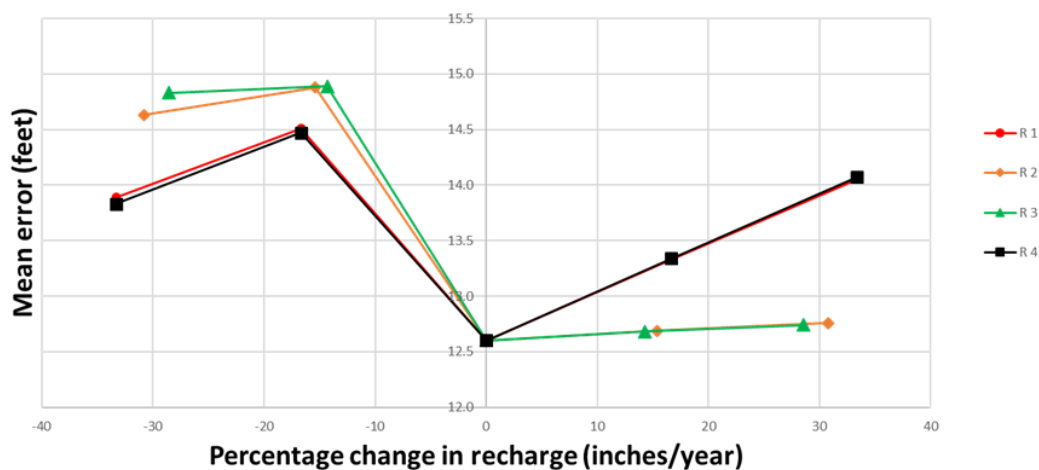
Figure 7.17 First steady state models. Sensitivity analysis of the recharge values for the four areas.

7.2 Second steady state model

Six monitoring shafts distributed within the Meigs Complex were included in the groundwater flow model as pumping and observation wells because of their possible influence on the flow regime of the model. Information about where the miners were pumping when the mine was active was not available. For that reason, it was decided to simulate pumping in each shaft until we could replicate the observed heads in the shaft in January 2004. Data for water levels in the shafts is presented in Appendix B. Table 7.5 shows the parameters of the monitoring shafts based on the variables determined from the Meigs Mine Complex map and post-mining water data. According to (Borch, 2008) the Meigs Mine Complex was pumping at a rate of 5000 gpm after January 2008 when the water levels stabilized and were not rising. Based on an initial pumping rate of 5000 gpm and the parameters of the pumping and observation wells the model was calibrated at steady-state conditions. Pumping and observation wells were simulated at each shaft location. The steady-state model was calibrated changing the pumping rate in each shaft

until the lowest error values based on calculated heads and observed heads was obtained.

Table 7.6 shows the modeled pumping rates to reproduce the water level in the shafts in

January 2004. The parameters of the calibration of the first steady state model were the

same in these simulations.

Figure 7.19 (Aquifer A) and Figure 7.20 (Aquifer B) shows large areas of

unsaturation with groundwater flow towards the pumping wells suggesting that shallower

wells probably became dry. In comparison, Figure 7.21 (deepest aquifer) shows large

areas of saturation with flow towards the pumping wells.

Table 7.5. Parameters of the monitoring shafts for the second steady state model.

			Pumping		Observation	
Monitoring Shafts	X-coordinates (feet)	Y-coordinates (feet)	Screen top elevation (feet)	Screen bottom elevation (feet)	Observation point elevation (feet)	Observation head (feet)
Dansville	2035488	370619	486	361.23	381.23	381.23
NE	2037086	424317	495	449.86	469.86	469.86
Roving crew	2045389	384639	491	353.9	373.9	373.9
NW	2023889	422599	494	488	512.17	512.17
Grange seal	2028487	410648	494	488	495.4	495.4
South bleeder	2024516	383718	486	480	495.5	495.5
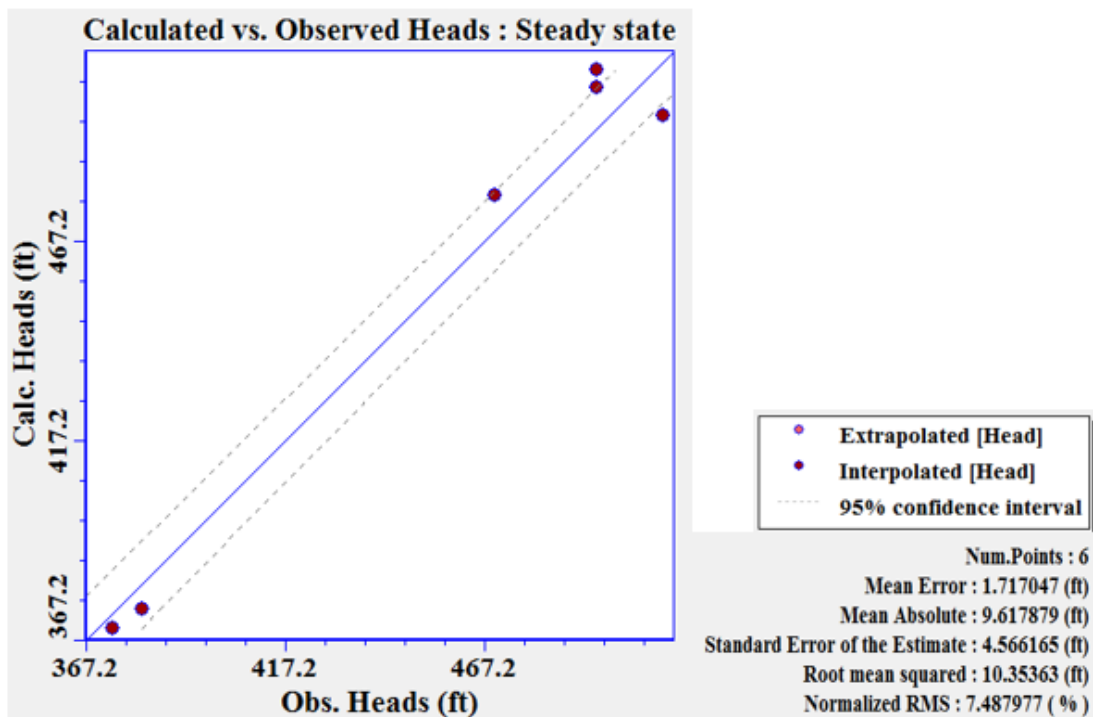
Figure 7.18. Second steady state model. Graph showing the calculated heads versus the observed heads for the second steady state calibrated model. This model was calibrated by changing the pumping rates in each shaft until the lowest errors values were observed.

Figure 7.19. Second steady state model. Aquifer A showing equipotential head contours at an interval of 20ft. Olive areas constitute areas of unsaturation whiles white areas constitute areas of saturation. Observation wells are represented with the white and green squares within the model.
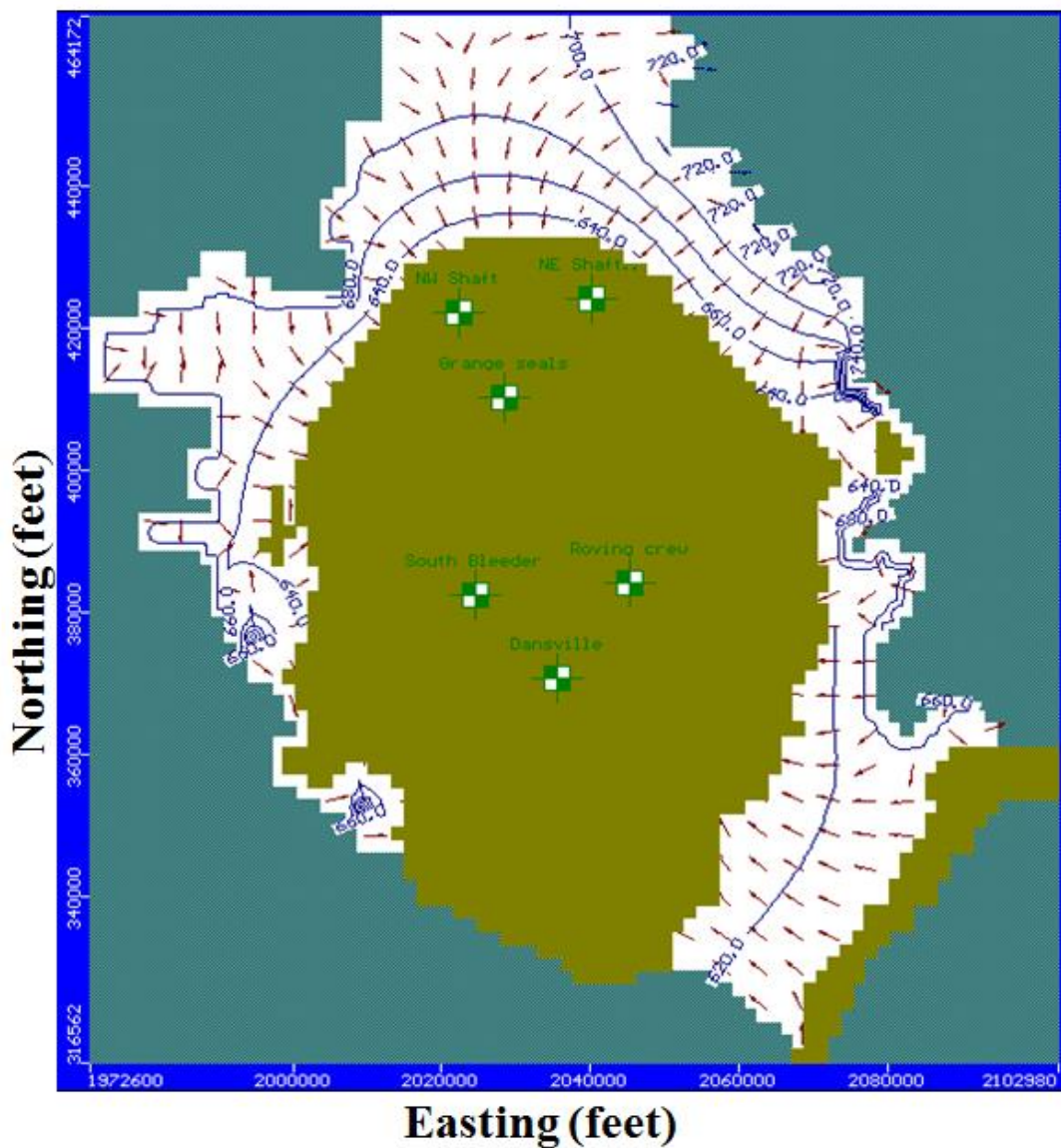
Figure 7.20. Second steady state model. Aquifer B flow regime showing equipotential head contours at interval of 20ft. Olive areas constitute areas of unsaturation whiles white areas constitute areas of saturation. Observation wells are represented with the white and green squares within the model.
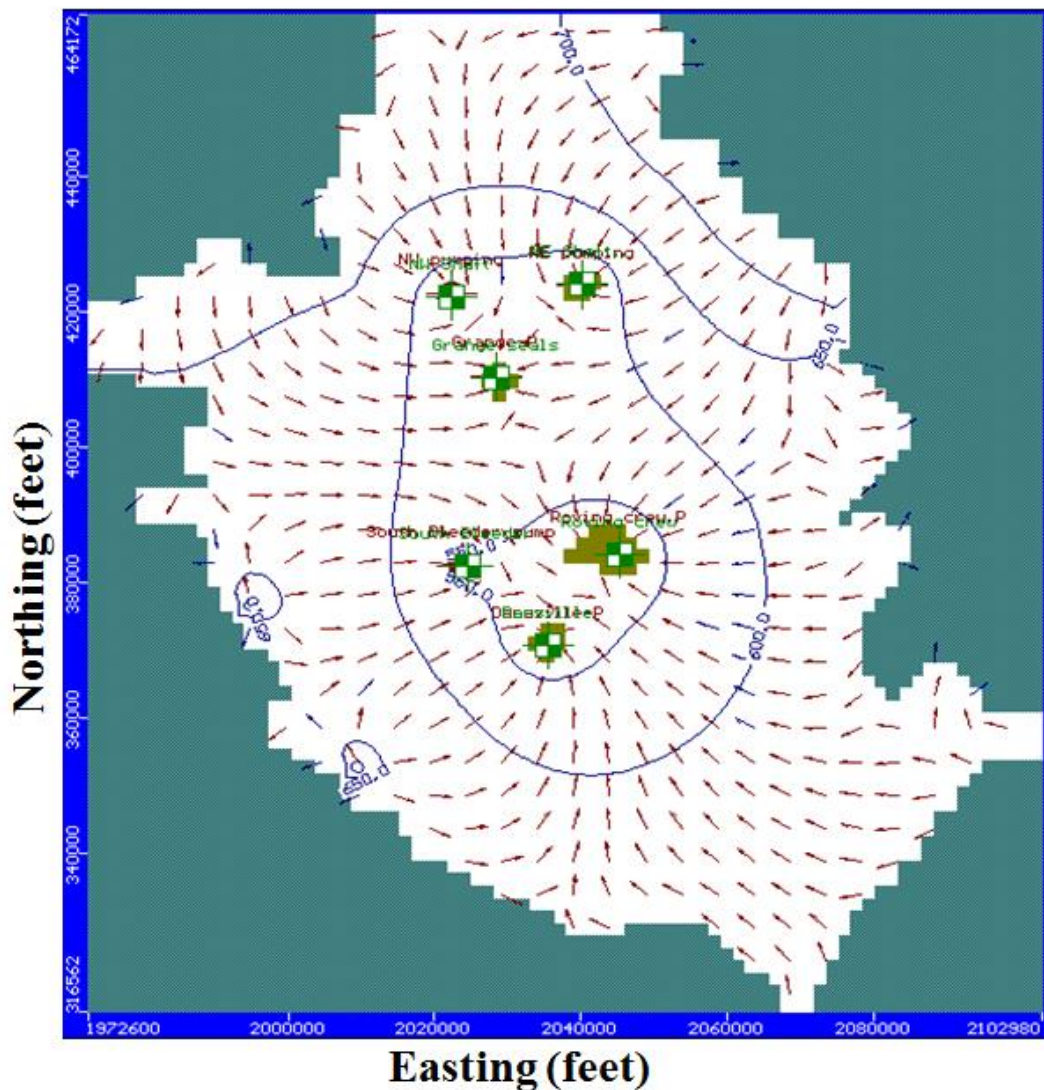
Figure 7.21. Second steady state model. Aquifer C flow regime showing equipotential head contour intervals of 20ft. Olive areas constitute areas of unsaturation whiles white areas constitute areas of saturation. Observation wells are represented with the white and green squares within the model. Groundwater flow was towards the wells due to the pumping.

Table 7.6 Pumping rate of the calibrated model second steady state model

Monitoring Shafts	X-coordinates (feet)	Y- coordinates (feet)	Pumping rates (gpm)
Dansville	2035488	370619	10,000
NE	2037086	424317	10,000
Roving crew	2045389	384639	9500
NW	2023889	422599	7000
Grange seal	2028487	410648	4500
South bleeder	2024516	383718	4200

7.3. Transient State Model

Transient simulations were conducted to establish the changes in groundwater flow conditions throughout the modeled area with respect to time, and to calibrate hydrogeological parameter during the recovery period of the Meigs Mine Complex. Those conditions are our interest because they should reflect what happens to these properties after mining. Variables such as hydraulic conductivity, specific yield, specific storage, and recharge were calibrated for transient simulation. The initial conditions for the model were the conditions of the calibrated second steady state model. Initial hydraulic conductivity parameters for the nine layers were taken from Table 7.3. Initial recharge values for the four areas were taken from Table 7.4. Initial specific storage, initial specific yield and porosity values were taken from table 7.2. The transient model was simulated for 1470 days starting in January 2008. Values for the hydraulic heads at every shaft were taken from Table B.1, B.2, B.3, B.4, B.5 and B.6 in Appendix B. Observation wells were simulated in each shaft. The hydraulic conductivities, specific yield, and specific storage for each layer, as well as the recharge values were changed one at a time until the error between the observed and the simulated heads was minimized. However, it was not possible to calibrate the model without doing some changes. It was thought that part of the shale overlying the exploited coal could have

fractured and be different from the rest of the shale layer 4. For that reason the model was altered as it can be seen in Figure 7.22 and Figure 7.23. Shale 4 was divided into shale 4A and 4B representing the region directly above the mine and the rest of the shale layer in the model. Adding this new complexity made the calibration of the model possible. The bottom coal layer was probably fractured but the value of the hydraulic conductivity was already high in the steady state models and we only have to calibrate the whole layer again in the transient model to obtain calibration.

Table 7.7, Table 7.8, Table 7.9 and Table 7.10 shows the calibration values for the different strata. Figure 7.24 shows the calculated heads versus the observed heads graph for the transient simulation given by MODFLOW and the corresponding error values obtained in the calibrated simulation. Note that the NW shaft is an outlier since the transient values of the simulated heads get farther from the line of equal simulated vs observed head, as time progresses. For that reason, the same simulation was repeated without the NW shaft and the error was dramatically improved (Figure 7.25). Figures 7.26, 7.27, and 7.28 show the flow regime in the three aquifers for the transient simulations. Groundwater flow is directed towards the mine void to illustrate that the water is filling the void.
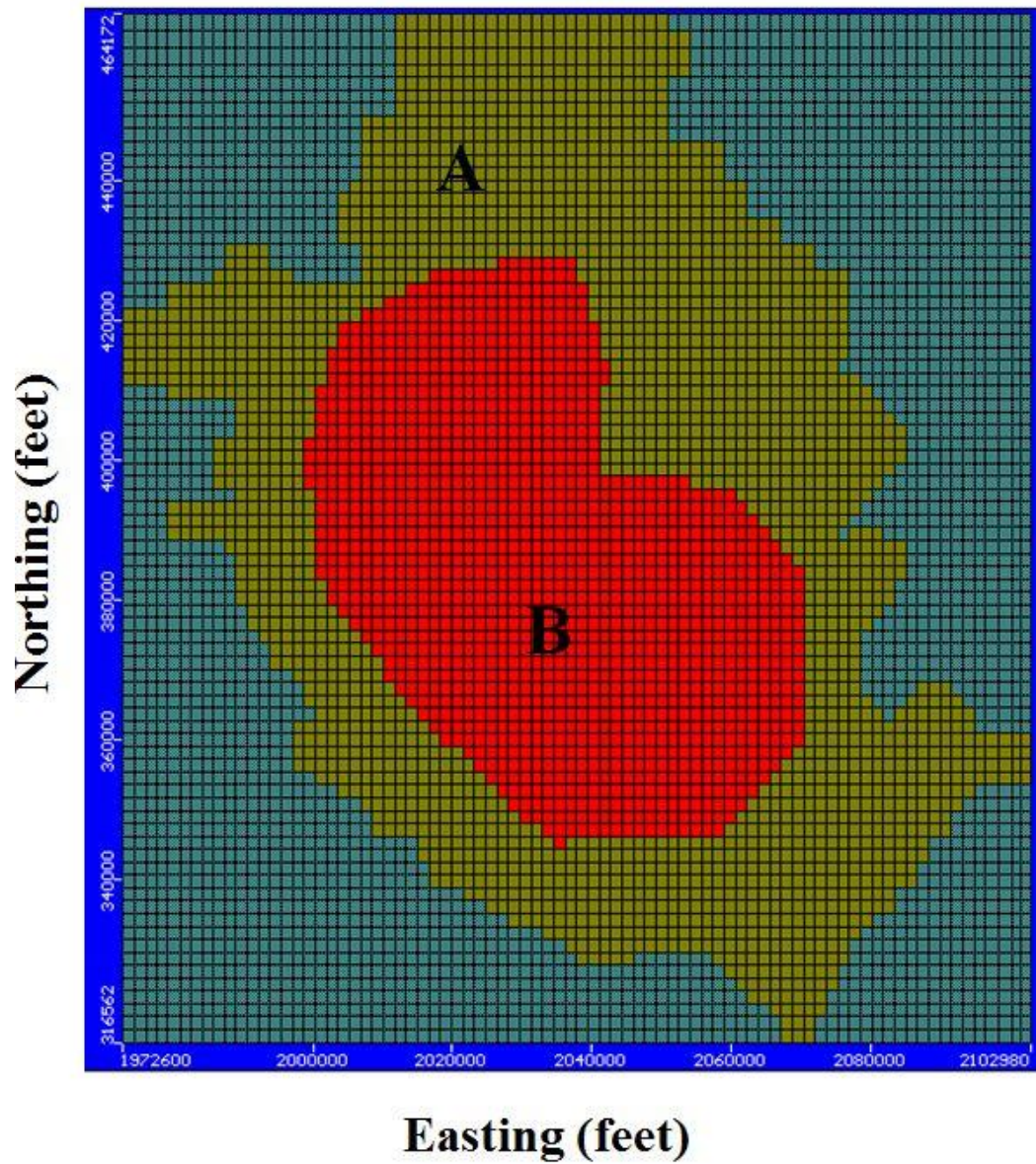
Figure 7.22 Map views of shale 4A and Shale 4B over the exploited coal
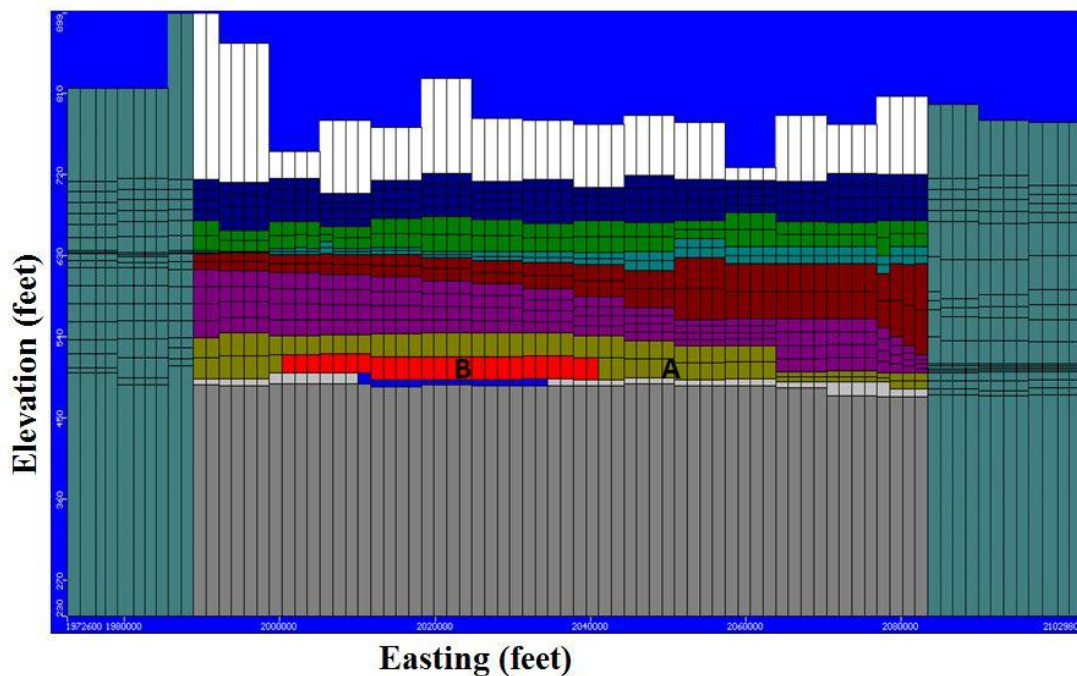
Figure 7.23 Cross sectional map of shale 4A and Shale 4B in the E-W direction.

Table 7.7. Calibrated hydraulic conductivity values for the transient-state model.

Lithological Units	Hydraulic conductivity (feet/day)		
	Kx	Ky	Kz
Layer 1 (Shales)	1.1	1.1	1.1
Layer 2 (Sandstones)	6.5	6.5	6.5
Layer 3 (shales)	0.04	0.04	0.04
Layer 4 (sandstones)	0.1	0.1	0.1
Layer 5 (shales)	0.8	0.8	0.8
Layer 6 (sandstones)	14	14	14
Layer 7 (shales 4A)	0.00009	0.00009	0.00009
Layer 7 (shales 4B)	0.0005	0.0005	0.0005
Layer 8 (coal)	0.0001	0.0001	0.0001
Voids	45	45	45
Layer 9 (shale)	0.02	0.02	0.02

Table 7.8. Calibrated Recharge values for the transient-state model.

Property	Recharge (Inches/year)
R1	0.1
R2	1.5
R3	1.4
R4	0.01

Table 7.9. Calibrated specific yield values for the transient-state model.

Property	Specific yield
Layer 1 (shale)	0.11
Layer 2 (sandstone)	0.27
Layer 3(shale)	0.12
Layer 4(sandstone)	0.27
Layer 5(shale)	0.12
Layer 6(sandstone)	0.27
Layer 7(shale)	0.12
Layer 8 (coal)	0.12
Layer 9(shale)	0.12
Voids	0.99

Table 7.10. Calibrated specific storage values for the transient-state model.

Property	Specific storage (1/ft)
Layer 1 (shale)	0.0001
Layer 2 (sandstone)	0.001
Layer 3(shale)	0.0001
Layer 4(sandstone)	0.001
Layer 5(shale)	0.0001
Layer 6(sandstone)	0.001
Layer 7(shale)	0.0001
Layer 8 (coal)	0.0001
Layer 9(shale)	0.0001
Voids	0.001
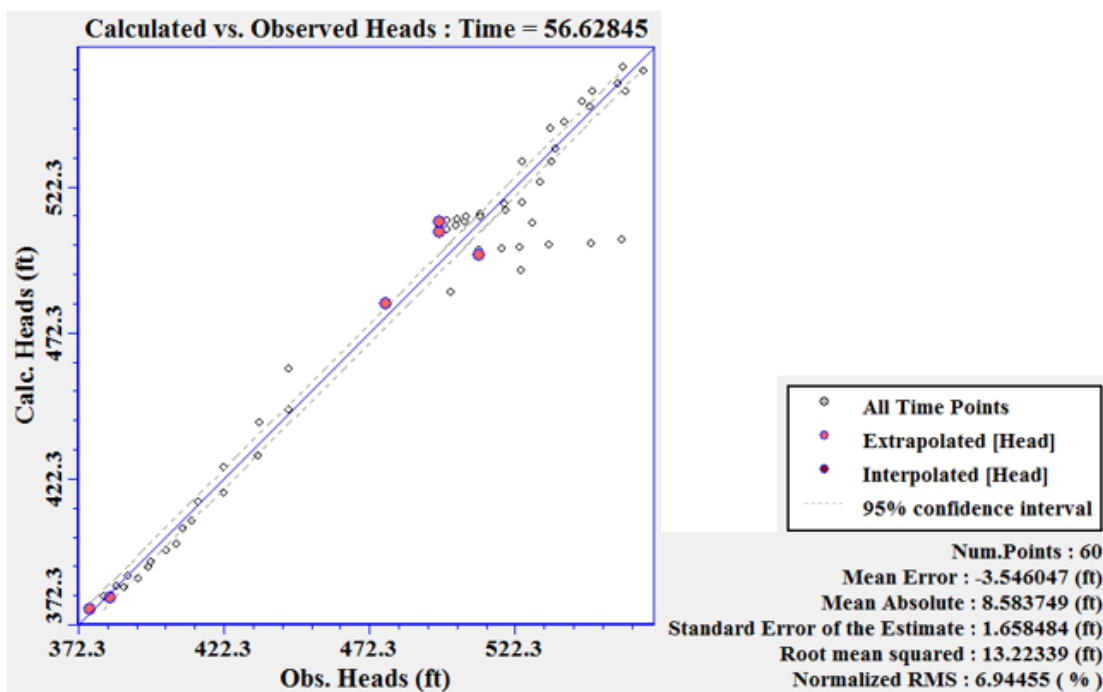
Figure 7.24. Transient model. Calculated heads versus the observed heads for the transient state simulation and the corresponding error values obtained in the calibrated simulation.
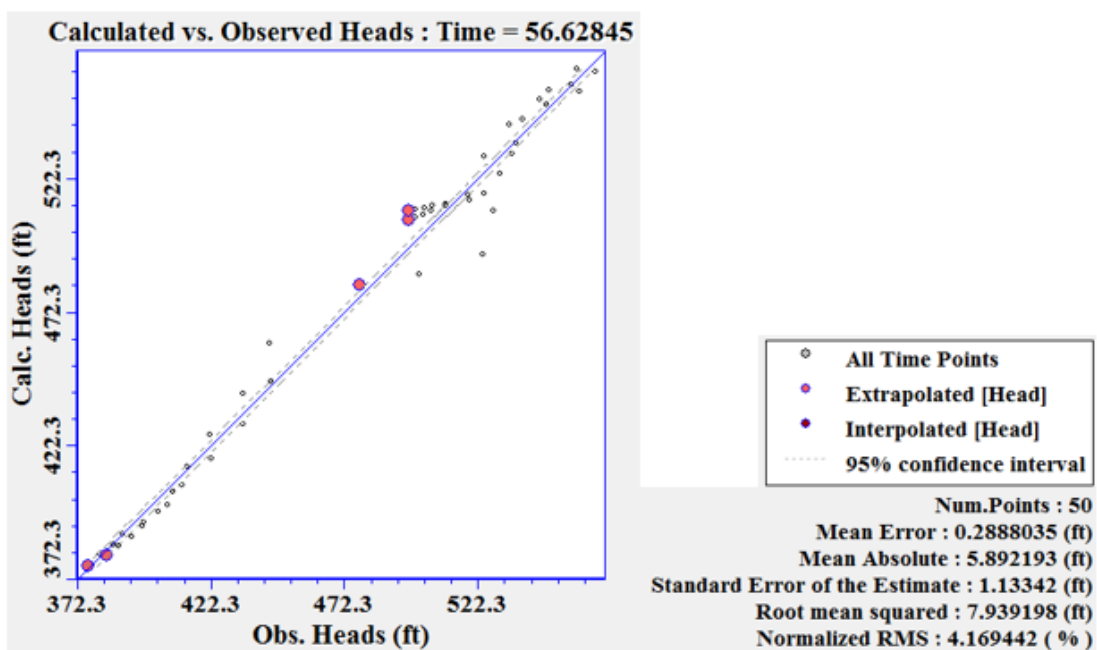
Figure 7.25. Transient model. Calculated heads versus the observed heads for the transient state simulation without the NW shaft. NW shaft is an outlier since its transient values of the simulated heads get farther from the line of equal simulated vs observed head, as time progresses.
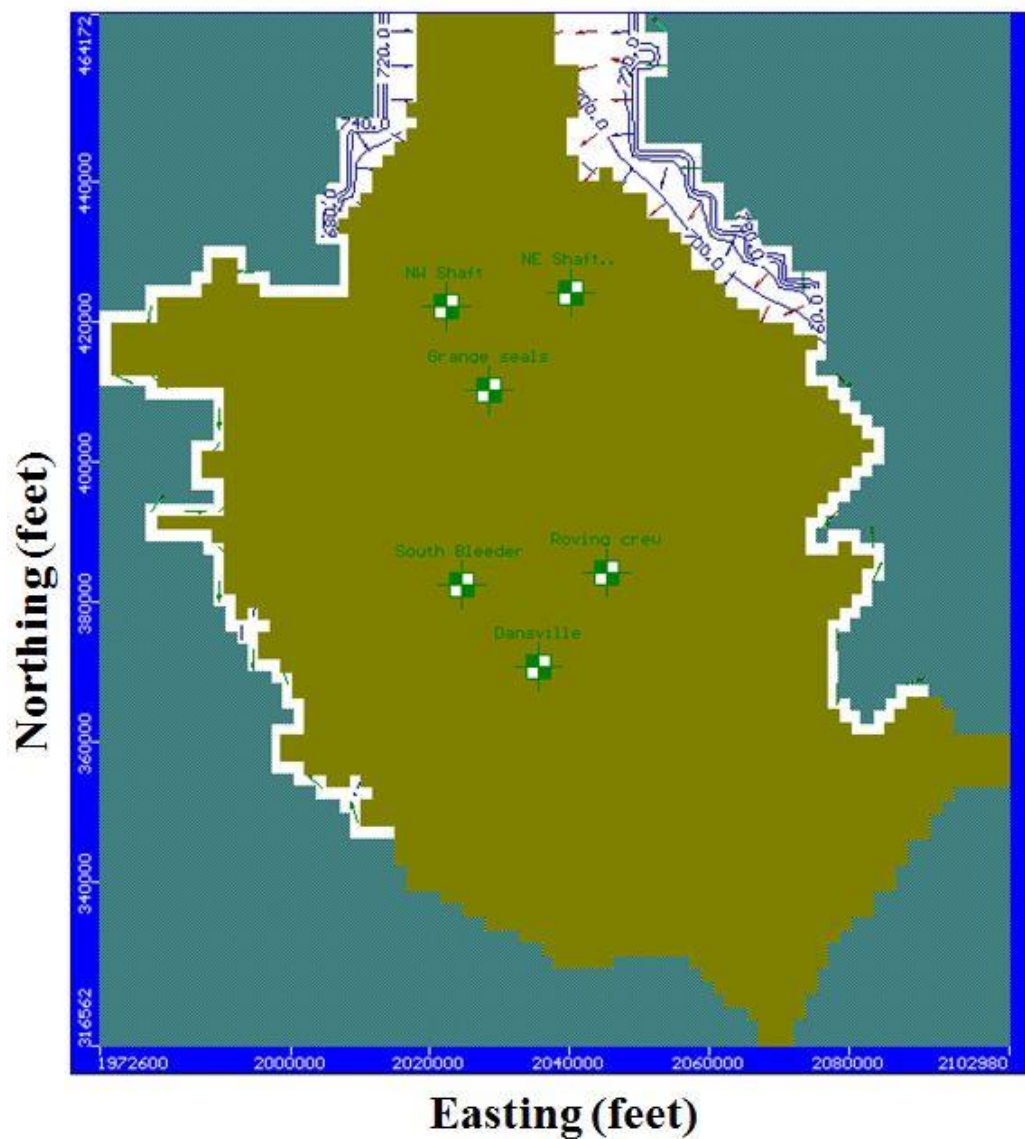
Figure 7.26. Transient model. Aquifer A showing equipotential head contours at an interval of 20ft. Olive areas constitute areas of unsaturation whiles white areas constitute areas of saturation. Observation wells are represented with the white and green squares within the model.
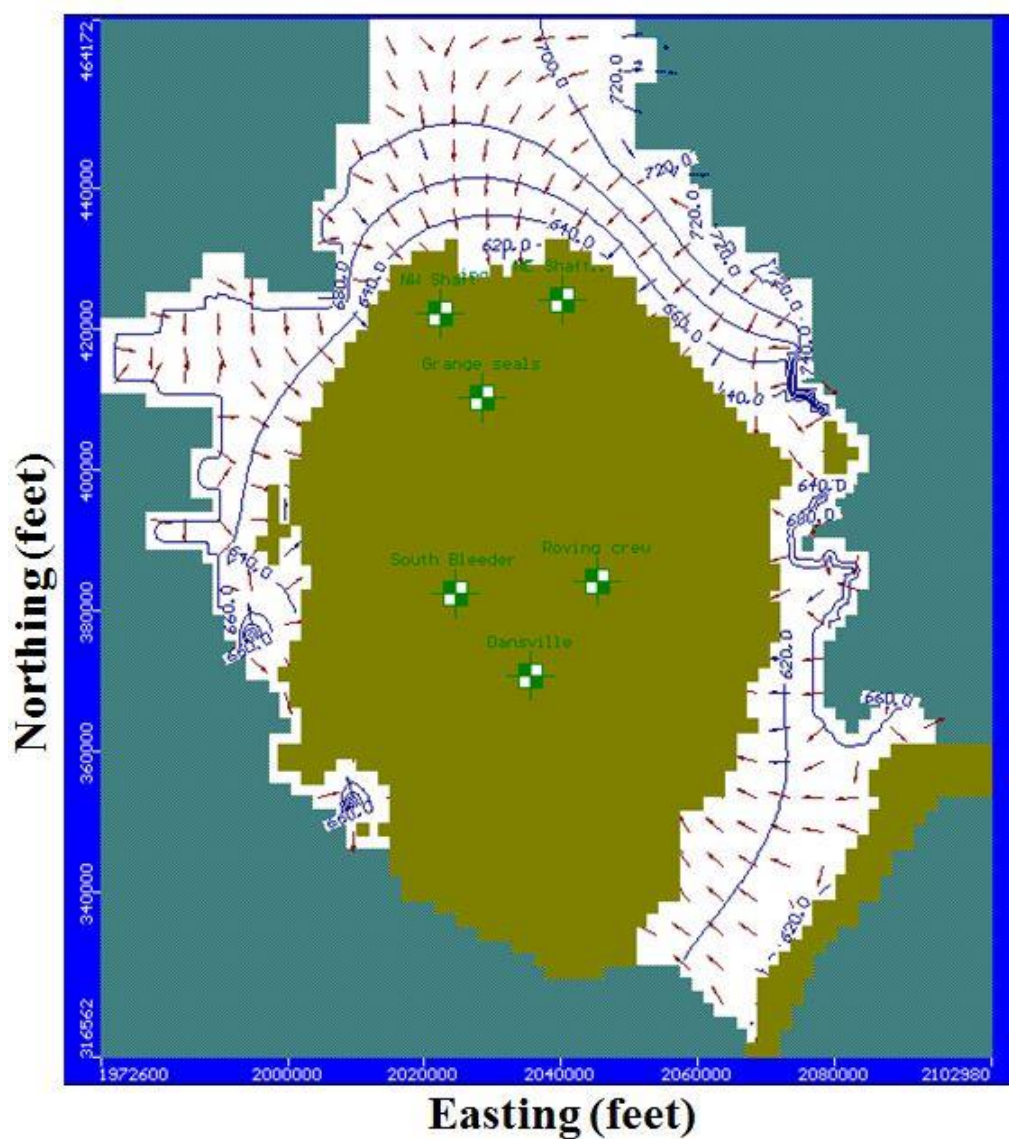
Figure 7.27. Transient model. Aquifer B flow regime showing equipotential head contours at interval of 20ft. Olive areas constitute areas of unsaturation whiles white areas constitute areas of saturation. Observation wells are represented with the white and green squares within the model.
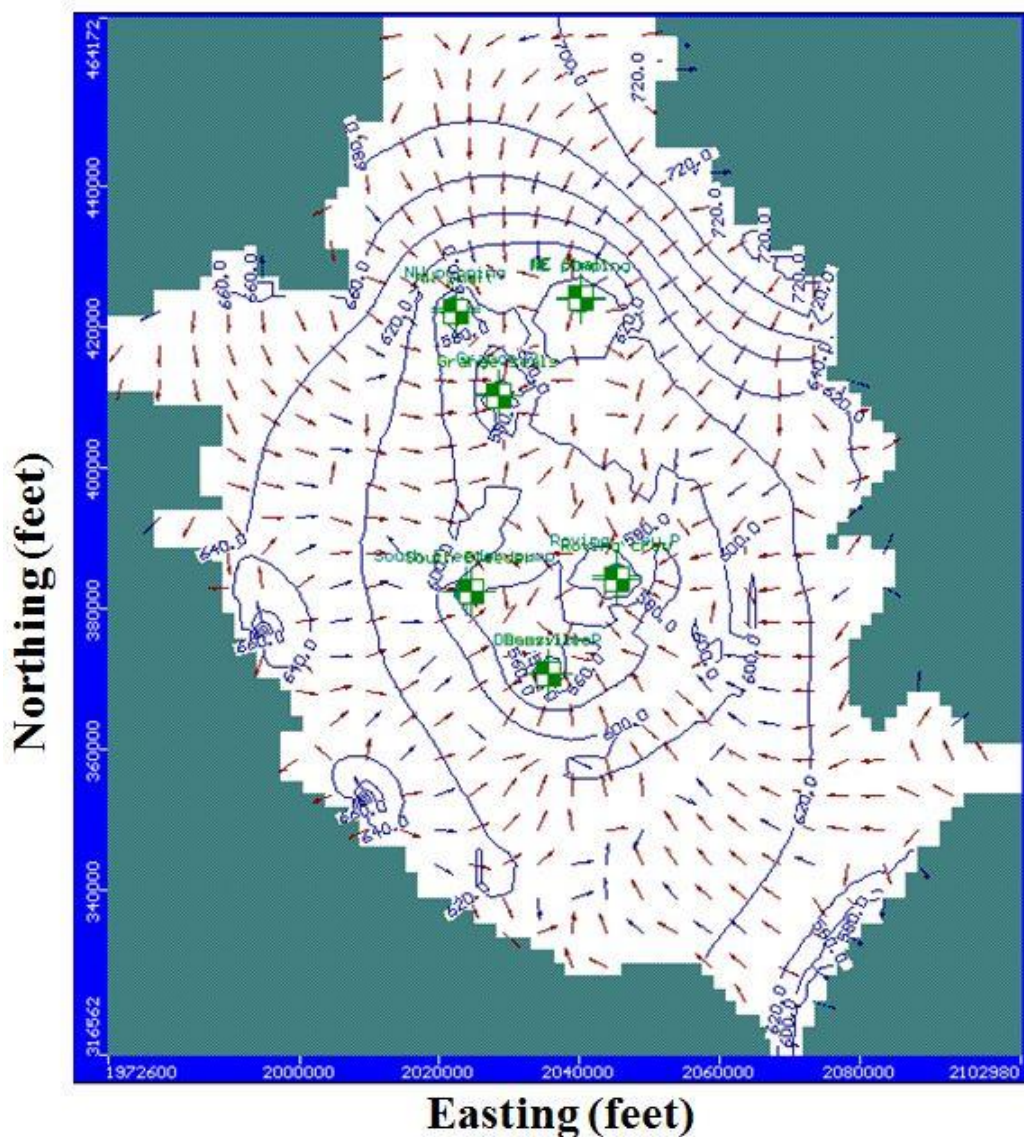
Figure 7.28. Transient model. Aquifer C flow regime showing equipotential head contour intervals of 20ft. Olive areas constitute areas of unsaturation whiles white areas constitute areas of saturation. Observation wells are repres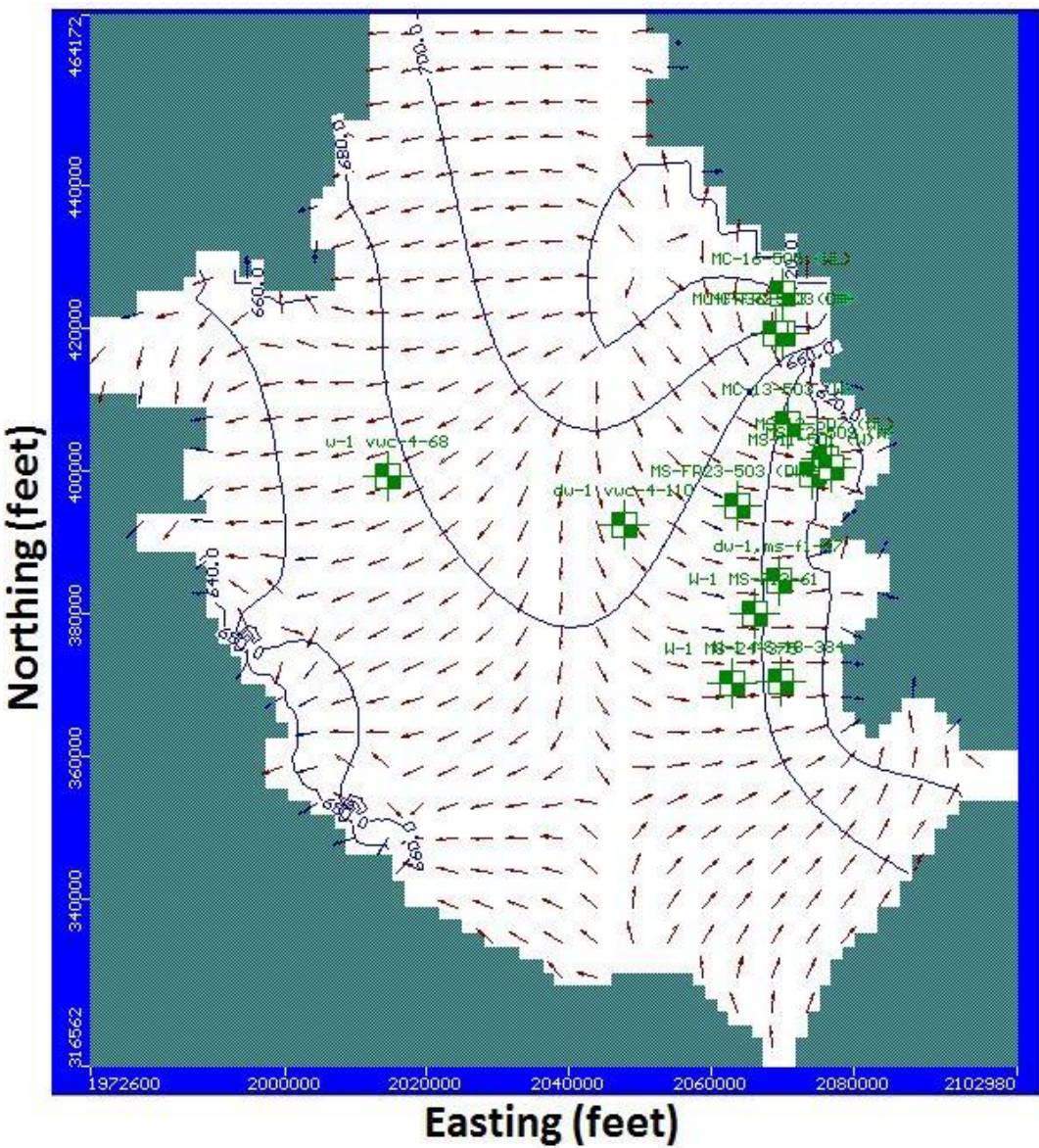ented with the white and green squares within the model. Groundwater flow was towards the wells due to unsaturated mine cavity.

A sensitivity analysis was performed for the transient model calibrated input parameters. The calibrated input parameters of shales specific yield, sandstones specific yield, coal specific yield, recharges (R1, R2, R3 and R4), shales specific storage, sandstones specific storage, coal specific storage, shales hydraulic conductivity, coal

hydraulic conductivity and hydraulic conductivity of the sandstones were each evaluated separately.

Figure 7.29 shows the sensitivity analysis of shales hydraulic conductivity for the transient state simulation. The model was very sensitive to both an increase and decrease in shale 5 hydraulic conductivity and also sensitive to an increase and decrease in shale 4A and shale 4B hydraulic conductivity. Shale 1, shale 2, and shale 3 were not sensitive to the model and maintained the same values than in the steady state models.

Figure 7.30 shows the sensitivity analysis of aquifers hydraulic conductivity. The model was sensitive to an increase and decrease in aquifer A and aquifer B. The model was very sensitive to an increase in aquifer C hydraulic conductivity and less sensitive to a decrease in aquifer C hydraulic conductivity.
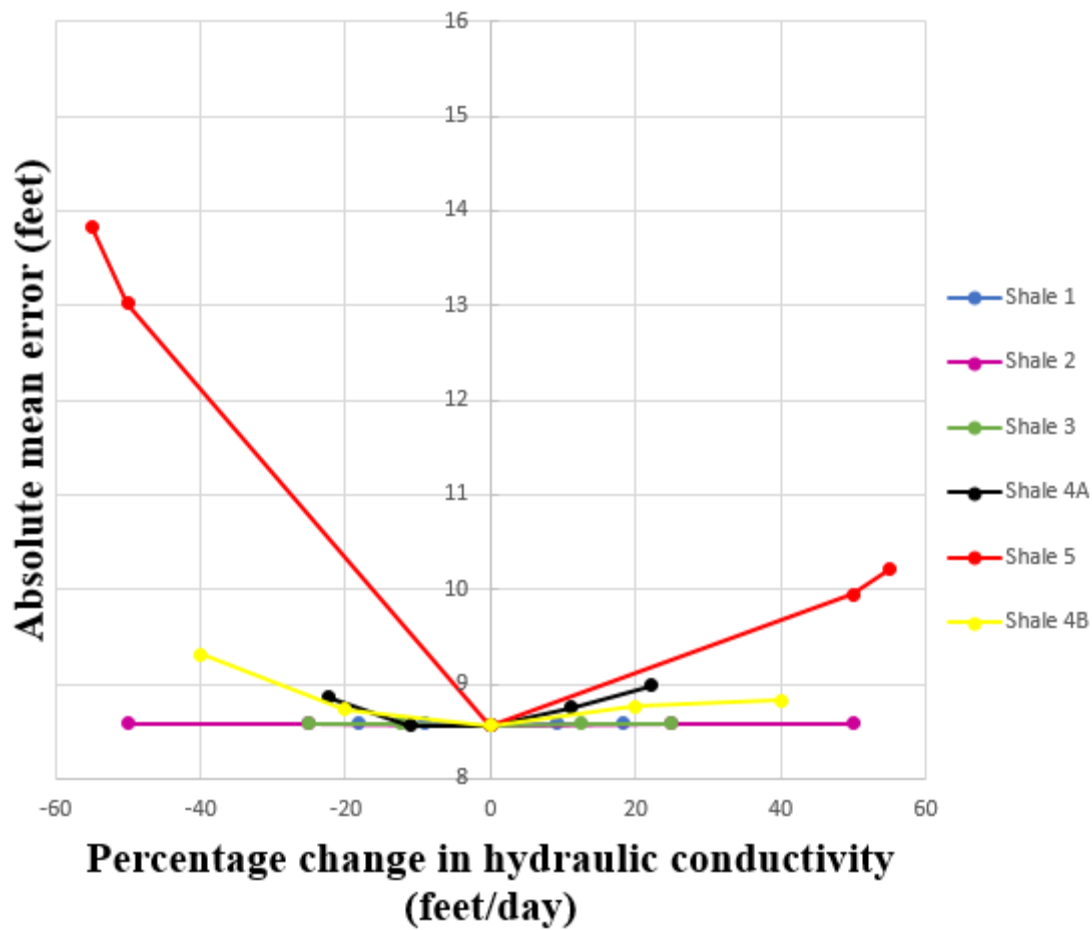
Figure 7.29 Sensitivity analysis of shales hydraulic conductivity for the transient state simulation.
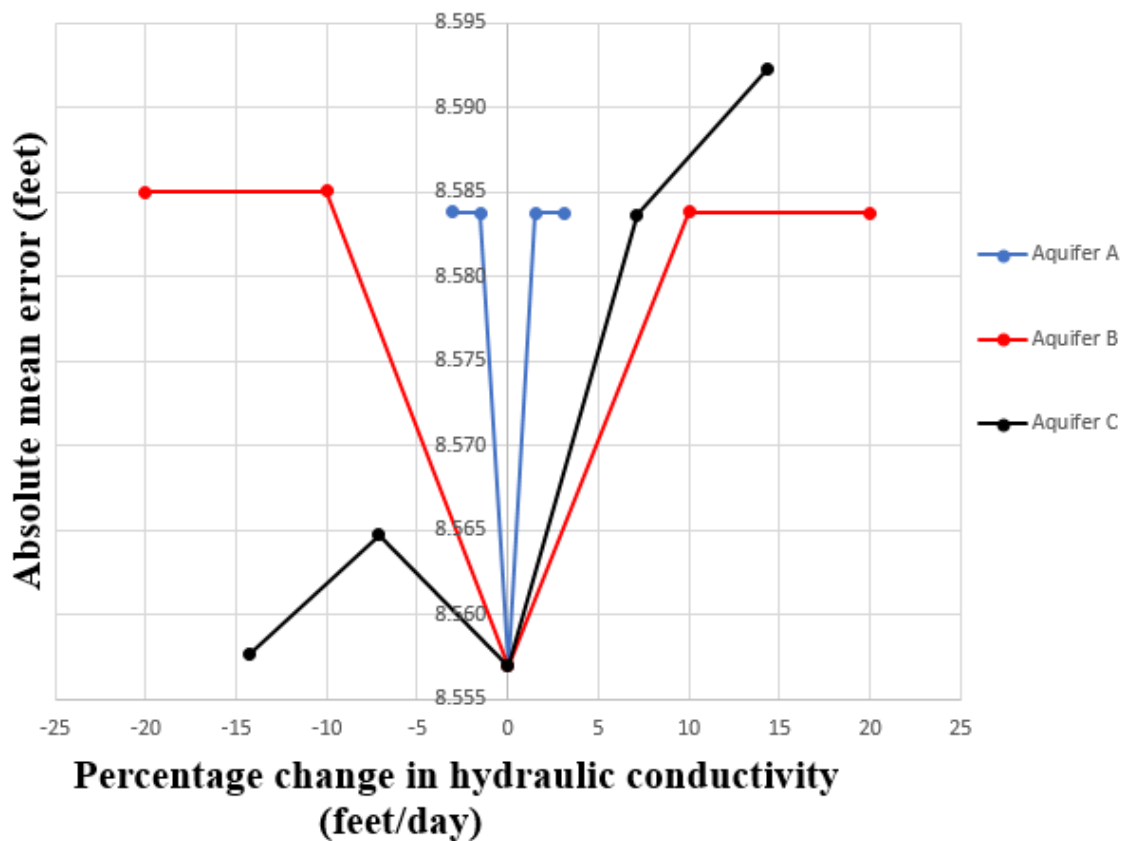
Figure 7.30 Sensitivity analysis of aquifers hydraulic conductivity for the transient state simulation.

Figure 7.31 shows the sensitivity analysis of coal hydraulic conductivity. The model was very sensitive to a decrease in hydraulic conductivity of the coal and slightly sensitive to an increase in hydraulic conductivity. The model was also sensitive to the hydraulic conductivity of the voids in the coal when the hydraulic conductivity were increased and decreased.
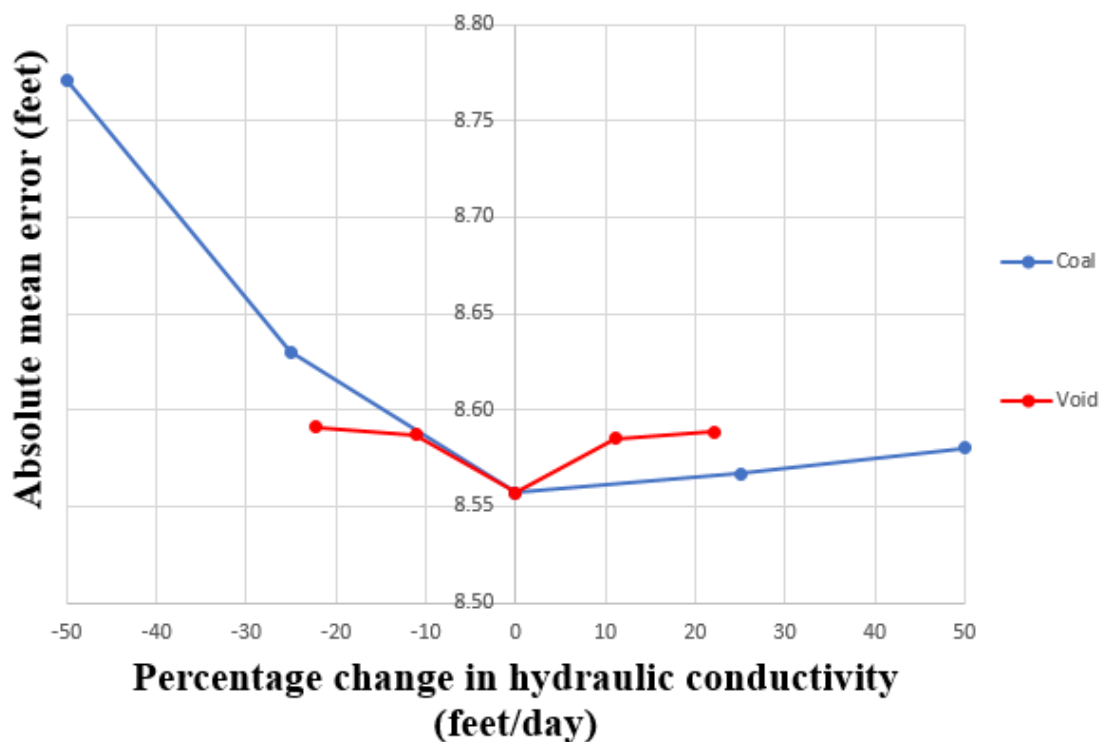
Figure 7.31 Sensitivity analysis of coal hydraulic conductivity for the transient state simulation.

Figure 7.32 shows the sensitivity analysis of recharge for the transient state simulation. An increase and decrease in recharge for the four areas resulted in the sensitivity of the model. The model was sensitive to the four recharge areas.

Specific storage and specific yield are parameters that are important in the transient groundwater flow equations and they were calibrated in this model. In Figure 7.33 for specific yield of the shales, the model was very sensitive to an increase and decrease in the specific yield of shale 1. The model was not sensitive to the specific yield of shale 2, shale 3, shale 4 and shale 5.
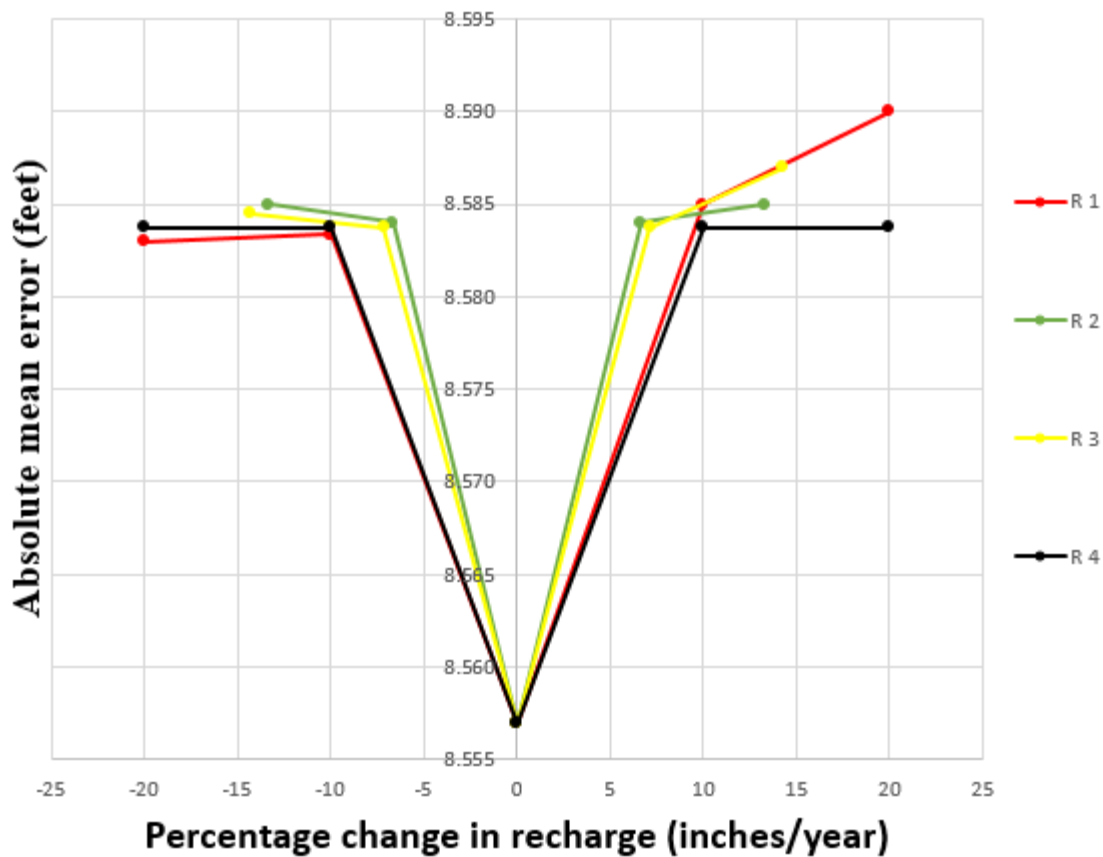
Figure 7.32 Sensitivity analysis of recharge for the transient state simulation.
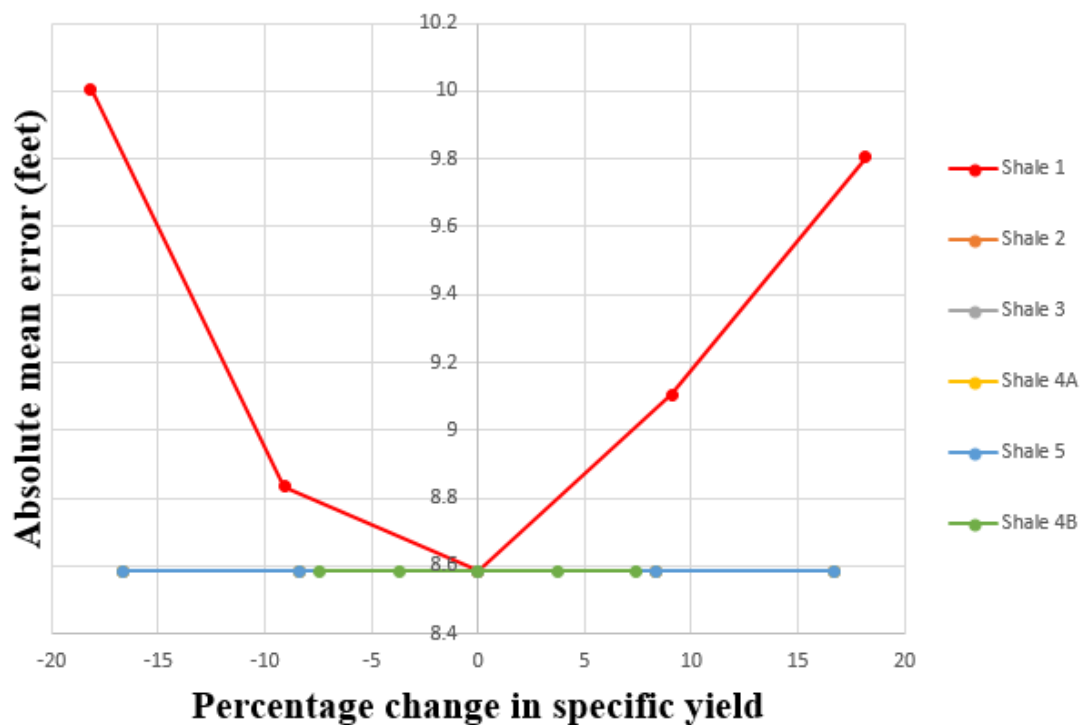
Figure 7.33 Sensitivity analysis of shale specific yield for the transient state simulation.

In Figure 7.34 for the sensitivity of the specific yield of the aquifers, the model was sensitive to aquifer C when the specific yield was increased and decreased. aquifer B and aquifer C were not sensitive to the model when their specific yields were increased and decreased.

Figure 7.35 shows the sensitivity analysis of coal specific yield for the transient state simulation. In this analysis the model was sensitive to the void in the coal layer when the specific yields were increased and decreased. The specific yield of the coal layer was not sensitive in the model when the specific yields were increased and decreased. In Figure 7.36 for the sensitivity of the coal and mine void, the model was sensitive when the specific yield of the mine void was increased and decreased. The coal layer was not sensitive to the model when the specific yield was increased and decreased.
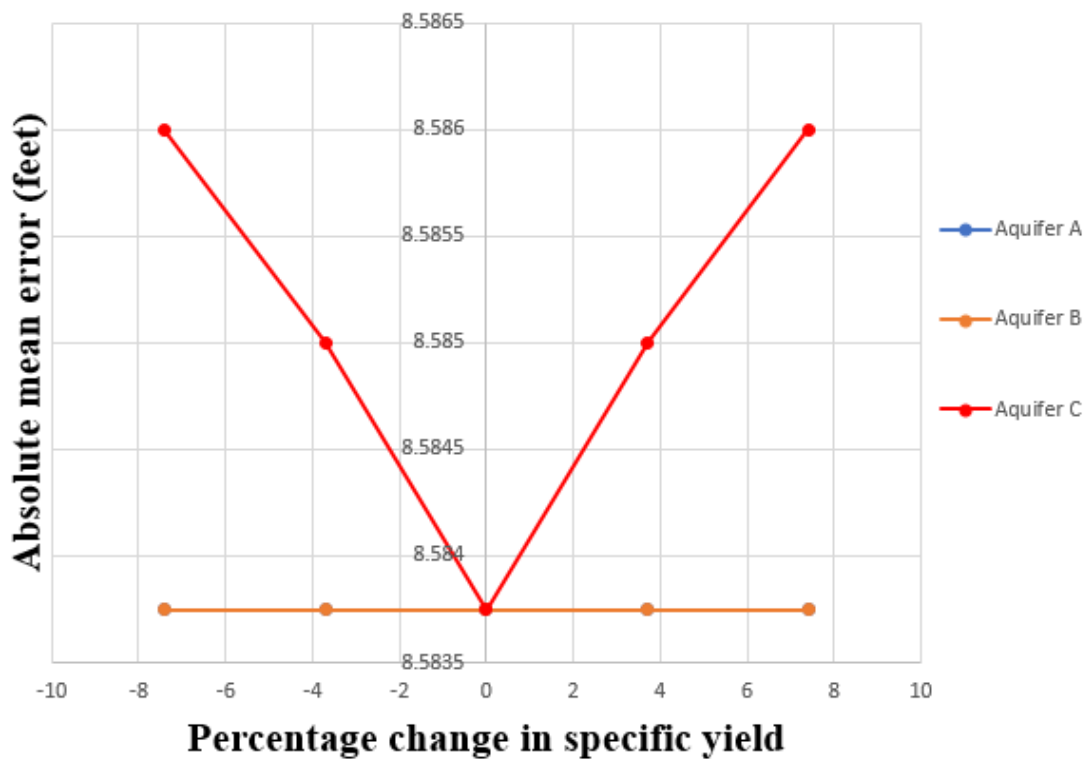
Figure 7.34 Sensitivity analysis of aquifer specific yield for the transient state simulation
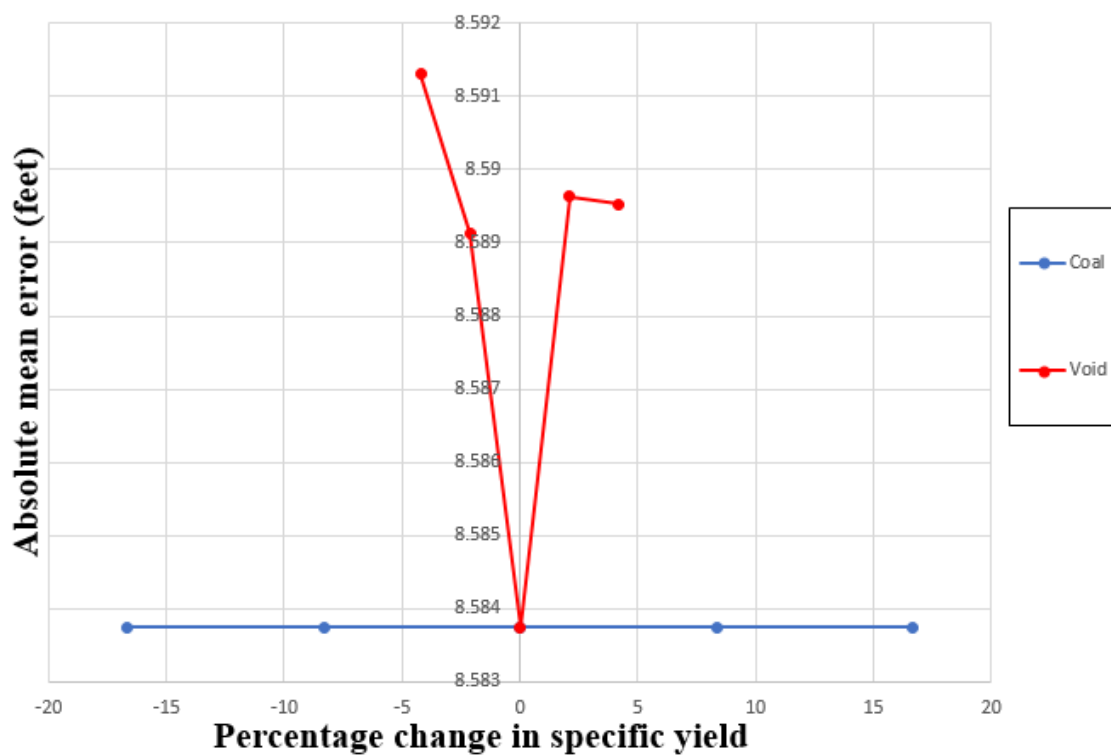
Figure 7.35 Sensitivity analysis of coal specific yield for the transient state simulation
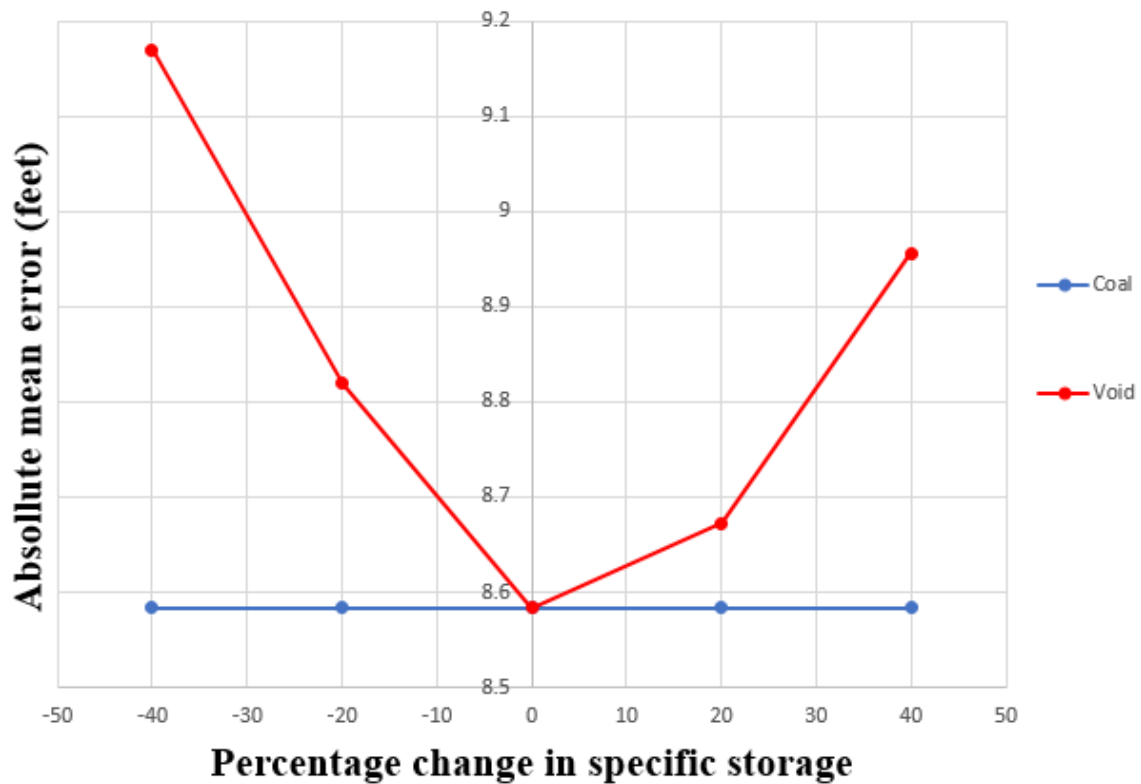
Figure 7.36 Sensitivity analysis of coal specific storage for the transient state simulation

Figure 7.37 shows that aquifer C was sensitive to the model when the specific storage was increased and decreased but aquifer A and aquifer B were not sensitive to the model with an increase and decrease in specific storage. In Figure 7.38 the model was very sensitive to a decrease in specific storage and less sensitive to an increase in specific storage for shale 1. The model was not sensitive to shale 2, shale 3, shale 4 and shale 5.
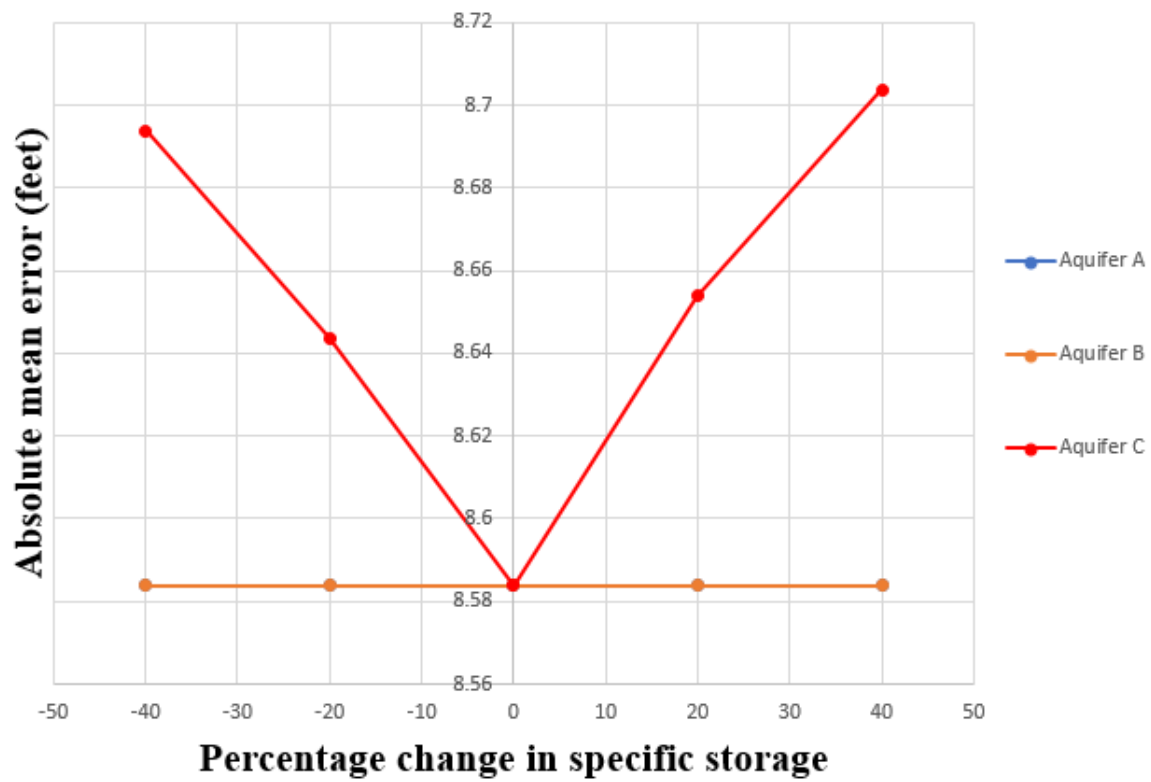
Figure 7.37 Sensitivity analysis of aquifer specific storage for the transient state simulation
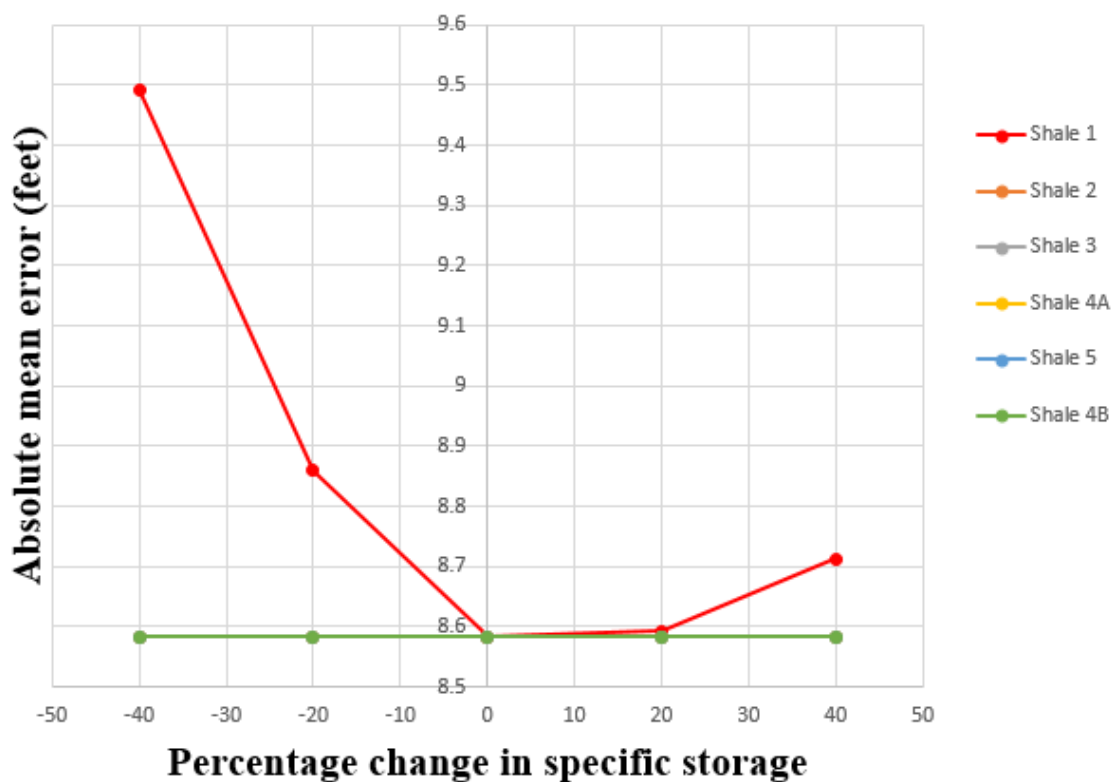
Figure 7.38 Sensitivity analysis of shale specific storage for the transient state simulation.

7.4 Summary of numerical model of the Meigs Mine Complex

Input parameters that were affected during the first steady-state calibration were the four recharge areas and the hydraulic conductivity of the layers as seen in Table 7.4 and Table 7.3, respectively. Porosity, specific yield, specific storage, stream sediment conductance, etc. had no effect on the output of the model during steady state calibration. It was observed that the first steady state model was sensitive to the aquifer and shale's closer to the mined coal (aquifer C, shale 4 and 5) when the hydraulic conductivity values were increased or decreased. Calibrated hydraulic conductivity values for the lithology's of the first model was very high because pumping of water in the mine was not simulated. Water levels in the six shafts in January 2004 were reproduced by estimating the pumping rate during the second steady state model.

In the transient simulation the calibrated hydraulic conductivity values for the lithologies were lower than in the first steady state model as seen in Table 7.5. This is probably due to pumping and dewatering of the mine when the mine was active and the fact that pumping was not considered in this first model. The transient model was also very sensitive to an increase and decrease in the hydraulic conductivity of the aquifer and shale's closer to the mined coal (aquifer C, shale 4A, shale 4B, and shale 5). Input parameters that were affected during the transient simulation were the hydraulic conductivity, recharge, specific yield, and specific storage.

CHAPTER 8: ARTIFICIAL NEUTRAL NETWORK

Artificial neutral network was used to build predictive models for mine pool development due to the empirical predictable relationship between potentiometric heads of the mines, overburden thickness, surface elevation, bottom of well, coal thickness, thickness of mined coal seam, thickness of sandstones, thickness of limestone, thickness of shales, cumulative coal volume extracted, water withdraw, underground mine area, average annual precipitation, and the development of mine pool. These parameters served as input variables for NeuroShell 2.

During the 35 years that cover the data for the 11 mines and their wells, water withdraw is only reported in the NPDES web site for the period of time 2007 to 2017. This situation reduces the number of wells that are available for regression analysis. For that reason two different data sets were analyzed: parameters that include the list given above with water withdraw and that contains 111 wells, and a second data set that contains the data collected for all the wells but does not contain water withdraw with a total of 381 wells. It should be noted that even if this data set does not contain water withdraw, it contains the accumulated coal extracted at the time of well monitoring, which is a parameter that should be related to the dewatering of the mine for working underground. The two data sets were analyzed in NeuroShell 2 to obtain polynomial regression of the potentiometric head as function of the variables listed above. The Group Method of Data Handling was used in NeuroShell 2 to produce first, second, and third degree polynomial regressions.

Simulation of the elevation of water in relation with the coal layer is the purpose of this research. For that reason, the resulting second degree polynomial equation was

used to model the elevation of water in the coal layer after mine closure. For this simulation, the bottom of coal elevation was used instead of the bottom of well to simulate the potentiometric head at the bottom of the mined coal layer and this was achieved by subtracting the overburden thickness and the thickness of coal from the surface elevation of the wells, and the maximum value for accumulated coal volume was used for each permit area.

8.1. Modeling potentiometric heads using the data set containing water withdraw

Different polynomial regression was analyzed with the neural networks program for the data set that contains water withdraw. Table 8.1 shows the mean square error, R squared, correlation coefficient and normalized mean square error for the maximum, average and minimum input variables of the parameters for the different polynomial regressions.

Table 8.1. Statistical data for the parameters with water withdraw. Maximum, average, and minimum refer to the potentiometric heads obtained at the different wells for the monitoring period.

		Parameters with water withdraw		
		Maximun	Average	Mininum
Polynomial 1	Mean square error	0.01	0.02	0.02
	R squared	0.96	0.95	0.94
	Correlation coefficient	0.98	0.98	0.97
	Norm. mean square error	0.03	0.04	0.04
Polynomial 2	Mean square error	0.01	0.01	0.01
	R squared	0.98	0.98	0.98
	Correlation coefficient	0.99	0.99	0.99
	Norm. mean square error	0.01	0.01	0.01
Polynomial 3	Mean square error	0.002	0.002	0.002
	R squared	0.99	0.99	0.99
	Correlation coefficient	1.00	1.00	1.00
	Norm. mean square error	0.005	0.006	0.005

In terms of the mean square errors and correlation coefficients, the third degree polynomials seem to reproduce the data better. However, when the outputs of the models were analyzed, the third degree polynomials found the accumulated coal volume extracted as one of the least significant variables and the third degree polynomial equations did not have that variable. For our purposes, the accumulated coal volume extracted is a key parameter to be able to predict the heads after the mine closes. To predict post-mining water level, accumulated coal volume is set to the maximum value for a planned mine (estimated coal that will be extracted) and the water withdraw is set to zero for steady-state conditions. For that reason, it was decided to use the second degree polynomial that includes these key variables and gives marginal difference in regression coefficient with respect to the third degree polynomial.

Table 8.2 shows the second degree polynomial equation, most significant variables, and least significant variables for the average head. Tables for maximum and minimum heads are presented in Appendix D.

Table 8.2. Second degree polynomial equation and significant variables for average heads in wells for the data set with water withdraw

Best formula:	$Y=-2.1E-002*X10-0.11*X11-4.4E-002*X6-0.2+0.61*X1+0.36*X2+0.18*X1^2-0.28*X1*X2+6.2E-002*X9^2+0.34*X10^2-0.13*X11^2+9.1E-002*X2^2$
Legend:	X1=2.*(Surface Elevation for Sampling Station (msl)-602.)/738.-1.
	X2=2.*(Bottom of well elevation (msl)-244.04)/1053.96-1.
	X3=2.*(Overburden thickness (ft)-65.)/475.4-1.
	X4=2.*(Thickness of mined coal seam (ft)-2.25)/9.51-1.
	X5=2.*(Thickness Shale + Clay (ft)-13.9)/333.16-1.
	X6=2.*Thickness Sandstone (ft)/258.71-1.
	X7=2.*Thickness Limestone (ft)/187.04-1.
	X8=2.*Thickness Coal (ft)/26.19-1.
	X9=2.*(Accumulative Coal Volume (Mm^3)-.07)/146.11-1.
	X10=2.*(Underground Mine Area 4mi (acres)-617.98)/110430.52-1.
	X11=2.*(Average Annual Precipitation (in)-38.)/3.-1.
	X12=2.*W/D (MGD / ft)/.-1.
	Y=2.*(Average Head (msl)-457.17)/841.26-1.
Most significant variables:	Surface Elevation for Sampling Station (msl)
	Bottom of well elevation (msl)
	Thickness Sandstone (ft)
	Accumulative Coal Volume (Mm^3)
	Underground Mine Area 4mi (acres)
	Average Annual Precipitation (in)
Least significant variables:	Thickness Coal (ft)

Based on the equation reported in Table 8.2 and the statistical data for the parameters with water withdraw; polynomial 2 sets of observed heads were plotted against its calculated heads as seen in Figure 8.1.

Figure 8.1 (and Figs. D.2 and D.3 in the Appendix D) shows that the observed and calculated heads are closely reproduced by the artificial neural networks model with a correlation coefficient close to 1.
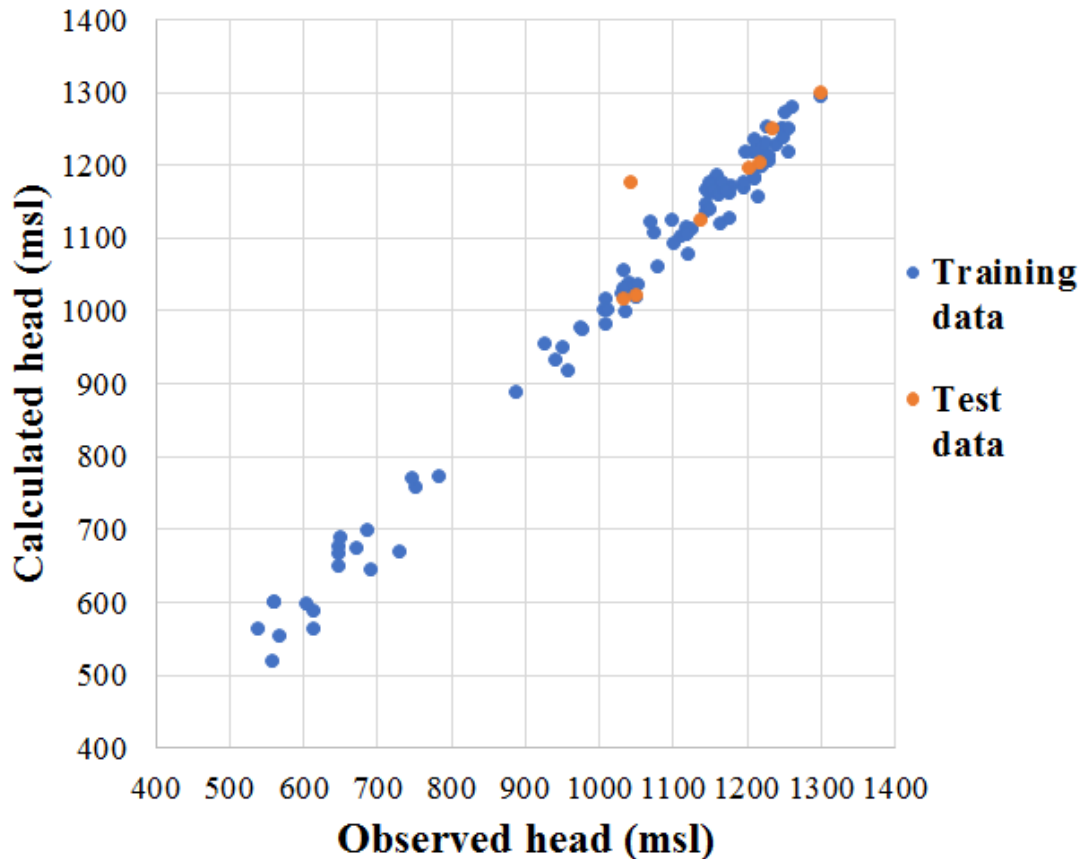
Figure 8.1 Correlation between observed and calculated heads for the average head for mine data with water withdraw.

8.2. Modeling potentiometric heads using the data set without water withdraw

In a similar way that with the previous data set, the mine data without water withdraw was modeled with NeuroShell 2 using first, second, and third degree polynomials (see table 8.3). Again, the second degree polynomial was chosen because it gave very good statistical results and included the accumulated coal volume extracted.

Table 8.3. Statistical data for the parameters without water withdraw. Maximum, average, and minimum refer to the potentiometric heads obtained at the different wells for the monitoring period.

		Parameters without water withdraw		
		Maximum	Average	Mininum
Polynomial 1	Mean square error	0.01	0.01	0.01
	R squared	0.97	0.96	0.94
	Correlation coefficient	0.98	0.98	0.97
	Norm. mean square error	0.01	0.02	0.03
Polynomial 2	Mean square error	0.003	0.003	0.006
	R squared	0.98	0.98	0.97
	Correlation coefficient	0.99	0.99	0.98
	Norm. mean square error	0.01	0.01	0.02
Polynomial 3	Mean square error	0.002	0.002	0.004
	R squared	0.99	0.99	0.98
	Correlation coefficient	1.00	0.99	0.99
	Norm. mean square error	0.004	0.005	0.01

Table 8.4 shows the second degree polynomial equation, most significant variables, and less significant variables for the average head. Tables for maximum and minimum heads are presented in Appendix D. Figure 8.2 shows the observed and calculated heads for the average head for the second degree polynomial. It shows that the model reproduces the observed data with high precision as it is evident in the correlation coefficient very close to 1. Similar Figures were constructed for the maximum and average heads as presented in Appendix D.

Table 8.4. Second degree polynomial equation and most significant variables for the average head for the mine data set without water withdraw.

Best formula:	$Y = -1.7E\text{-}002*X11 + 4.5E\text{-}004*X10 - 2.3E\text{-}002*X4 + 1.6E\text{-}002*X5 - 8.3E\text{-}002 - 1.5E\text{-}002*X7 - 1.4E\text{-}002*X6 - 4.9E\text{-}002*X9 + 0.73*X1 + 0.37*X2 + 0.2*X1^2 + 0.24*X2^2 - 0.52*X1*X2 + 4.7E\text{-}002*X1*X9 + 2.3E\text{-}002*X2*X9 + 1.4E\text{-}002*X1^2*X9 + 1.5E\text{-}002*X2^2*X9 - 3.3E\text{-}002*X1*X2*X9 - 4.3E\text{-}002*X11^2 - 1.8E\text{-}002*X7^2 - 1.6E\text{-}002*X5^2 + 9.5E\text{-}002*X10^2$
Legend:	X1=2.*(Surface Elevation for Sampling Station (msl)-545.)/835.-1.
	X2=2.*(Bottom of well elevation (msl)-80.)/1220.-1.
	X3=2.*(Overburden thickness (ft)-56.)/506.6-1.
	X4=2.*(Thickness of mined coal seam (ft)-1.17)/10.59-1.
	X5=2.*(Thickness Shale + Clay (ft)-13.9)/452.53-1.
	X6=2.*Thickness Sandstone (ft)/258.71-1.
	X7=2.*Thickness Limestone (ft)/204.97-1.
	X8=2.*Thickness Coal (ft)/33.23-1.
	X9=2.*Accumulative Coal Volume (Mm^3)/146.18-1.
	X10=2.*(Underground Mine Area 4mi (acres)-617.98)/110430.52-1.
	X11=2.*(Average Annual Precipitation (in)-37.)/4.-1.
	Y=2.*(Average Head (msl)-400.)/930.67-1.
Most significant variables:	Surface Elevation for Sampling Station (msl)
	Bottom of well elevation (msl)
	Thickness of mined coal seam (ft)
	Thickness Shale + Clay (ft)
	Thickness Sandstone (ft)
	Thickness Limestone (ft)
	Accumulative Coal Volume (Mm^3)
	Underground Mine Area 4mi (acres)
	Average Annual Precipitation (in)
Least significant variables:	Thickness Coal (ft)

Figure 8.2 Correlation between average observed and calculated heads for the data set without water withdraw.

8.3. Simulations to determine the potentiometric head in the coal layer after mine closure and recovery of the hydrogeological regime

Simulation of the elevation of water with respect to the coal layer is the purpose of this research. For that reason, the second degree polynomial equations were used to model the elevation of water in the coal layer after mine closure as well as the potentiometric head of the wells used in each regression after the mine closes. For this simulation, in the polynomial equations, the bottom of coal elevation was used instead of the bottom of well to simulate the potentiometric head at the bottom of the mined coal layer. This parameter was calculated by subtracting the overburden thickness and the thickness of coal from the surface elevation of the wells, the maximum value for accumulated coal volume was used for each permit area. For the equation that contains

water withdraw, zero water withdraw was simulated because free recovery of the water in the system is assumed and pumping is expected to cease.

Figure 8.3 shows the average potentiometric head at the bottom of the mined coal layer after mine closure. The small differences for the two curves produced by the simulation vary along the wells, in some cases the simulation with water withdraw gives lower values and in some other cases it gives higher values than the simulation values without water withdraw. This is consistent with the low errors reported in Tables 8.1 and 8.3.

Figure 8.4 shows the average potentiometric head at the bottom of the 381 wells after mine closure. It can be seen in this Figure, that the two equations give similar results and could be used with confidence to simulate the head recovery in these wells after the mine closes.

Figure 8.5 shows the average potentiometric heads and the differences between the observed and calculated head at the bottom of the 381 well after mine closure.

To predict if a mine pool may form, the calculated potentiometric heads at the bottom of the coal layer should be compared with the elevation of the top contact between the coal and the overlying rocks, usually shale. Figure 8.6 shows the average calculated potentiometric head at the bottom of the coal layer with the two model equations, and the top of the coal layer as reported in the borehole logs. This Figure shows that the elevation of the water will be higher than the elevation of the top of the coal, suggesting that all the mines that have been considered in this study will develop mine pools if the hydrogeological regime is allowed to recover without any other perturbation.
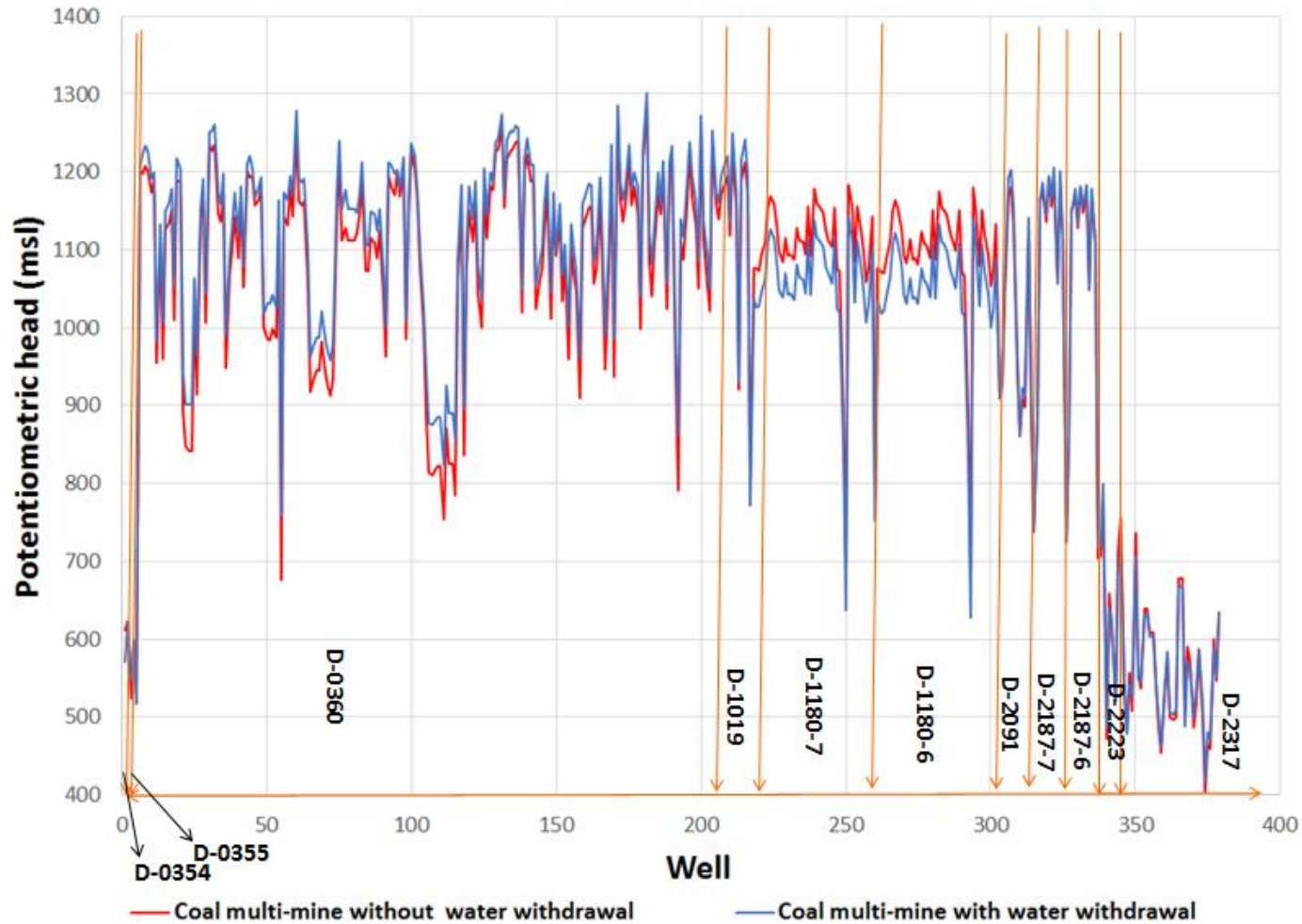
Figure 8.3. Average calculated heads at the bottom of the mined coal layer after mine closure using the second polynomial regression for the data set that contains water withdraw according to the NPDES reports, and the mine data without water withdraw for each mine studied in this research.
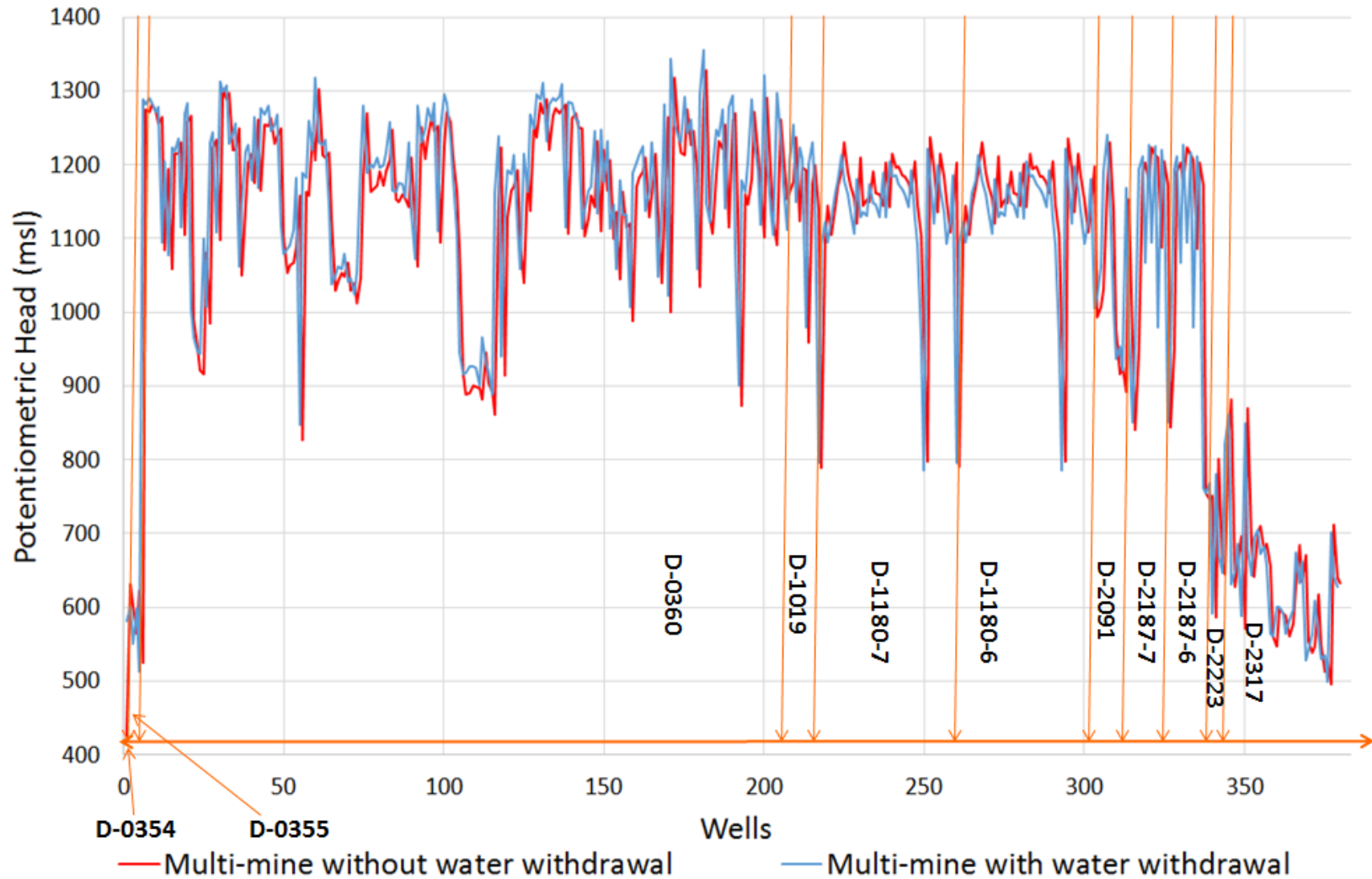
Figure 8.4. Average calculated potentiometric heads for the 381 wells used for this work after mine closure and well recovery. The second polynomial regression equations were used to construct this graph for the mines studied in this research.
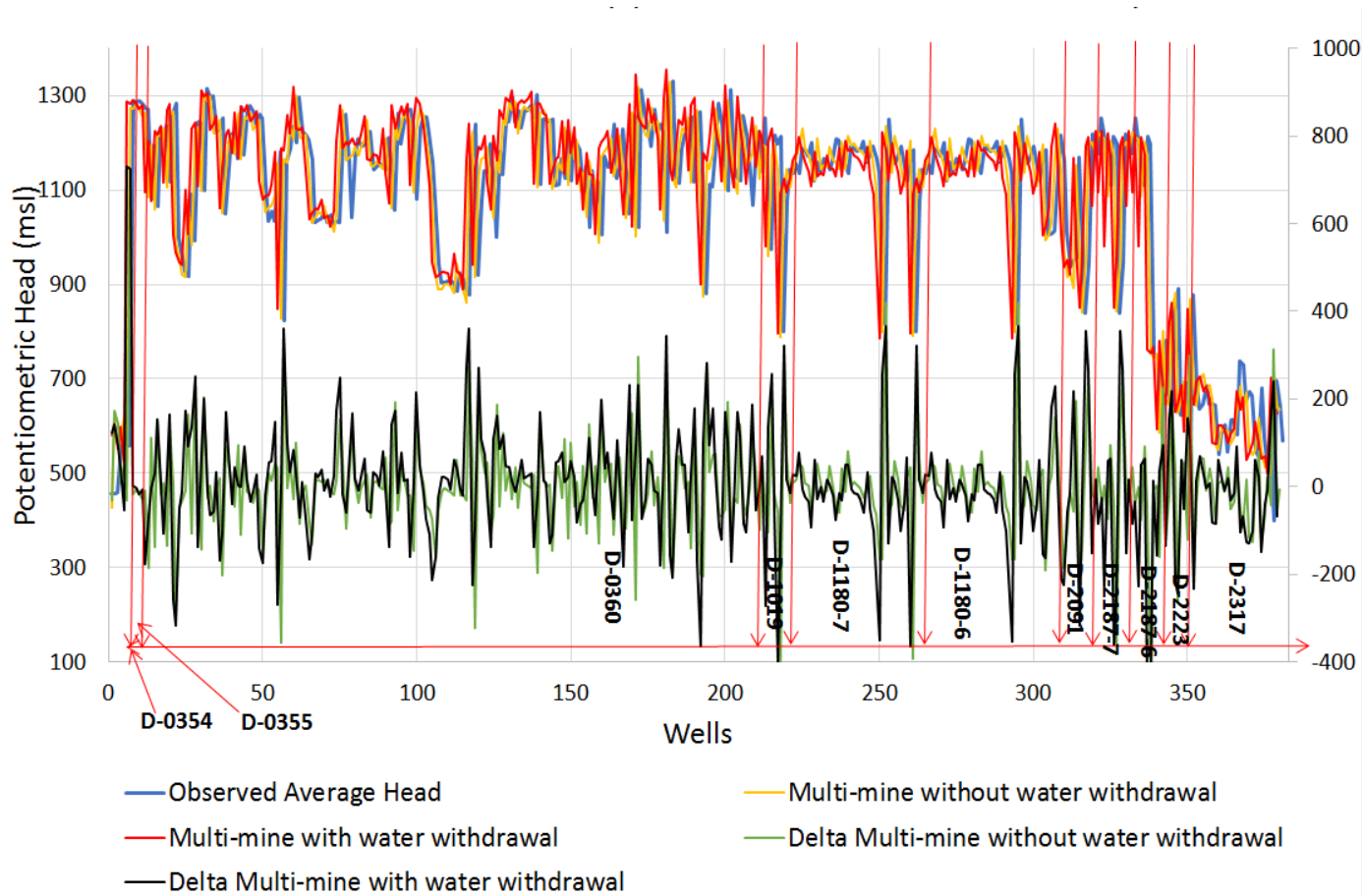
Figure 8.5. A graph showing the average potentiometric heads and the differences between the average observed and calculated heads at the bottom of the 381 wells. The second polynomial regression equation was used to construct this graph for the mines studied in this research. Note that the difference between heads is not error, but the difference between the heads at the wells after mine closes and the measured head during mining activity.
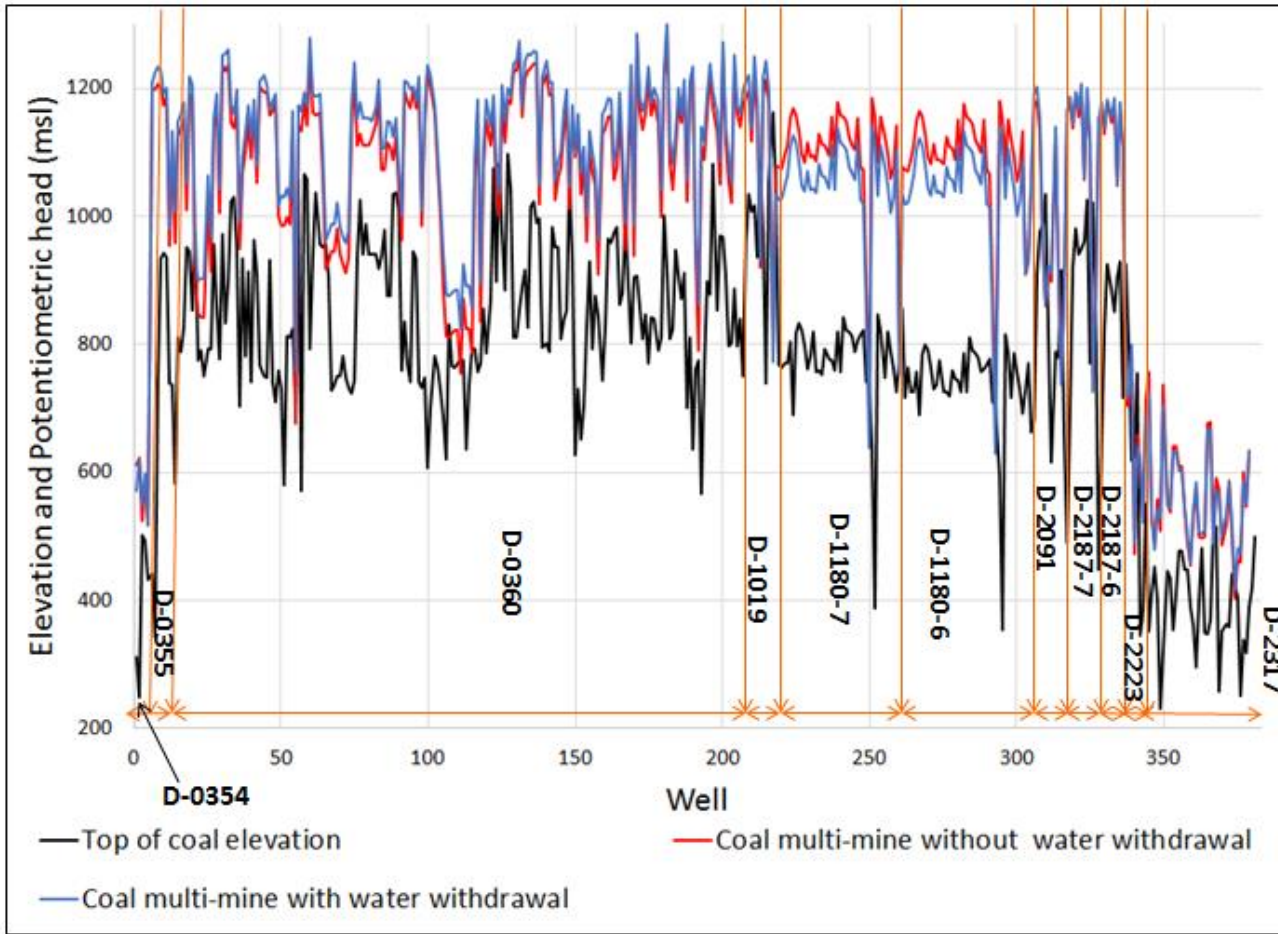
Figure 8.6. Average calculated heads at the bottom of the mined coal layer in each mine after mine closure using the two modeling approaches and the top of the coal layer. The Figure shows that all the mines considered in this study will develop mine pools because the water heads are higher than the top of the coal.

CHAPTER 9: CONCLUSION AND RECOMMENDAATION

For the Meigs Mine groundwater modeling, correlation of the water potentiometric maps for each aquifer was compared with the elevation of the upper contact of the formation hosting the aquifer. These maps were inversely correlated and areas of the aquifer that have the highest elevation have the lower potentiometric head and the areas with lower elevation have the highest potentiometric head. This indicates that groundwater flow towards the southern part of the model (Ohio River) under normal conditions. However, in our modeling results, water flows away from the Ohio River. This is due to the pumping during mining activities and the filling of the mine cavity during recovery of the hydrogeological regime after the mine closes. This should be a temporary situation and the flow regime should return towards the river when the system finally stabilizes.

For the steady state models, lithological units in the model have very high hydraulic conductivities, higher than those expected for the sandstones, shales and coals. These results are consistent with highly fractured rocks and secondary permeability due to the exploitation of the coal. A network of fractures that rapidly transport groundwater flow could probably be present even when the matrix rocks have low permeability's. The relative fast water flow in the modeled rocks is also supported by transient data analysis work of the response of water elevation within the mines to precipitation. A flow velocity of 2.4 feet/day is consistent with highly fractured rocks and secondary permeability.

Lithological units (shale 4, shale 5 and aquifer C) closer to the mined coal were very sensitive to the model when their hydraulic conductivity values were increased or decreased in both steady-and transient state simulations. aquifer C (sandstone) has a very

unusually high hydraulic conductivity of 14 feet/day in the more realistic transient model, and a channel like shape due to its variable thickness within the catchment area. The shale layer at the bottom of the coal layer had an unusually high hydraulic conductivity in all the models.

The transient model was then run for a total of 4 years (January 2004 to December 2007) to simulate the evolution of the potentiometric head (free recovery of the water levels). During the transient simulation hydraulic conductivity values for the lithologies were decreased. The hydraulic conductivity values obtained during the first model were too high because water pumping in the mine was not simulated. The more reliable parameters obtained in the transient simulations suggest that the rocks closer to the mine void present very high hydraulic conductivities compared with normal ranges of hydraulic conductivity for each kind of rock. This is consistent with the great perturbation in the mine zone produced by the explosives and fracturing of the rocks and coal.

For the artificial neural networks simulations of the potentiometric head as function of the different parameters collected in this work, the most significant variables were surface elevation, bottom of well elevation, thickness of sandstones, limestone, and shales, average annual precipitation, neighboring underground mined area and accumulative coal volume. The thickness of the mined coal and the total thickness of coal layers in the boreholes were the least significant variables that often were not included in the regression equation. The average parameters without water withdraw regression equation as seen in Table 8.7 is the best equation that will aid in the prediction of the potentiometric heads. The reason is that the regressions are good because there was more

data. Water withdraw data are sometimes not reported but the extracted coal is reported by law.

The thickness of the sandstones, shales and coal are significant variables that contributed to the generation of the regression equation that will be used in the prediction of potentiometric heads. Hydraulic conductivity values of the sandstones, shales and coal were also significant in the MODFLOW modeling. The model was very sensitive to these variables.

Recommendations to improve prediction models include changing regulations such that parameters such as water withdraw pumping rates and location of the pumps should be reported by law, also a detailed program of periodic monitoring of water elevation in wells should be established by each mining company.

REFERENCES

Anderson, M.P., and Woessner, W.W., 1992, Applied Groundwater Modeling Simulation of flow and advective transport, academic press. San Diego, California.

Akcil, A., and Koldas, S., 2006, Acid Mine Drainage (AMD): causes, treatment and case studies J. Clean. Prod., 14 (2006), pp. 1139-1145.

Austin, M.E., 1965, Land resource regions and major land resource areas of the United States. U.S. Dep. Agric. Handb. 296.

Aznarte, J.L.M., Benitez, S.J.M., and Lugilde, D.N., 2007, Forecasting airborne pollen concentration time series with neural and neuro-fuzzy models. Expert Syst. Appl. 32, 1218-1225.

Baratti, R., Cannas, B., Fanni, A., Pintus, M., Sechi, G.M., and Toreno, N., 2003, River flow forecast for reservoir management through neural networks. Neurocomputing 55: 421–437.

Borch, M.A., 2008, Flooding Conditions in the Meigs Mine Pool Complex. Ohio Department of Natural Resources, Division of Mineral Resources Management. Ohio.

Bowman, J., and Johnson, K., 2015, Stream Health Report – An evaluation of water quality, biology, and acid mine drainage reclamation in five watersheds: Raccoon Creek, Monday Creek, Sunday Creek, Huff Run, and Leading Creek: http://www.watersheddata.com/userview_file.aspx6 (accessed July 2017).

Brown, H., Skousen, J., and Renton, J., 1994b, Volume and composition of flocs from chemical neutralization of acid mine drainage. Green lands 24 (1): 33-51.

Civil and Environmental Consultants, Inc., 2005. Meigs No. 2 and Meigs No.31 Mines:

Mine Drainage Handling and Treatment Feasibility Study, unpublished report.

Crowell, D. L., 1995, History of the coal-mining industry in Ohio: Ohio Division of Geological Survey Bulletin 72, 204 p. (Accessed April 2017).

Crowell, D. L., 1997b, History of coal mining in Ohio: Ohio Division of Geological Survey GeoFacts 14. (Accessed April 2017).

Currie, R.J., 1999, Identification of Ecosystem Stressors in Developing an Enhancement Plan for the Leading Creek Watershed, Meigs County, Ohio.Virginia Tech. Doctoral Thesis presented to the Department of Biology. <http://scholar.lib.vt.edu/theses/available/etd-042299-053420

Ferguson, H. F., 1974, Geological observations and geotechnical effects of valley stress relief in the Allegheny plateau. ASCE National Meeting on Water Resources, Los Angeles, CA, 1974.

Fetter, C., 2001, Applied hydrogeology: Fourth Edition. Upper Saddle River, New Jersey: Prentice-Hall, Inc. pp. 40-47, 81-89, 307.

Franz, T., and Guiger, N., 1990, FLOWPATH, two –dimensional horizontal aquifer simulation model.Waterloo hydrogeologic software, Waterloo, Ontario.

Freeze, R.A., and Cherry, J.A., 1979, Groundwater. Prentice-Hall, Inc., England Cliffs, New Jersey, p.190.

Gopalsamy, K., 2004, Stability of artificial neural networks with impulses. Applied Mathematics and Computation, v. 154, p. 783-813, doi: 10.1016/S0096-3003(03)00750-1

Heiat, A., 2002, Comparison of artificial neural network and regression models for estimating software development effort. Information and Software Technology. v44 i15. 911-922.

Hunt, B., 1999, Unsteady stream depletion from ground-water pumping, Ground Water, 37(1), 98 – 102.

Ince, R., 2004, Prediction of fracture parameters of concrete by artificial neural networks. Engng Fract Mech ;71:2143–59.

Kendorski, F.S., 1993, Effect of High-Extraction Coal Mining on Surface Subsidence and Ground Water, Proceedings 12th Conference on Ground Control in Mining, West Virginia University, Morgantown, WV.

Khadri, S.F.R., and Chaitanya, P., 2016, Ground water flow modeling for calibrating steady state using MODFLOW software: a case study of Mahesh River basin, India. Model Earth Syst Environ 2:39. doi: 10.1007/s40808-015-0049-7

Kissi, O., 2004, River flow modelling using artificial neural networks. Journal of hydrologic Engineering 9, 60-63. Doi: 10.1061/ (ASCE) 1084-0699(2004)9:1(60)

Kruse, N .A., Derose, L., Korenowsky, R., Bowman, J., R., Lopez, D.L., Johnson, K.s., and Rankin, E., 2013, The role of remediation, natural alkalinity sources and physical stream parameters in stream recovery. Journal of Environmental Management.128 (2013) 1000-1011.

Maier, H.R., and Dandy, G.C., 2000, Neural networks for the prediction and forecasting of water resources variables: a review of modelling issues and applications. Environmental Modelling and Software 15, 101-124. doi: 10.1016/S1364-8152(99)00007-9

McDonald, M.G., and Harbaugh, A.W., 1998, A modular three-dimensional finite

    difference   ground-water flow model, U.S.G.S. Techniques of Water-Resources

    Investigations, Book 6 chapter A1, 586pp.

Meigs county Ohio, 2017, Online auditor: http://meigscountyauditor.org/Search.aspx

    (Accessed November 2017).

Mine Safety and Health Administration, 2018, Mine data retrieval system:

    https://arlweb.msha.gov/drs/drshome.htm (Accessed March 2018).

Moody and Associates, Inc., 2006, A Probable Hydrologic Consequence (PHC)

    Statement, unpublished report prepared for CONSOL Energy and ODNR

    DMRM.

ODNR, 2011, A Citizen's Guide to Mining and Reclamation in Ohio, Ohio Department

    of Natural Resources Division of Mineral Resources Management,

    www.ohiodnr.com/portals/11/publications/pdf/citizens_guide.pdf (Accessed:

    April 2018).

Ohio Division of Geological Survey, 2006, Bedrock geologic map of Ohio: Ohio

    Department of Natural Resources, Division of Geological Survey Map BG-1,

    generalized page-size version with text, 2 p., scale 1:2,000,000 (Accessed May

    2017).

Ohio Division of Geological Survey, 2012, Abandoned underground mines of Ohio: Ohio

    Department of Natural Resources, Division of Geological Survey Map EG-3,

    generalized page-size version with text, scale 1:2,000,000, 2 p. (Accessed June

    2017).

Ohio Environmental Protection Agency, Public Interest Center, 2005, News Releases: Ohio EPA and Ohio Power Company Reach Agreement on Two Environmental Projects. http://www.epa.state.oh.us/pic/nr/2005/january/ohiopow2.html

Recknagel, F., French, M., Harkonen, P., Yabunaka, K.I., 1997, Artificial neural network approach for modelling and prediction of algal blooms. Ecological Modelling 96, 11-28. doi:10.1016/S0304-3800(96)00049-X

Sánchez, M.J.A., Galán, C., Martínez, J.A., and Hervás, C., 2002, The use of a neural network to forecast daily grass pollen concentration in a Mediterranean region: the southern part of the Iberian Peninsula. Clin Exp Allergy 32:1606–1612.

Schaap, M. G., Leij, F. J., Van Genuchenten, M.T., 1998, Neural Network Analysis for Hierarchical Prediction of Soil Hydraulics Properties. Soil Science Society of America Journal 62, 845-855.

Schafer, L., 2018, Statistical analysis of mining parameters to create empirical models to predict mine pool formation in underground coal mines [Master thesis]: Ohio University.

Skousen, J., Simmons, J., and Ziemkiewicz, P., 2002, Acid-base accounting to predict post-mining drainage quality on surface mines. J. Environ. Qual. 31(6): 2034-2044.

Siplivy, William, P.E. Inc., 2004. Mine Pool Audit, Meigs No. 2 and No. 31 Mines, January 2005 – unpublished report.

Sozen, A., and Arcakliolu, E., 2005, Solar potential in Turkey, Applied Energy, v. 80, no. 1, p.35–45.

Tan, A.H., and Pan, H., 2005, Predictive neural networks for gene expression data analysis. Neural Network. 18, 297–306.

United States Department of Justice, 1996.Southern Ohio Coal Company to Restore Ohio River Tributaries Devastated by Discharges of Mine Wastes. <http://www.usdoj.gov/opa/pr/1996/February96/034.txt (Accessed March 2018).

USEIA, 2002, Coal Disposition, Number of Mines, and Average Price, by State and County, 2000. <http://www.eia.doe.gov/cneaf/coal/cia/html/tb184p01p2.html> (Accessed April 2018).

United States Environmental Protection Agency, 2018, National Pollutant Discharge Elimination System (NPDES): https://www.epa.gov/npdes (Accessed April 2018).

USDA-NRCS, 1991, Soil Survey Report for Meigs County, Ohio: Web Soil Survey. http://websoilsurvey.nrcs.usda.gov/app/. (Accessed: January 2018).

Venkatasubramanian, V., Rengaswamy, R., and Kavuri, S.N., 2003, A review of process fault detection and Diagnosis Computers and Chemical Engineering, 27 (2003), pp. 293-311.

Walker J.A., 1975, The stratigraphic and facies relationships of selected road cuts in Coshocton, Guernsey, and Tuscarawas Counties, Ohio, M.S. Thesis, Ohio University, Athens, p.82.

Wickstrom, L.H., Venteris, E.R., and Harper, J.A., 2005, Characterization of geologic sequestration opportunities in the MRCSP region: Final report under DOE cooperative agreement DE-PS26-05NT42255,p. 152.

Wyrick, G.G., and Borchers, J.W., 1981, Hydrologic effects of stress-relief fractures in an Appalachian valley, USGS Water-Supply Paper 2177.

Yu, B., Lam, W. H., and Tam, M. L., 2011, Bus arrival time prediction at bus stop with multiple routes. Transportation Research Part C: Emerging Technologies, 19(6), 1157-1170.

Zheng, C., and Bennett, G.,1995, Applied contaminant transport modeling, van nostrand reinhold, New York.

APPENDIX A: LITHOLOGICAL CONTACT MAPS

Table A.1 shows the lithological contact elevations for the 30 boreholes of the Meigs Mine Complex.

Borehole ID	X	Y	Surface Elevation	Shale/Sandstone Contact Elevation 1	Sandstone/shale contact Elevation 2	Shale/Sandstone contact Elevation 3	Sandstone/Shale contact Elevation 4	Shale/Sandstone contact Elevation 5	Sandstone/shale contact elevation 6	Shale/coal contact elevation 7	Coal/Shale contact Elevation 8
1816	2049634	394966	799.6	744.1	689.3	635.0	613.1	585.1	528.9	504.3	497.6
774	2068674	418212	654.1	593.3	575.6	501.8	485.4	478.1	468.2	439.9	434.9
790	2068322	414346	747.4	604.1	585.9	560.5	552.5	476.0	472.6	457.1	452.9
1828	2068550	424475	649.0	574.5	570.0	550.0	540.0	476.0	470.0	434.0	428.8
1561	2067840	399716	770.0	650.3	643.2	588.0	574.2	567.5	515.4	432.7	428.8
1566	2061055	397936	686.5	630.4	623.4	614.2	602.3	585.2	545.6	456.0	451.3
1570	2067016	398279	623.0	571.4	512.1	497.5	468.3	453.7	435.5	422.2	417.6
1572	2069760	398395	612.5	556.3	490.3	458.7	453.5	424.9	413.1	395.9	390.9
1574	2073305	398078	749.7	626.5	616.4	606.8	568.4	541.9	527.6	388.5	385.6
1576	2061776	396692	693.2	622.0	585.9	568.1	526.8	482.9	472.6	446.3	441.6
1578	2064775	396769	738.8	708.2	684.5	570.2	511.5	461.6	435.1	428.7	423.9
1580	2067755	396710	706.5	669.7	646.7	482.8	458.9	435.2	421.1	408.0	403.3
1587	2064118	395419	772.6	744.9	730.3	547.8	520.4	445.6	420.3	408.2	403.3
A-266	2054342	396585	687.2	588.4	574.1	566.6	542.5	520.5	493.4	472.9	468.4
A-992	2056740	393803	671.7	613.0	595.7	586.5	564.8	494.1	461.9	460.5	455.7
A-637	2068900	379155	841.9	692.2	653.1	571.1	505.7	434.5	387.7	366.9	360.3
A-1218	2068988	374742	766.8	700.0	655.9	605.2	450.4	431.4	398.6	374.9	370.8
A-1235	2069007	372153	786.8	746.3	720.5	670.3	631.1	561.7	431.7	356.7	352.1
1830	2064880	423953	656.0	596.0	592.0	550.0	545.0	524.2	517.1	497.1	493.1
916	2072218	410363	778.9	678.8	618.7	566.8	539.8	425.8	415.1	406.0	397.6
A-208	2075437	379143	728.1	661.1	623.5	600.2	448.9	406.0	365.8	344.4	340.2
A-482	2051789	388351	692.0	632.6	626.5	623.5	618.4	587.3	511.1	486.8	482.5
A-271	2056442	389332	723.6	567.2	553.2	516.9	510.5	501.5	484.6	464.4	459.7
787	2072141	413025	723.0	674.0	624.6	609.8	603.8	558.7	548.5	448.9	447.8
A-1266	2066198	365568	836.7	689.7	658.7	612.6	565.4	515.4	384.6	373.1	369.1
A-1231	2075375	371814	889.6	630.2	619.1	554.1	539.0	507.9	356.7	321.8	317.3
1750	2075119	404472	741.9	669.0	583.2	556.6	540.5	528.9	503.1	410.8	407.1
A-1121	2061156	375129	772.3	651.5	605.7	598.8	501.1	488.4	419.6	408.0	403.8
A-1259	2062069	368218	792.3	718.7	686.9	669.8	660.1	642.7	418.0	392.1	387.6
Testhole	2048867	386061	721.7	666.9	659.0	607.7	591.1	565.5	515.4	496.5	491.9

Figure A.1 Map of Shale/Sandstone contacts 1 with a contour interval of 10 feet.
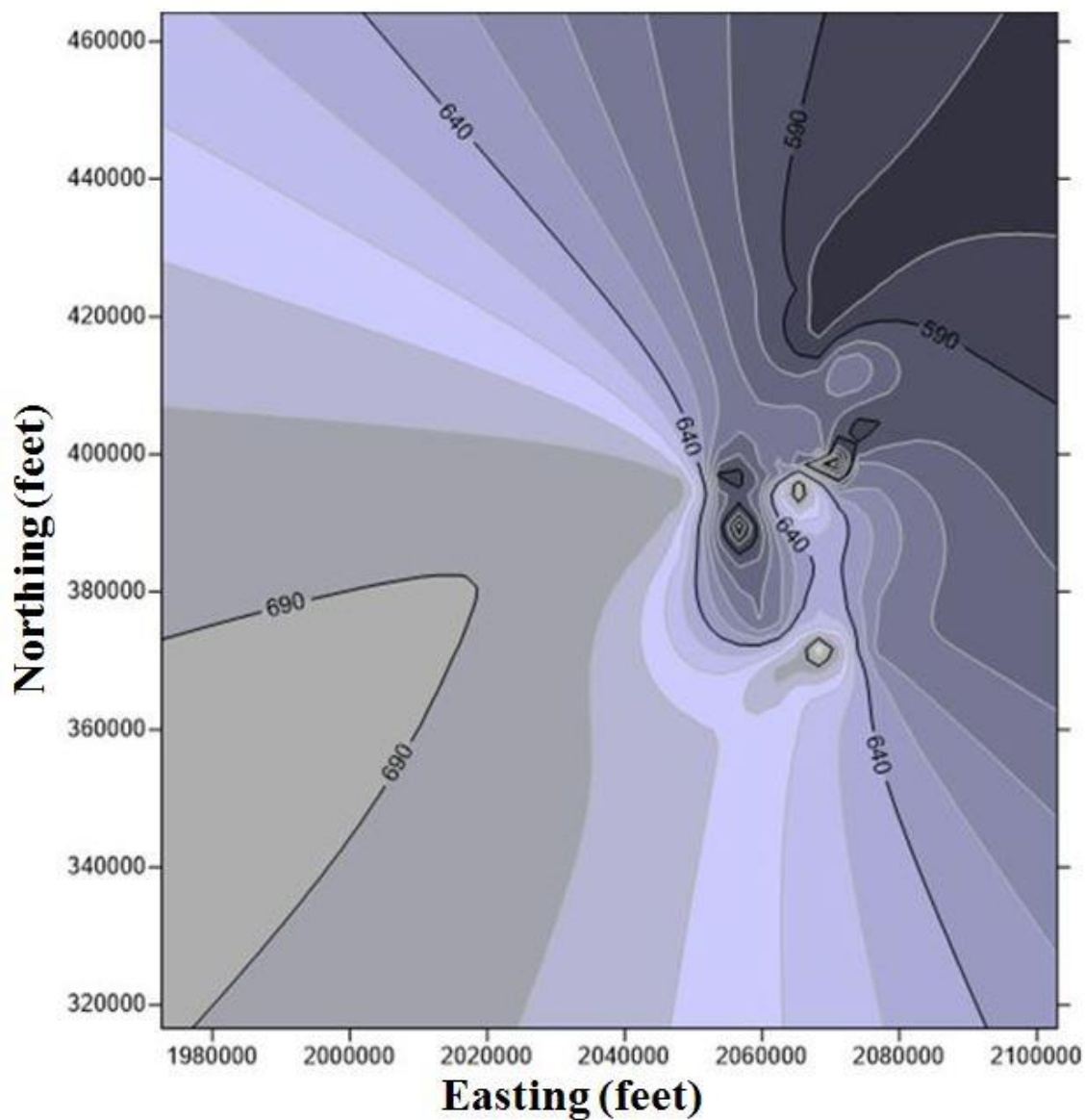
Figure A.2. Map of Sandstone/Shale contact 2 with a contour interval of 10 feet.
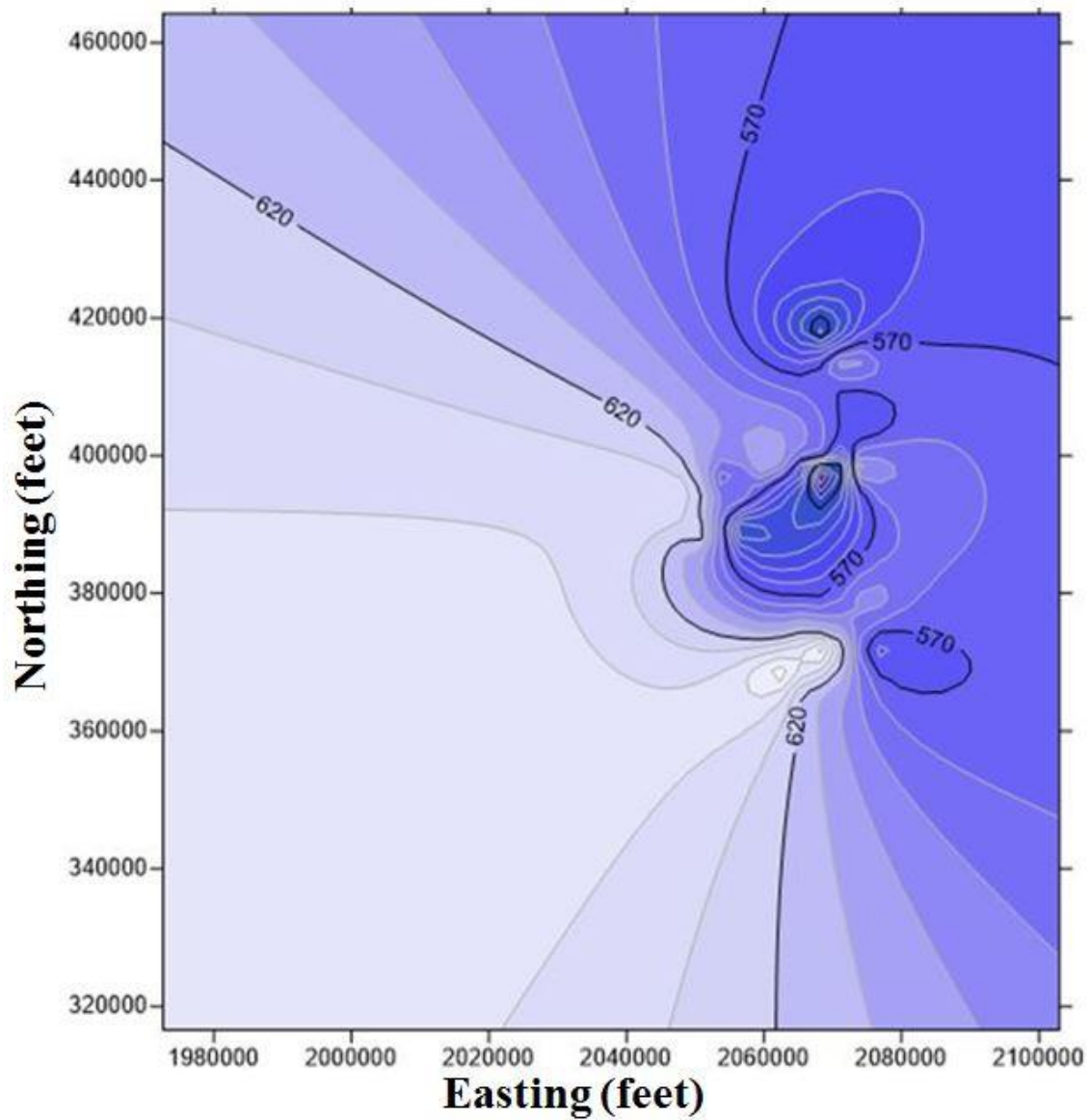
Figure A.3 Map of Shale/Sandstone contact 3 with a contour interval of 10 feet.
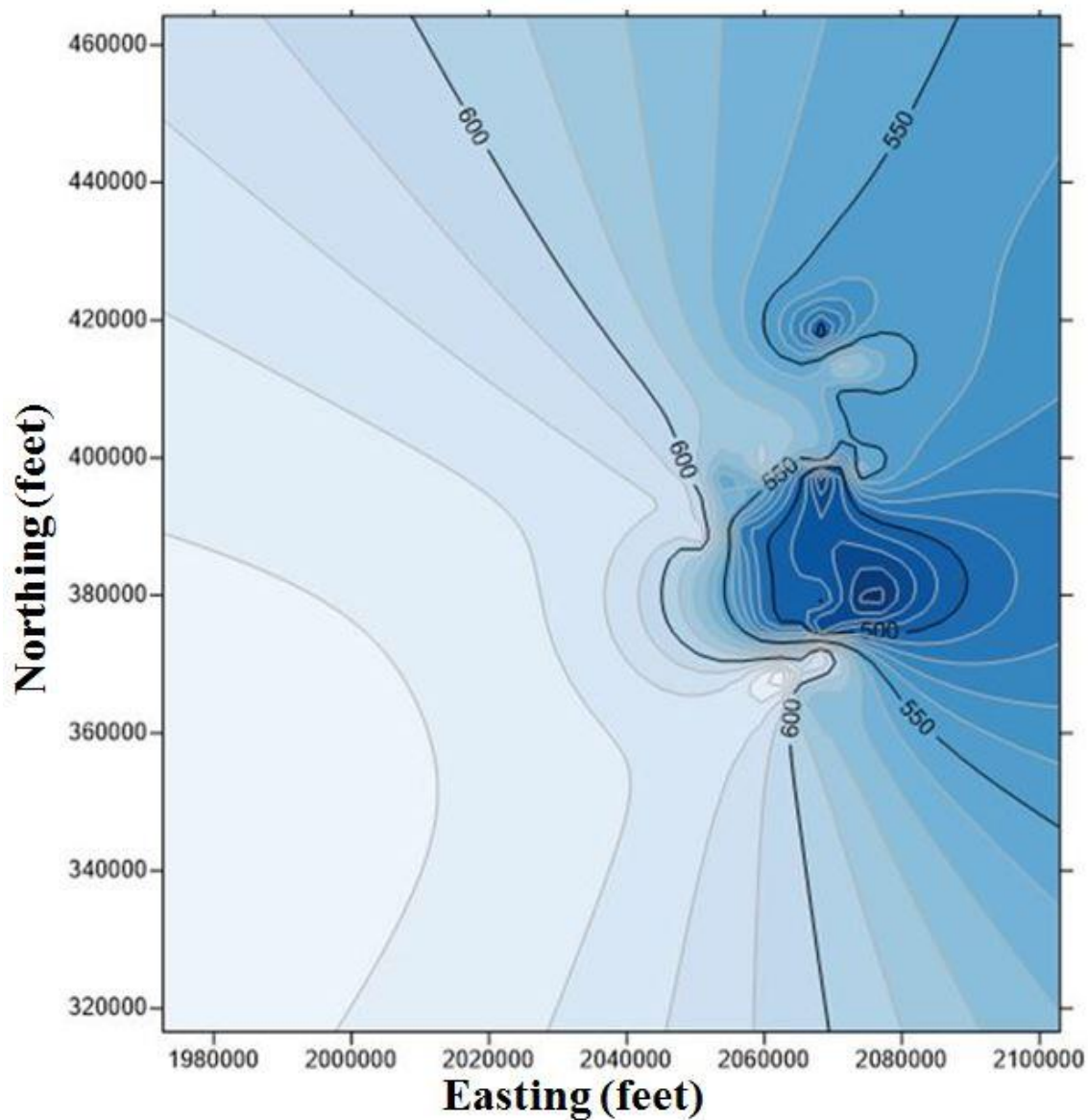
Figure A.4. Map of Sandstone/Shale contact 4 with a contour interval of 10 feet.
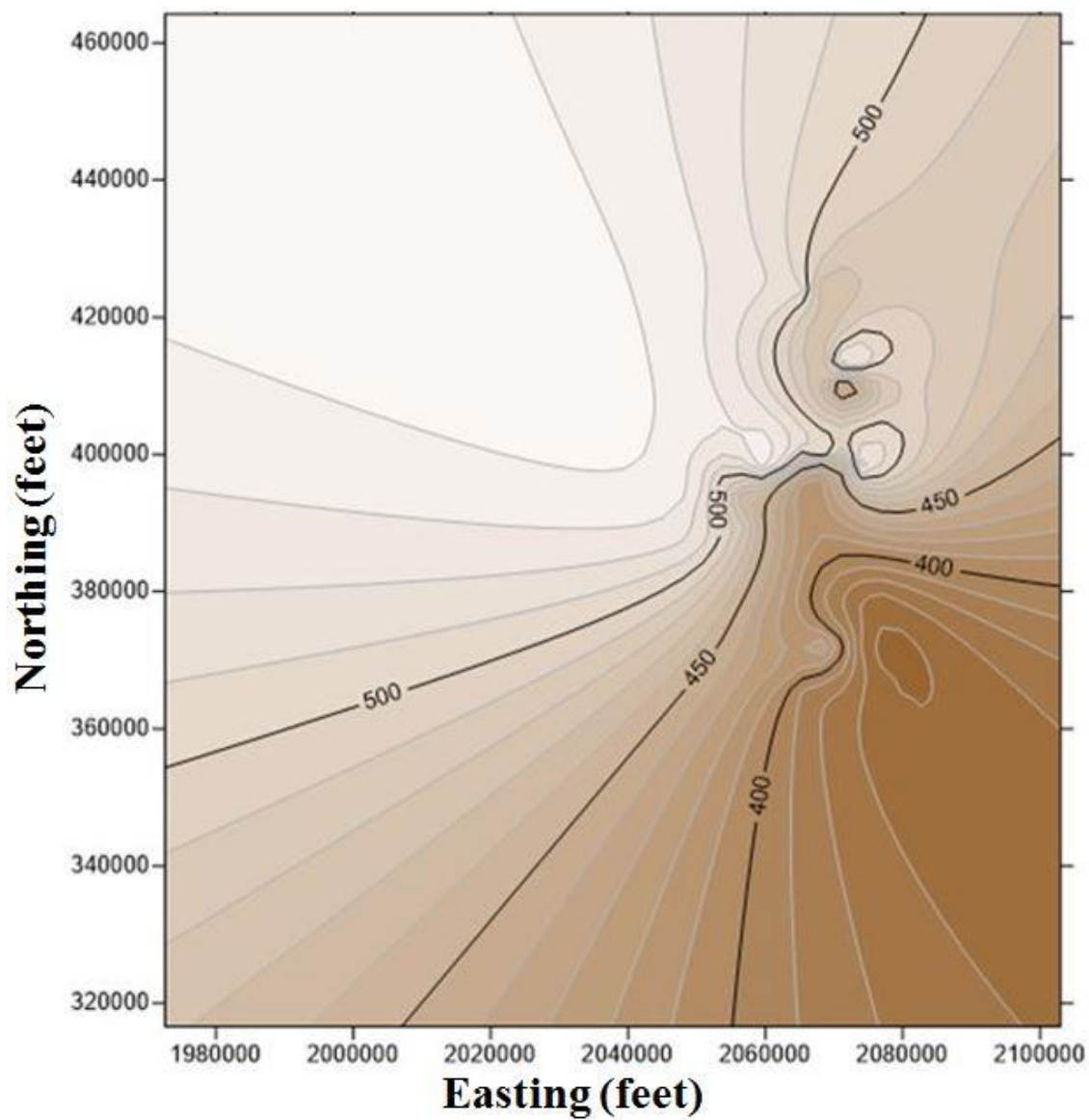
Figure A.5. Map of Sandstone/Shale contact 6 with a contour interval of 10 feet.
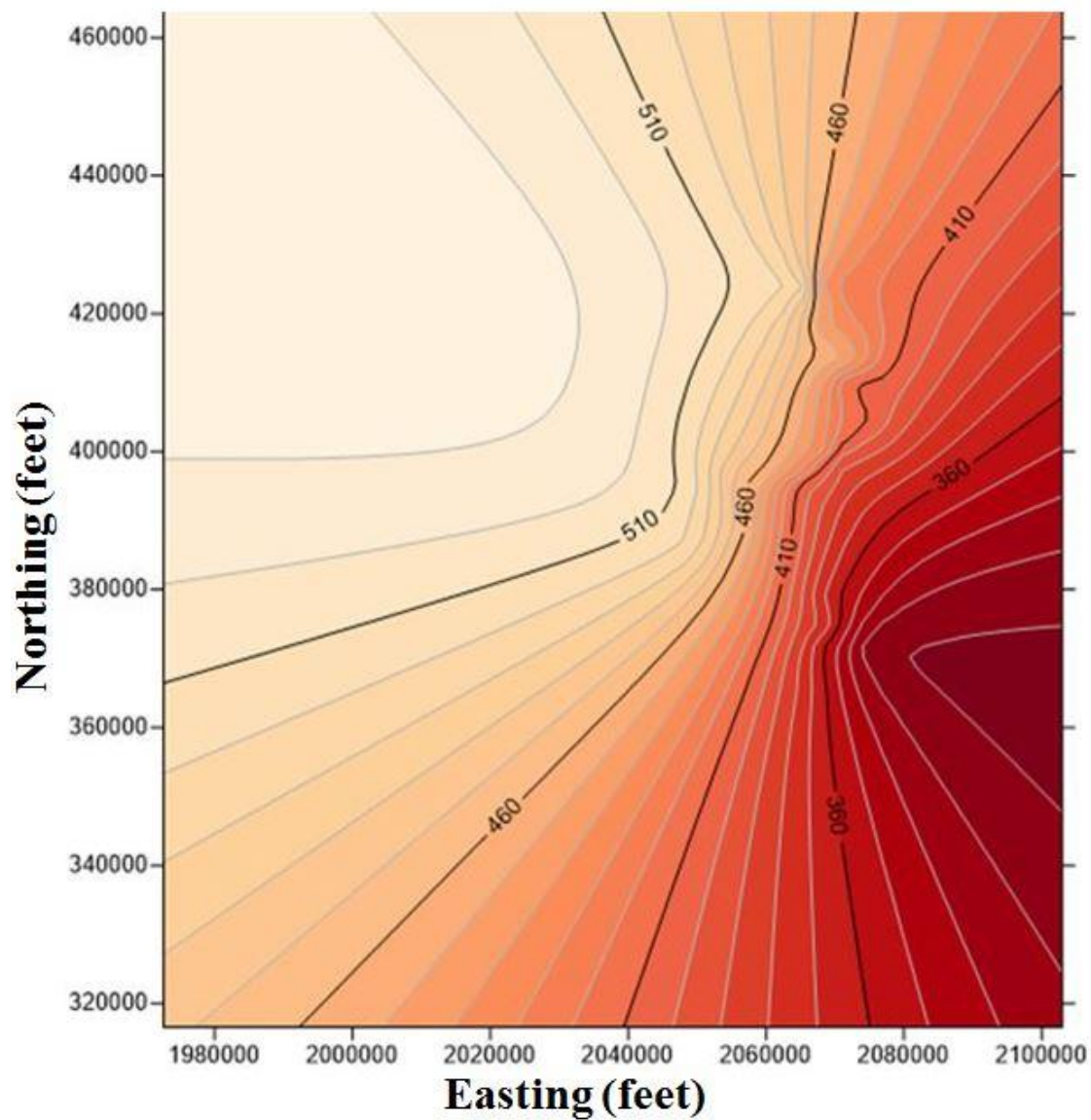
Figure A.6. Map of Shale/Coal contact 7 with a contour interval of 10 feet.
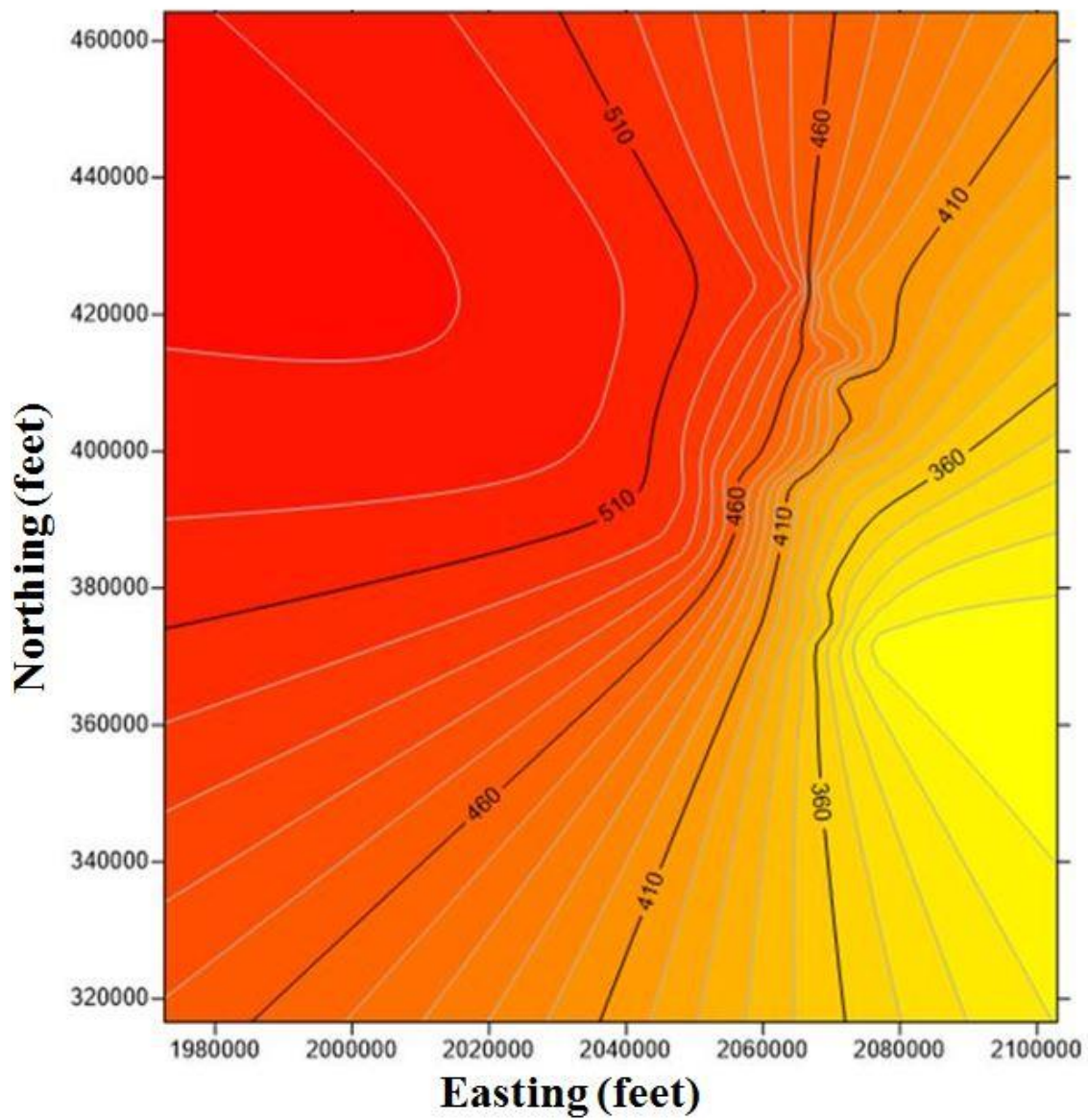
Figure A.7. Map of Coal/shale contact 8 with a contour interval of 10 feet.

APPENDIX B: PARAMETERS FOR THE SIX POST MINING MONITORING SHAFTS

Table B.1 NE Post Mining Monitoring Shaft for the Meigs Mine Complex.

3rd North East Intake Shaft					
new 3-13-07 pipe top - 647.54'					
floor elevation- 438.81'					
total depth- 208.7' (560)					
Date	to water	elevation	Time	Precipitation	Acc PP
11-21-03	189.3	460.06		2.89	2.89
12-23-03	185.4	463.96		2.78	5.67
1-22-04	179.5	469.86	22	5.08	10.75
2-17-04	173.8	475.56	49	2.02	12.77
3-18-04	164.5	484.86	78	3.27	16.04
4-16-04	155.2	494.16	107	3.96	20
5-19-04	143.8	505.56	140	5.93	25.93
6-17-04	135.9	513.46	169	5.34	31.27
7-12-04	127.1	522.26	194	5.6	36.87
8-18-04	121.4	527.96	231	3.43	40.3
9-16-04	121.6	527.76	264	2.98	43.28
10-19-04	120.9	528.46	293	3.33	46.61
11-17-04	121.1	528.26	322	4.12	50.73
12-17-04	121	528.36	352	3.36	54.09
1-21-05	119.9	529.46	386	8.95	63.04
2-17-05	118.8	530.56	414	1.27	64.31
3-18-05	117.8	531.56	443	3.53	67.84
4-14-05	116.7	532.66	470	4.36	72.2
5-18-05	115.2	534.16	504	3.36	75.56
6-15-05	113.8	535.56	532	2.69	78.25
7-18-05	112.9	536.46	565	1.79	80.04
8-16-05	112.2	537.16	594	5.09	85.13
9-14-05	111.8	537.56	623	2.91	88.04
10-14-05	111.4	537.96	653	1.33	89.37
11-17-05	111.1	538.26	688	3.31	92.68
12-20-05	110.4	538.96	720	1.67	94.35
1-18-06	109.7	539.66	749	2.67	97.02
2-17-06	109.1	540.26	779	1.36	98.38
3-15-06	108.3	541.06	805	3.48	101.86

Cont'd

4-18-06	107.1	542.26	839	2.52	104.38
5-17-06	106	543.36	868	3.25	107.63
6-14-06	105.5	543.86	896	4.3	111.93
7-20-06	104.1	545.26	932	5.77	117.7
8-18-06	103.1	546.26	961	2.94	120.64
9-19-06	101.7	547.66	993	5.35	125.99
10-18-06	100.5	548.86	1022	6.7	132.69
11-21-06	98.9	550.46	1056	2.12	134.81
12-15-06	96.5	552.86	1080	3.18	137.99
1-16-07	95.3	554.06	1112	4.25	142.24
2-19-07	92.6	556.76	1146	2.06	144.3
3-13-07	90.7	556.84	1168	6.67	150.97
4-18-07	88.2	559.34	1204	2.31	153.28
5-18-07	87.1	560.44	1237	1.4	154.68
6-18-07	85.8	561.74	1265	2.78	157.46
7-20-07	84.9	562.64	1297	3.02	160.48
8-21-07	83.9	563.64	1329	4.73	165.21
9-21-07	83.2	564.34	1360	2.53	167.74
10-18-07	82.3	565.24	1387	3.58	171.32
11-21-07	81.8	565.74	1421	2.18	173.5
12-28-07	81	566.54	1458	4.34	177.84
1-31-08	80.32	567.22		1.64	179.48
2-28-08	81.09	566.45		3.88	183.36
3-28-08	79.73	567.81		7.58	190.94
4-24-08	78.78	568.76		2.16	193.1
5-29-08	79.59	567.95		3.14	196.24
6-26-08	79.91	567.63		10.39	206.63
7-31-08	80.14	567.4		1.65	208.28
8-28-08	80.06	567.48		3.73	212.01
9-25-08	79.71	567.83		2.5	214.51
10-30-08	79.25	568.29		1.44	215.95
11-20-08	79.37	568.17		2.49	218.44
12-18-08	79.59	567.95		4.84	223.28
1-22-09	78.84	568.7		2.73	226.01
2-19-09	78.32	569.22		1.93	227.94

Cont'd

3-27-09	78.4	569.14		1.15	229.09
4-30-09	78.1	569.44		4.23	233.32
5-28-09	77.25	570.29		2.42	235.74
6-24-09	77.14	570.4		3.44	239.18
7-29-09	77.14	570.4		4.9	244.08
8-26-09	77.44	570.1		3.27	247.35
9-2-09	77.61	569.93		2.5	249.85
10-28-09	79.37	568.17		4.89	254.74
11-25-09	81.03	566.51		0.42	255.16
12-30-09	83.03	564.51		3.6	258.76
1-28-10	83.51	564.03		2.22	260.98
2-24-10	82.95	564.59		2.42	263.4
3-31-10	82.47	565.07		2.75	266.15
4-28-10	82.13	565.41		2.51	268.66
5-26-10	81.8	565.74		3.89	272.55
6-30-10	81.14	566.4		5.38	277.93
7-28-10	80.92	566.62		6.01	283.94
8-25-10	82.32	565.22		2.23	286.17
9-29-10	82.64	564.9		1.66	287.83
10-27-10	83.12	564.42		1.54	289.37
11-24-10	83.9	563.64		4.34	293.71
12-29-10	84.26	563.28		1.26	294.97
1-26-11	84.25	563.29		1.47	296.44
2-23-11	84.95	562.59		4.25	300.69
3-30-11	83.72	563.82		4.58	305.27
4-28-11	82.83	564.71		7.14	312.41
5-25-11	82.39	565.15		5.9	318.31
6-30-11	82.42	565.12		3.03	321.34
7-20-11	82.3	565.24		5.67	327.01
8-17-11	82.84	564.7		2.48	329.49
9-28-11	83	564.54		6.55	336.04
10-26-11	83.41	564.13		3.68	339.72
11-23-11	83.69	563.85		4.77	344.49
12-21-11	83.1	564.44		5.44	349.93
1-4-12	83.46	564.08		3.82	353.75
2-8-12	82.91	564.63		1.89	355.64

Cont'd

3-22-12	82.31	565.23		4.92	360.56
4-18-12	82.04	565.5		3.6	364.16
5-30-12	81.39	566.15		2.3	366.46
6-27-12	82.36	565.18		2.01	368.47
7-12-12	82.58	564.96		2.54	371.01
8-29-12	83.15	564.39		1.8	372.81
9-26-12	84.66	562.88		3.97	376.78
10-24-12	85.32	562.22		4.06	380.84
11-21-12	85.64	561.9		0.66	381.5
12-19-12	86.03	561.51		5.7	387.2
1-23-13	86.2	561.34		2.25	389.45
2-20-13	85.24	562.3		1.82	391.27
3-20-13	84.59	562.95		3.12	394.39
4-17-13	84.3	563.24		3.66	398.05
5-29-13	83.9	563.64		0.94	398.99
6-26-13	83.82	563.72		4.46	403.45
7-30-13	84.23	563.31		6.87	410.32
8-28-13	83.81	563.73		2.84	413.16
9-26-13	84.28	563.26		2.52	415.68
10-23-13	84.4	563.14		5.91	421.59
11-19-13	85.19	562.35		2.18	423.77
12-18-13	85.12	562.42		4.3	428.07
1-22-14	84.23	563.31		2.4	430.47
2-19-14	82.51	565.03		2.39	432.86
3-19-14	82.05	565.49		2.59	435.45
29-Apr-2014	81.3	566.24		5.47	440.92
16-May-2014	82	565.54		4	444.92
25-Jun-2014	81.08	566.46		5.29	450.21
30-Jul-2014	81.35	566.19		3.47	453.68
27-Aug-2014	81.77	565.77		4.9	458.58
24-Sep-2014	82.55	564.99		0.65	459.23
22-Oct-2014	83.03	564.51		2.77	462
19-Nov-2014	83.63	563.91		1.46	463.46
30-Dec-2014	84.82	562.72		2.7	466.16
28-Jan-2015	85.15	562.39		2.69	468.85
25-Feb-2015	84.42	563.12		1.7	470.55

Cont'd

25-Mar-2015	83.15	564.39	3.92	474.47
30-Apr-2015	79.93	567.61	4.09	478.56
26-May-2015	78.6	568.94	3.56	482.12
25-Jun-2015	77.62	569.92	6.72	488.84
9-Jul-2015	77.05	570.49	5.41	494.25
28-Aug-2015	76.21	571.33	3.59	497.84
21-Sept-2015	74.84	572.7	3.21	501.05
10-Oct-2015	74.19	573.35	2.68	503.73
11-Nov-2015	73.45	574.09	2.37	506.1
7-Dec-2015	72.7	574.84	4.88	510.98
4-Jan-2016	72.21	575.33	1.12	512.1
1-Feb-2016	70.85	576.69	3.29	515.39
1-Mar-2016	68.95	578.59	4.27	519.66
4-Apr-2016	66.37	581.17	2.31	521.97
5-May-2016	64.5	583.04	2.74	524.71
13-Jun-2016	63.24	584.3	5.22	529.93
7-Jul-2016	62.3	585.24	2.49	532.42
8-Aug-2016	61.12	586.42	5.82	538.24
8-Sep-2016	60.1	587.44	4.68	542.92
5-Oct-2016	59.39	588.15	1.73	544.65

Table B.2 Grange Seal Post Mining Monitoring Shaft for the Meigs Mine Complex.

Mine 2 NE Seals (grange)					
new 3-13-07 735.03' elevation					
Critical Elevation 560'					
Date	to water	Elevation	Time	Precipitation	Accumulated precipitation
11-21-03	242.1	493.14		2.89	2.89
12-23-03	241	494.24		2.78	5.67
1-22-04	239.8	495.44	22.00	5.08	10.75
2-17-04	239.4	495.84	49.00	2.02	12.77
3-18-04	238.1	497.14	78.00	3.27	16.04
4-16-04	237.2	498.04	107.00	3.96	20
5-19-04	235.9	499.34	140.00	5.93	25.93
6-17-04	234.8	500.44	169.00	5.34	31.27
7-12-04	233.6	501.64	194.00	5.6	36.87
8-18-04	232.2	503.04	231.00	3.43	40.3
9-17-04	231.1	504.14	264.00	2.98	43.28
10-19-04	230.5	504.74	293.00	3.33	46.61
11-17-04	229.7	505.54	322.00	4.12	50.73
12-17-04	228.7	506.54	352.00	3.36	54.09
1-20-05	226.8	508.44	386.00	8.95	63.04
2-17-05	225.1	510.14	414.00	1.27	64.31
3-18-05	223.8	511.44	443.00	3.53	67.84
4-14-05	222.2	513.04	470.00	4.36	72.2
5-18-05	219.9	515.34	504.00	3.36	75.56
6-15-05	217.8	517.44	532.00	2.69	78.25
7-18-05	216.1	519.14	565.00	1.79	80.04
8-16-05	215.1	520.14	594.00	5.09	85.13
9-14-05	213.8	521.44	623.00	2.91	88.04
10-14-05	212.8	522.44	653.00	1.33	89.37
11-17-05	212.1	523.14	688.00	3.31	92.68
12-20-05	211	524.24	720.00	1.67	94.35
1-18-06	209.8	525.44	749.00	2.67	97.02
2-17-06	208.7	526.54	779.00	1.36	98.38
3-15-06	207.2	528.04	805.00	3.48	101.86
4-18-06	205.1	530.14	839.00	2.52	104.38
5-17-06	203.6	531.64	868.00	3.25	107.63
6-14-06	202.4	532.84	896.00	4.3	111.93

Cont'd

7-20-06	200.4	534.84	932.00	5.77	117.7
8-18-06	199.1	536.14	961.00	2.94	120.64
9-19-06	197.8	537.44	993.00	5.35	125.99
10-18-06	196.6	538.64	1022.00	6.7	132.69
11-22-06	194.9	540.34	1056.00	2.12	134.81
12-15-06	193.2	542.04	1080.00	3.18	137.99
1-16-07	191.8	543.44	1112.00	4.25	142.24
2-19-07	188.9	546.34	1146.00	2.06	144.3
3-13-07	187	548.03	1168.00	6.67	150.97
4-18-07	184.2	550.8	1204.00	2.31	153.28
5-21-07	182.4	552.63	1237.00	1.4	154.68
6-18-07	181.2	553.83	1265.00	2.78	157.46
7-20-07	180.4	554.63	1297.00	3.02	160.48
8-21-07	179.1	555.93	1329.00	4.73	165.21
9-21-07	178.4	556.63	1360.00	2.53	167.74
10-18-07	177.4	557.63	1387.00	3.58	171.32
11-21-07	176.8	558.23	1421.00	2.18	173.5
12-28-07	175.8	559.23	1458.00	4.34	177.84
1-31-08	174.92	560.11		1.64	179.48
2-28-08	176.39	558.64		3.88	183.36
3-28-08	175.25	559.78		7.58	190.94
4-24-08	173.9	561.13		2.16	193.1
5-29-08	175.02	560.01		3.14	196.24
6-26-08	175.48	559.55		10.39	206.63
7-31-08	175.72	559.31		1.65	208.28
8-28-08	175.59	559.44		3.73	212.01
9-25-08	175	560.03		2.5	214.51
10-30-08	174.38	560.65		1.44	215.95
11-20-08	174.64	560.39		2.49	218.44
12-18-08	174.75	560.28		4.84	223.28
1-22-09	173.95	561.08		2.73	226.01
2-12-09	173.72	561.31		1.93	227.94
3-27-09	173.51	561.52		1.15	229.09
4-30-09	173.32	561.71		4.23	233.32
5-28-09	172.44	562.59		2.42	235.74
6-24-09	172.4	562.63		3.44	239.18
7-29-09	172.23	562.8		4.9	244.08
8-26-09	172.78	562.25		3.27	247.35

Cont'd

9-30-09	173.2	561.83		2.5	249.85
10-28-09	175.27	559.76		4.89	254.74
11-25-09	177.55	557.48		0.42	255.16
12-30-09	180.2	554.83		3.6	258.76
1-28-10	180.82	554.21		2.22	260.98
2-24-10	180.28	554.75		2.42	263.4
3-31-10	179.94	555.09		2.75	266.15
4-28-10	179.45	555.58		2.51	268.66
5-26-10	179.02	556.01		3.89	272.55
6-30-10	178.69	556.34		5.38	277.93
7-28-10	178.39	556.64		6.01	283.94
8-25-10	179.73	555.3		2.23	286.17
9-29-10	180	555.03		1.66	287.83
10-27-10	180.5	554.53		1.54	289.37
11-24-10	181.2	553.83		4.34	293.71
12-29-10	181.55	553.48		1.26	294.97
1-26-11	181.54	553.49		1.47	296.44
2-23-11	182.19	552.84		4.25	300.69
3-24-11	181.32	553.71		4.58	305.27
4-28-11	180.5	554.53		7.14	312.41
5-25-11	179.8	555.23		5.9	318.31
6-30-11	179.4	555.63		3.03	321.34
7-20-11	179.12	555.91		5.67	327.01
8-17-11	179.7	555.33		2.48	329.49
9-28-11	179.95	555.08		6.55	336.04
10-26-11	180.5	554.53		3.68	339.72
11-23-11	180.9	554.13		4.77	344.49
12-21-11	180.44	554.59		5.44	349.93
1-25-12	180.78	554.25		3.82	353.75
2-22-12	179.64	555.39		1.89	355.64
3-7-12	180.23	554.8		4.92	360.56
4-18-12	179.33	555.7		3.6	364.16
5-30-12	178.58	556.45		2.3	366.46
6-27-12	179.75	555.28		2.01	368.47
7-12-12	180	555.03		2.54	371.01
8-29-12	180.46	554.57		1.8	372.81

Cont'd

9-26-12	180.96	554.07		3.97	376.78
10-24-12	181.44	553.59		4.06	380.84
11-21-12	181.92	553.11		0.66	381.5
12-19-12	182.35	552.68		5.7	387.2
1-23-13	182.65	552.38		2.25	389.45
2-20-13	181.81	553.22		1.82	391.27
3-20-13	181.3	553.73		3.12	394.39
4-17-13	181.02	554.01		3.66	398.05
5-29-13	180.55	554.48		0.94	398.99
6-26-13	180.38	554.65		4.46	403.45
7-30-13	180.84	554.19		6.87	410.32
8-28-13	180.62	554.41		2.84	413.16
9-26-13	181.14	553.89		2.52	415.68
10-23-13	181.29	553.74		5.91	421.59
11-19-13	182.13	552.9		2.18	423.77
12-18-13	182.22	552.81		4.3	428.07
1-22-14	181.49	553.54		2.4	430.47
2-19-14	179.52	555.51		2.39	432.86
3/22/2014	179.4	556.1		2.59	435.45
29-Apr-2014	178.54	556.49		5.47	440.92
16-May-2014	179.24	555.79		4	444.92
25-Jun-2014	178.22	556.81		5.29	450.21
30-Jul-2014	178.29	556.74		3.47	453.68
27-Aug-2014	178.22	556.81		4.9	458.58
24-Sep-2014	179.45	555.58		0.65	459.23
22-Oct-2014	179.93	555.1		2.77	462
19-Nov-2014	180.46	554.57		1.46	463.46
30-Dec-2014	181.56	553.47		2.7	466.16
28-Jan-2015	181.9	553.13		2.69	468.85
25-Feb-2015	180.62	554.41		1.7	470.55
25-Mar-2015	178.93	556.1		3.92	474.47
30-Apr-2015	176.21	558.82		4.09	478.56
26-May-2015	174.68	560.35		3.56	482.12
25-Jun-2015	173.05	561.98		6.72	488.84
9-Jul-2015	172.32	562.71		5.41	494.25
28-Aug-2015	170.07	564.96		3.59	497.84

Cont'd

23-Sept-2015	168.94	566.09		3.21	501.05
10-Oct-2015	168.36	566.67		2.68	503.73
7-Nov-2015	166.3	568.73		2.37	506.1
4-Jan-2016	165.78	569.25		1.12	507.22
1-Feb-2016	164.1	570.93		3.29	510.51
1-Mar-2016	162.56	572.47		4.27	514.78
4-Apr-2016	160.23	574.8		2.31	517.09
5-May-2016	158.24	576.79		2.74	519.83
13-Jun-2016	156.45	578.58		5.22	525.05
7-Jul-2016	155.08	579.95		2.49	527.54
8-Aug-2016	153.64	581.39		5.82	533.36
8-Sep-2016	152.2	582.83		4.68	538.04
5-Oct-2016	151.12	583.91		1.73	539.77

Table B.3 NW Post Mining Monitoring Shaft for the Meigs Mine Complex.

Date	to water	elevation	Time	Precipitation	Acc PP
NW Shaft					
new 3-13-07 TOC 2" 693.11'					
Critical Elevation 560'					
11-21-03	181.25	511.72		2.89	2.89
12-23-03	180.1	512.87		2.78	5.67
1-22-04	180.8	512.17	22	5.08	10.75
2-18-04	183.1	509.87	49	2.02	12.77
3-18-04	183.1	509.87	78	3.27	16.04
4-16-04	183.1	509.87	107	3.96	20
5-19-04	183.1	509.87	140	5.93	25.93
6-17-04	183.1	509.87	169	5.34	31.27
7-12-04	183.2	509.77	194	5.6	36.87
8-18-04	183.2	509.77	231	3.43	40.3
9-20-04	183.2	509.77	264	2.98	43.28
10-19-04	183.2	509.77	293	3.33	46.61
11-17-04	183.3	509.67	322	4.12	50.73
12-17-04	183.2	509.77	352	3.36	54.09
1-20-05	183.2	509.77	386	8.95	63.04
2-17-05	183.2	509.77	414	1.27	64.31
3-18-05	182.1	510.87	443	3.53	67.84
4-14-05	180.6	512.37	470	4.36	72.2
5-18-05	178.4	514.57	504	3.36	75.56
6-15-05	176.4	516.57	532	2.69	78.25
7-18-05	175	517.97	565	1.79	80.04
8-16-05	173.7	519.27	594	5.09	85.13
9-14-05	172.4	520.57	623	2.91	88.04
10-14-05	171.6	521.37	653	1.33	89.37
11-18-05	170.7	522.27	688	3.31	92.68
12-20-05	169.5	523.47	720	1.67	94.35
1-18-06	168.3	524.67	749	2.67	97.02
2-17-06	167.4	525.57	779	1.36	98.38
3-15-06	166	526.97	805	3.48	101.86
4-18-06	163.9	529.07	839	2.52	104.38
5-17-06	162	530.97	868	3.25	107.63
6-14-06	160.9	532.07	896	4.3	111.93
7-20-06	159.3	533.67	932	5.77	117.7

Cont'd

8-18-06	158	534.97	961	2.94	120.64
9-19-06	156.5	536.47	993	5.35	125.99
10-18-06	155.2	537.77	1022	6.7	132.69
11-21-06	153.8	539.17	1056	2.12	134.81
12-15-06	151.4	541.57	1080	3.18	137.99
1-16-07	150.2	542.77	1112	4.25	142.24
2-19-07	147.2	545.77	1146	2.06	144.3
3-13-07	145.3	547.81	1168	6.67	150.97
4-18-07	142.7	550.41	1204	2.31	153.28
5-21-07	141	552.11	1237	1.4	154.68
6-18-07	139.8	553.31	1265	2.78	157.46
7-20-07	138.6	554.51	1297	3.02	160.48
8-21-07	137.6	555.51	1329	4.73	165.21
9-21-07	136.8	556.31	1360	2.53	167.74
10-18-07	135.8	557.31	1387	3.58	171.32
11-21-07	135.2	557.91	1421	2.18	173.5
12-28-07	134.2	558.91	1458	4.34	177.84
1-31-08	133.64	559.47		1.64	179.48
2-28-08	135.15	557.96		3.88	183.36
3-28-08	133.81	559.3		7.58	190.94
4-24-08	132.41	560.7		2.16	193.1
5-29-08	133.63	559.48		3.14	196.24
6-26-08	133.98	559.13		10.39	206.63
7-31-08	134.3	558.81		1.65	208.28
8-28-08	134.09	559.02		3.73	212.01
9-25-08	133.37	559.74		2.5	214.51
10-30-08	132.97	560.14		1.44	215.95
11-20-08	133.21	559.9		2.49	218.44
12-18-08	133.22	559.89		4.84	223.28
1-22-09	132.6	560.51		2.73	226.01
2-19-09	132.26	560.85		1.93	227.94
3-27-09	132.38	560.73		1.15	229.09
4-30-09	131.85	561.26		4.23	233.32
5-28-09	131.07	562.04		2.42	235.74
6-24-09	130.92	562.19		3.44	239.18
7-29-09	130.84	562.27		4.9	244.08
8-26-09	131.38	561.73		3.27	247.35

Cont'd

9-30-09	131.86	561.25		2.5	249.85
10-28-09	134.09	559.02		4.89	254.74
11-25-09	136.23	556.88		0.42	255.16
12-30-09	138.92	554.19		3.6	258.76
1-28-10	139.34	553.77		2.22	260.98
2-24-10	138.84	554.27		2.42	263.4
3-31-10	138.36	554.75		2.75	266.15
4-28-10	138	555.11		2.51	268.66
5-26-10	137.46	555.65		3.89	272.55
6-30-10	137.15	555.96		5.38	277.93
7-28-10	136.97	556.14		6.01	283.94
8-25-10	138.4	554.71		2.23	286.17
9-29-10	138.6	554.51		1.66	287.83
10-27-10	139.04	554.07		1.54	289.37
11-24-10	139.8	553.31		4.34	293.71
12-29-10	140.09	553.02		1.26	294.97
1-26-11	140.1	553.01		1.47	296.44
2-23-11	140.78	552.33		4.25	300.69
3-30-11	139.73	553.38		4.58	305.27
4-28-11	138.95	554.16		7.14	312.41
5-25-11	138.2	554.91		5.9	318.31
6-30-11	137.8	555.31		3.03	321.34
7-20-11	137.62	555.49		5.67	327.01
8-17-11	138.25	554.86		2.48	329.49
9-28-11	138.58	554.53		6.55	336.04
10-26-11	139	554.11		3.68	339.72
11-23-11	139.44	553.67		4.77	344.49
12-21-11	138.97	554.14		5.44	349.93
1-25-12	139.2	553.91		3.82	353.75
2-22-12	138.15	554.96		1.89	355.64
3-22-12	138.06	555.05		4.92	360.56
4-18-12	137.71	555.4		3.6	364.16
5-30-12	137.05	556.06		2.3	366.46
6-27-12	138.43	554.68		2.01	368.47
7-12-12	138.42	554.69		2.54	371.01
8-29-12	138.92	554.19		1.8	372.81

Cont'd

9-26-12	139.45	553.66		3.97	376.78
10-24-12	139.95	553.16		4.06	380.84
11-21-12	140.39	552.72		0.66	381.5
12-19-12	141	552.11		5.7	387.2
1-23-13	140.97	552.14		2.25	389.45
2-20-13	140.21	552.9		1.82	391.27
3-20-13	139.74	553.37		3.12	394.39
4-17-13	139.39	553.72		3.66	398.05
5-29-13	138.97	554.14		0.94	398.99
6-26-13	138.82	554.29		4.46	403.45
7-18-13	139.09	554.02		6.87	410.32
8-28-13	139.11	554		2.84	413.16
9-26-13	139.73	553.38		2.52	415.68
10-23-13	139.88	553.23		5.91	421.59
11-19-13	140.72	552.39		2.18	423.77
12-18-13	140.8	552.31		4.3	428.07
1-8-14	140.85	552.26		2.4	430.47
2-19-14	138	555.11		2.39	432.86
3-19-14	137.8	555.31		2.59	435.45
29-Apr-2014	136.99	556.12		5.47	440.92
16-May-2014	137.62	555.49		4	444.92
25-Jun-2014	136.7	556.41		5.29	450.21
30-Jul-2014	136.79	556.32		3.47	453.68
27-Aug-2014	137.22	555.89		4.9	458.58
24-Sep-2014	137.94	555.17		0.65	459.23
22-Oct-2014	138.49	554.62		2.77	462
19-Nov-2014	138.98	554.13		1.46	463.46
30-Dec-2014	140.09	553.02		2.7	466.16
28-Jan-2015	140.44	552.67		2.69	468.85
25-Feb-2015	138.83	554.28		1.7	470.55
25-Mar-2015	137.15	555.96		3.92	474.47
30-Apr-2015	134.42	558.69		4.09	478.56
26-May-2015	132.89	560.22		3.56	482.12
25-Jun-2015	131.32	561.79		6.72	488.84
9-Jul-2015	130.55	562.56		5.41	494.25
28-Aug-2015	128.32	564.79		3.59	497.84

Cont'd

28-Aug-2015	128.32	564.79		3.59	497.84
21-Sept-2015	127.19	565.92		3.21	501.05
10-Oct-2015	126.59	566.52		2.68	503.73
11-Nov-2015	125.7	567.41		2.37	506.1
7-Dec.-2015	124.4	568.711		4.88	510.98
4-Jan-2016	123.71	569.4		1.12	512.1
1-Feb-2016	122.37	570.74		3.29	515.39
1-Mar-2016	120.44	572.67		4.27	519.66
4-Apr-2016	118.34	574.77		2.31	521.97
5-May-2016	116.32	576.79		2.74	524.71
13-Jun-2016	114.53	578.58		5.22	529.93
7-Jul-2016	113.13	579.98		2.49	532.42
8-Aug-2016	111.56	581.55		5.82	538.24
8-Sep-2016	110.05	583.06		4.68	542.92
5-Oct-2016	108.94	584.17		1.73	544.65

Table B.4 Roving Crew Post Mining Monitoring Shaft for the Meigs Mine Complex.

Roving Crew					
636.2' elevation at ground level					
new 3-13-07 TOC elevation - 637.76'					
Date	to water	elevation	time	Precipitation	Acc PP
11-25-03	268.5	369.5		2.89	2.89
12-22-03	266.7	371.3		2.78	5.67
1-21-04	264.1	373.9	22	5.08	10.75
2-18-04	262.4	375.6	49	2.02	12.77
3-18-04	260.4	377.6	78	3.27	16.04
4-19-04	258.2	379.8	107	3.96	20
5-19-04	256	382	140	5.93	25.93
6-17-04	254.3	383.7	169	5.34	31.27
7-13-04	252.8	385.2	194	5.6	36.87
8-18-04	251.9	386.1	231	3.43	40.3
9-17-04	250.5	387.5	264	2.98	43.28
10-19-04	249.2	388.8	293	3.33	46.61
11-18-04	248.1	389.9	322	4.12	50.73
12-17-04	246.5	391.5	352	3.36	54.09
1-20-05	243.7	394.3	386	8.95	63.04
2-17-05	241.4	396.6	414	1.27	64.31
3-18-05	239.5	398.5	443	3.53	67.84
4-14-05	237.1	400.9	470	4.36	72.2
5-18-05	234.3	403.7	504	3.36	75.56
6-15-05	233.1	404.9	532	2.69	78.25
7-15-05	231.9	406.1	565	1.79	80.04
8-16-05	230.8	407.2	594	5.09	85.13
9-14-05	230.2	407.8	623	2.91	88.04
10-14-05	229.7	408.3	653	1.33	89.37
11-18-05	228.6	409.4	688	3.31	92.68
12-20-05	227.4	410.6	720	1.67	94.35
1-18-06	225.2	412.8	749	2.67	97.02
2-17-06	223.9	414.1	779	1.36	98.38
3-16-06	221.7	416.3	805	3.48	101.86

Cont'd

4-18-06	219.7	418.3	839	2.52	104.38
5-17-06	218.7	419.3	868	3.25	107.63
6-14-06	217.5	420.5	896	4.3	111.93
7-20-06	215.8	422.2	932	5.77	117.7
8-18-06	215.8	422.2	961	2.94	120.64
9-18-06	213.6	424.4	993	5.35	125.99
10-18-06	212.3	425.7	1022	6.7	132.69
11-22-06	210.8	427.2	1056	2.12	134.81
12-15-06	209.2	428.8	1080	3.18	137.99
1-16-07	207.9	430.1	1112	4.25	142.24
2-19-07	205.6	432.4	1146	2.06	144.3
3-13-07	204.3	433.46	1168	6.67	150.97
4-18-07	201.9	435.86	1204	2.31	153.28
5-18-07	200.6	437.16	1237	1.4	154.68
6-18-07	199.6	438.16	1265	2.78	157.46
7-20-07	198.6	439.16	1297	3.02	160.48
8-21-07	197.3	440.46	1329	4.73	165.21
9-21-07	196.1	441.66	1360	2.53	167.74
10-18-07	194.9	442.86	1387	3.58	171.32
11-21-07	194.1	443.66	1421	2.18	173.5
12-28-07	193.2	444.56	1458	4.34	177.84
1-31-08	191.93	445.83		1.64	179.48
2-28-08	187.04	450.72		3.88	183.36
3-28-08	184.03	453.73		7.58	190.94
4-24-08	182.9	454.86		2.16	193.1
5-29-08	179.09	458.67		3.14	196.24
6-26-08	176.03	461.73		10.39	206.63
7-31-08	171.78	465.98		1.65	208.28
8-28-08	169.97	467.79		3.73	212.01
9-25-08	171.62	466.14		2.5	214.51
10-30-08	172.33	465.43		1.44	215.95
11-20-08	171.31	466.45		2.49	218.44
12-30-08	171.54	466.22		4.84	223.28

Cont'd

1-22-09	171.1	466.66		2.73	226.01
2-27-09	168.62	469.14		1.93	227.94
3-27-09	166.69	471.07		1.15	229.09
4-30-09	164.89	472.87		4.23	233.32
5-28-09	163.75	474.01		2.42	235.74
6-24-09	163.13	474.63		3.44	239.18
7-29-09	167.3	470.46		4.9	244.08
8-26-09	172.68	465.08		3.27	247.35
9-30-09	178.26	459.5		2.5	249.85
10-28-09	179.35	458.41		4.89	254.74
11-25-09	180.94	456.82		0.42	255.16
12-30-09	183.19	454.57		3.6	258.76
1-28-10	183.64	454.12		2.22	260.98
2-24-10	183.01	454.75		2.42	263.4
3-31-10	182.7	455.06		2.75	266.15
4-28-10	181.5	456.26		2.51	268.66
5-26-10	180.62	457.14		3.89	272.55
6-30-10	180.33	457.43		5.38	277.93
7-28-10	180.5	457.26		6.01	283.94
8-25-10	181.21	456.55		2.23	286.17
9-29-10	180.61	457.15		1.66	287.83
10-27-10	183.49	454.27		1.54	289.37
11-24-10	183.68	454.08		4.34	293.71
12-29-10	184.02	453.74		1.26	294.97
1-26-11	183.75	454.01		1.47	296.44
2-23-11	183.75	454.01		4.25	300.69
3-30-11	183.33	454.43		4.58	305.27
4-28-11	182.14	455.62		7.14	312.41
5-25-11	180.75	457.01		5.9	318.31
6-30-11	180.79	456.97		3.03	321.34
7-20-11	180.55	457.21		5.67	327.01
8-17-11	181.13	456.63		2.48	329.49
9-28-11	182.42	455.34		6.55	336.04

Cont'd

10-26-11	183.15	454.61		3.68	339.72
11-23-11	183.11	454.65		4.77	344.49
12-21-11	181.94	455.82		5.44	349.93
1-25-12	182.62	455.14		3.82	353.75
2-22-12	181.41	456.35		1.89	355.64
3-22-12	181.03	456.73		4.92	360.56
4-18-12	180.9	456.86		3.6	364.16
5-30-12	180.86	456.9		2.3	366.46
6-27-12	182.98	454.78		2.01	368.47
7-12-12	182.61	455.15		2.54	371.01
8-29-12	182.23	455.53		1.8	372.81
9-26-12	182.12	455.64		3.97	376.78
10-24-12	181.5	456.26		4.06	380.84
11-21-12	181.52	456.24		0.66	381.5
12-19-12	180.68	457.08		5.7	387.2
1-23-13	181.03	456.73		2.25	389.45
2-20-13	180.38	457.38		1.82	391.27
3-20-13	180.65	457.11		3.12	394.39
4-17-13	182.05	455.71		3.66	398.05
5-29-13	181.22	456.54		0.94	398.99
6-26-13	181.46	456.3		4.46	403.45
7-30-13	181.1	456.66		6.87	410.32
8-28-13	181	456.76		2.84	413.16
9-26-13	180.4	457.36		2.52	415.68
10-23-13	179.25	458.51		5.91	421.59
11-19-13	180.32	457.44		2.18	423.77
12-18-13	179.8	457.96		4.3	428.07
1-22-14	180.61	457.15		2.4	430.47
2-19-14	180.95	456.81		2.39	432.86
3-19-14	180.75	457.01		2.59	435.45
29-Apr	179.4	458.36		5.47	440.92
16-May	180.95	456.81		4	444.92
25-Jun	180.28	457.48		5.29	450.21

Cont'd

30-Jul	179.97	457.79		3.47	453.68
27-Aug	179.85	457.91		4.9	458.58
24-Sep	180.05	457.71		0.65	459.23
22-Oct	180.92	456.84		2.77	462
19-Nov-2014	181.65	456.11		1.46	463.46
30-Dec-2014	182.26	455.5		2.7	466.16
28-Jan-2015	181.99	455.77		2.69	468.85
25-Feb-2015	182.78	454.98		1.7	470.55
25-Mar-2015	183.59	454.17		3.92	474.47
30-Apr-2015	184.38	453.38		4.09	478.56
26-May-2015	184.72	453.04		3.56	482.12
25-Jun-2015	186.95	450.81		6.72	488.84
9-Jul-2015	186.18	451.58		5.41	494.25
28-Aug-2015	186.7	451.06		3.59	497.84
21-Sept-2015	186.62	451.14		3.21	501.05
10-Oct-2015	187.18	450.58		2.68	503.73
11-Nov-2015	187.1	450.66		2.37	506.1
7-Dec-2015	183.7	454.06		4.88	510.98
4-Jan-2016	187	450.76		1.12	512.1
1-Feb-2016	187.32	450.44		3.29	515.39
1-Mar-2016	187.8	449.96		4.27	519.66
4-Apr-2016	187.22	450.54		2.31	521.97
5-May-2016	187.28	450.48		2.74	524.71
13-Jun-2016	204.69	433.07		5.22	529.93
7-Jul-2016	204.89	432.87		2.49	532.42
8-Aug-2016	204.05	433.71		5.82	538.24
8-Sep-2016	188.61	449.25		4.68	542.92
5-Oct-2016	205.46	477.3		1.73	544.65

Table B.5 Danville Post Mining Monitoring Shaft For the Meigs Mine Complex.

Danville Shaft					
1 Left Borehole					
new2-1-11 TOC- elevation- 743.09'					
Date	to water	elevation	Time	Precipitation	Acc PP
12-22-03	364.3	378.73		2.78	2.78
1-21-04	361.8	381.23	22	5.08	7.86
2-18-04	360.1	382.93	49	2.02	9.88
3-18-04	358.2	384.83	78	3.27	13.15
4-19-04	356.2	386.83	107	3.96	17.11
5-19-04	354.2	388.83	140	5.93	23.04
6-17-04	352.3	390.73	169	5.34	28.38
7-13-04	350.8	392.23	194	5.6	33.98
8-18-04	349.3	393.76	231	3.43	37.41
9-16-04	348.4	394.63	264	2.98	40.39
10-19-04	347	396.03	293	3.33	43.72
11-17-04	345.9	397.13	322	4.12	47.84
12-17-04	344.3	398.73	352	3.36	51.2
1-20-05	342	401.03	386	8.95	60.15
2-17-05	340.9	402.13	414	1.27	61.42
3-18-05	339.6	403.43	443	3.53	64.95
4-14-05	338.1	404.93	470	4.36	69.31
5-18-05	336.6	406.43	504	3.36	72.67
6-15-05	335.4	407.63	532	2.69	75.36
7-15-05	334.9	408.13	565	1.79	77.15
8-17-05	333.9	409.13	594	5.09	82.24
9-14-05	332.9	410.13	623	2.91	85.15
10-14-05	332.1	410.93	653	1.33	86.48
11-18-05	331.1	411.93	688	3.31	89.79
12-20-05	330	413.03	720	1.67	91.46
1-18-06	328.5	414.53	749	2.67	94.13
2-17-06	327.4	415.63	779	1.36	95.49
3-16-06	326.1	416.93	805	3.48	98.97
4-18-06	324.2	418.83	839	2.52	101.49
5-17-06	323.4	419.63	868	3.25	104.74
6-14-06	322.4	420.63	896	4.3	109.04
7-20-06	321	422.03	932	5.77	114.81
8-18-06	319.7	423.33	961	2.94	117.75

Cont'd

9-18-06	318	425.03	993	5.35	123.1
10-18-06	316.8	426.23	1022	6.7	129.8
11-22-06	315.2	427.83	1056	2.12	131.92
12-15-06	314	429.03	1080	3.18	135.1
1-16-07	312.5	430.53	1112	4.25	139.35
2-19-07	310.1	432.93	1146	2.06	141.41
3-13-07	308.7	433.59	1168	6.67	148.08
4-18-07	305.5	436.79	1204	2.31	150.39
5-18-07	305.4	436.89	1237	1.4	151.79
6-18-07	304.2	438.09	1265	2.78	154.57
7-20-07	303.3	438.99	1297	3.02	157.59
8-21-07	302	440.29	1329	4.73	162.32
9-21-07	301	441.29	1360	2.53	164.85
10-18-07	299.6	442.69	1387	3.58	168.43
11-21-07	299.2	443.09	1421	2.18	170.61
12-27-07	297.9	444.39	1458	4.34	174.95
1-31-08	296.73	445.56		1.64	176.59
2-28-08	292.1	450.19		3.88	180.47
3-28-08	289	453.29		7.58	188.05
4-24-08	287.54	454.75		2.16	190.21
5-29-08	283.88	458.41		3.14	193.35
6-26-08	280.52	461.77		10.39	203.74
7-31-08	276.62	465.67		1.65	205.39
8-28-08	274.8	467.49		3.73	209.12
9-25-08	276.02	466.27		2.5	211.62
10-30-08	276.97	465.32		1.44	213.06
11-20-08	276	466.29		2.49	215.55
12-18-08	276.45	465.84		4.84	220.39
1-22-09	275.79	466.5		2.73	223.12
2-19-09	273.62	468.67		1.93	225.05
3-27-09	271.4	470.89		1.15	226.2
4-30-09	269.72	472.57		4.23	230.43
5-28-09	268.4	473.89		2.42	232.85
6-24-09	267.8	474.49		3.44	236.29
7-29-09	271.34	470.95		4.9	241.19
8-26-09	276.69	465.6		3.27	244.46
9-30-09	282.22	460.07		2.5	246.96

Cont'd

10-28-09	283.75	458.54		4.89	251.85
11-25-09	285.45	456.84		0.42	252.27
12-30-09	287.5	454.79		3.6	255.87
1-28-10	288.4	453.89		2.22	258.09
2-24-10	287.7	454.59		2.42	260.51
3-31-10	287.31	454.98		2.75	263.26
4-28-10	286.5	455.79		2.51	265.77
5-26-10	285.65	456.64		3.89	269.66
6-30-10	285.6	456.69		5.38	275.04
7/28/2010	285.65	456.54		6.01	281.05
8-25-10	286.31	455.98		2.23	283.28
9-29-10	285.9	456.39		1.66	284.94
10-27-10	288.1	454.19		1.54	286.48
11-24-10	288.72	453.57		4.34	290.82
12-2-10	288.78	453.51		1.26	292.08
1-12-11	289.01	453.28		1.47	293.55
2-23-11	290.1	452.99		4.25	297.8
3-30-11	289.15	453.94		4.58	302.38
4-28-11	287.9	455.19		7.14	309.52
5-25-11	287.23	455.86		5.9	315.42
6-30-11	256.79	456.3		3.03	318.45

Table B.6 South Bleeder Post Mining Monitoring Shaft for the Meigs Mine Complex

South Bleeder Mine 2					
new 12 /28 /07 hole top / 771.22' ele					
floor elevation /443.1'					
total depth /326.9' (560)					
Date	to water	elevation	Time	Precipitation	acc PP
1/22/2004	274.5	495.5	22	5.08	5.08
2/17/2004	273.9	496.1	49	2.02	7.1
3/18/2004	272.6	497.4	78	3.27	10.37
4/16/2004	271.8	498.2	107	3.96	14.33
5/19/2004	270.2	499.8	140	5.93	20.26
6/17/2004	269.1	500.9	169	5.34	25.6
7/12/2004	268.1	501.9	194	5.6	31.2
8/18/2004	266.8	503.2	231	3.43	34.63
9/16/2004	266.1	503.9	264	2.98	37.61
10/19/2004	265	505	293	3.33	40.94
11/18/2004	264.2	505.8	322	4.12	45.06
12/17/2004	263.3	506.7	352	3.36	48.42
1/20/2005	261.3	508.7	386	8.95	57.37
2/17/2005	260	510	414	1.27	58.64
3/18/2005	258.4	511.6	443	3.53	62.17
4/14/2005	256.9	513.1	470	4.36	66.53
5/18/2005	254.7	515.3	504	3.36	69.89
6/15/2005	252.6	517.6	532	2.69	72.58
7/18/2005	251.2	518.8	565	1.79	74.37
8/16/2005	250	520	594	5.09	79.46
9/14/2005	248.8	521.2	623	2.91	82.37
10/14/2005	247.9	522.1	653	1.33	83.7
11/17/2005	247.1	522.9	688	3.31	87.01
12/20/2005	245.9	524.1	720	1.67	88.68
1/18/2006	244.7	525.3	749	2.67	91.35
2/17/2006	243.9	526.1	779	1.36	92.71
3/15/2006	242.3	527.7	805	3.48	96.19
4/18/2006	240.4	529.6	839	2.52	98.71
5/17/2006	238.7	531.3	868	3.25	101.96
6/14/2006	237.2	532.8	896	4.3	106.26
7/20/2006	235.8	534.2	932	5.77	112.03
8/18/2006	234.5	535.5	961	2.94	114.97
9/19/2006	233.1	536.9	993	5.35	120.32

Cont'd

10/18/2006	232.7	537.3	1022	6.7	127.02
11/22/2006	230.1	539.9	1056	2.12	129.14
12/15/2006	228.2	541.8	1080	3.18	132.32
1/16/2007	227	543	1112	4.25	136.57
2/19/2007	224	546	1146	2.06	138.63
3/13/2007	222.2	547.48	1168	6.67	145.3
4/18/2007	219.6	550.08	1204	2.31	147.61
5/18/2007	218.2	551.48	1237	1.4	149.01
6/18/2007	216.8	552.88	1265	2.78	151.79
7/20/2007	215.8	553.88	1297	3.02	154.81
8/21/2007	214.7	554.98	1329	4.73	159.54
9/21/2007	213.9	555.78	1360	2.53	162.07
10/18/2007	212.9	556.78	1387	3.58	165.65
11/21/2007	212.3	557.38	1421	2.18	167.83
12/28/2007	211	560.22	1458	4.34	172.17
1/28/2008	210.3	560.92		1.64	173.81
2/28/2008	212.75	558.47		3.88	177.69
3/6/2008	212.92	558.3		7.58	185.27
4/3/2008	211.35	559.87		2.16	187.43
5/1/2008	210.02	561.2		3.14	190.57
6/26/2008	211.61	559.61		10.39	200.96
7/10/2008	212.59	558.63		1.65	202.61
8/15/2008	212.14	559.08		3.73	206.34
9/4/2008	211.29	559.93		2.5	208.84
10/2/2008	210.54	560.68		1.44	210.28
11/6/2008	210.47	560.75		2.49	212.77
12/30/2008	210.25	560.97		4.84	217.61
1/8/2009	209.7	561.52		2.73	220.34
2/5/2009	210.29	560.93		1.93	222.27
3/5/2009	209.95	561.27		1.15	223.42
4/30/2009	209.72	561.5		4.23	227.65
5/7/2009	209.51	561.71		2.42	230.07
6/24/2009	208.73	562.49		3.44	233.51
7/29/2009	208.65	562.57		4.9	238.41
8/26/2009	209.14	562.08		3.27	241.68
9/2/2009	209.26	561.96		2.5	244.18

Cont'd

10/28/2009	212	559.22		4.89	249.07
11/25/2009	214.06	557.16		0.42	249.49
12/30/2009	216.77	554.45		3.6	253.09
1/28/2010	217.22	554		2.22	255.31
2/24/2010	216.74	554.48		2.42	257.73
3/31/2010	216.3	554.92		2.75	260.48
4/28/2010	215.94	555.28		2.51	262.99
5/26/2010	215.25	555.97		3.89	266.88
6/30/2010	215.03	556.19		5.38	272.26
7/28/2010	214.9	556.32		6.01	278.27
8/25/2010	216.3	554.92		2.23	280.5
9/29/2010	216.48	554.74		1.66	282.16
10/27/2010	216.95	554.27		1.54	283.7
11/24/2010	217.55	553.67		4.34	288.04
12/29/2010	217.88	553.34		1.26	289.3
1/26/2011	217.89	553.33		1.47	290.77
2/23/2011	218.5	552.72		4.25	295.02
3/30/2011	217.47	553.75		4.58	299.6
4/28/2011	216.78	554.44		7.14	306.74
5/25/2011	216	555.22		5.9	312.64
6/2/2011	216	555.22		3.03	315.67
7/20/2011	215.44	555.78		5.67	321.34
8/17/2011	216.04	555.18		2.48	323.82
9/28/2011	216.36	554.86		6.55	330.37
10/12/2011	216.42	554.8		3.68	334.05
11/23/2011	217.25	553.97		4.77	338.82
12/21/2011	216.73	554.49		5.44	344.26
1/25/2012	217.01	554.21		3.82	348.08
2/22/2012	216	555.22		1.89	349.97
3/22/2012	216.01	555.21		4.92	354.89
4/18/2012	215.53	555.69		3.6	358.49
5/30/2012	214.91	556.31		2.3	360.79
6/27/2012	216.31	554.91		2.01	362.8
7/12/2012	216.21	555.01		2.54	365.34
8/29/2012	216.75	554.47		1.8	367.14
9/26/2012	217.31	553.91		3.97	371.11

Cont'd

10/24/2012	217.85	553.37		4.06	375.17
11/21/2012	218.19	553.03		0.66	375.83
12/19/2012	218.83	552.39		5.7	381.53
1/23/2013	218.71	552.51		2.25	383.78
2/20/2013	218.02	553.2		1.82	385.6
3/20/2013	217.58	553.64		3.12	388.72
4/17/2013	217.23	553.99		3.66	392.38
5/15/2013	216.7	554.52		0.94	393.32
6/26/2013	216.7	554.52		4.46	397.78
7/30/2013	217.16	554.06		6.87	404.65
8/28/2013	216.95	554.27		2.84	407.49
9/26/2013	217.59	553.63		2.52	410.01
10/23/2013	217.85	553.37		5.91	415.92
11/19/2013	218.56	552.66		2.18	418.1
12/18/2013	218.68	552.54		4.3	422.4
1/22/2014	217.5	553.72		2.4	424.8
2/19/2014	215.95	555.27		2.39	427.19
3/19/2014	215.85	555.37		2.59	429.78
4/29/2014	214.9	556.32		5.47	435.25
5/28/2014	214.7	556.52		4	439.25
6/25/2014	214.6	556.62		5.29	444.54
7/30/2014	214.69	556.53		3.47	448.01
8/27/2014	215.09	556.13		4.9	452.91
9/24/2014	216.9	554.32		0.65	453.56
10/22/2014	216.33	554.89		2.77	456.33
11/19/2014	216.82	554.4		1.46	457.79
12/30/2014	217.95	553.27		2.7	460.49
1/28/2015	217.42	553.8		2.69	463.18
2/25/2015	216.62	554.6		1.7	464.88
3/25/2015	214.94	556.28		3.92	468.8
4/30/2015	212.28	558.94		4.09	472.89
5/26/2015	210.6	560.62		3.56	476.45
6/25/2015	209.04	562.18		6.72	483.17
7/9/2015	208.32	562.9		5.41	488.58
8/28/2015	205.85	565.37		3.59	492.17
9/21/2015	204.87	566.35		3.21	495.38

Cont'd

10/10/2015	204.38	566.84		2.68	498.06
11/11/2015	203.42	567.8		2.37	500.43
12/7/2015	202.2	569.02		4.88	505.31
1/4/2016	201.6	569.62		1.12	506.43
2/1/2016	216.53	571		3.29	509.72
3/1/2016	198.38	572.84		4.27	513.99
4/4/2016	196.06	575.16		2.31	516.3
5/5/2016	194.1	577.12		2.74	519.04
6/13/2016	192.21	579.01		5.22	524.26
7 /July02016	190.9	580.32		2.49	526.75
8/8/2016	189.16	582.06		5.82	532.57
9/8/2016	187.74	583.48		4.68	537.25
10/5/2016	186.69	584.53		1.73	538.98

APPENDIX C: SENSITIVITY ANALYSIS DATA FOR MEIGS MINE MODEL.

Table.C.1. Sensitivity analysis data for the aquifers hydraulic conductivity (steady-state).

Aquifers	Calibrated Hydraulic Conductivity Values (feet/day)	Manipulated Hydraulic Condutivity Values (feet/day)	% Change in Hydraulic Conductivity Values (feet/day)	Mean error (feet)
A	20.00	16.00	-20.00	14.50
	20.00	18.00	-10.00	14.80
	20.00	20.00	0.00	12.60
	20.00	22.00	10.00	12.80
	20.00	24.00	20.00	13.00
B	27.00	25.00	-7.41	14.80
	27.00	26.00	-3.70	14.90
	27.00	27.00	0.00	12.60
	27.00	28.00	3.70	12.70
	27.00	30.00	11.11	12.80
C	60.00	56.00	-6.67	12.95
	60.00	58.00	-3.33	12.80
	60.00	60.00	0.00	12.60
	60.00	62.00	3.33	14.80
	60.00	64.00	6.67	14.60

Table.C.2. Sensitivity analysis data for recharge (steady-state)

Recharge	Calibrated Recharge Values (feet/day)	Manipulated Recharge Values (inches/year)	% Change in Recharge Values (inches/year)	Mean error (feet)
R1	1.2	0.8	-33.3	13.9
	1.2	1.0	-16.7	14.5
	1.2	1.2	0.0	12.6
	1.2	1.4	16.7	13.3
	1.2	1.6	33.3	14.1
R2	1.3	0.9	-30.8	14.6
	1.3	1.1	-15.4	14.9
	1.3	1.3	0.0	12.6
	1.3	1.5	15.4	12.7
	1.3	1.7	30.8	12.8
R3	1.4	1.0	-28.6	14.8
	1.4	1.2	-14.3	14.9
	1.4	1.4	0.0	12.6
	1.4	1.6	14.3	12.7
	1.4	1.8	28.6	12.7
R4	1.2	0.8	-33.3	13.8
	1.2	1.0	-16.7	14.5
	1.2	1.2	0.0	12.6
	1.2	1.4	16.7	13.3
	1.2	1.6	33.3	14.1

Table.C.3. Sensitivity analysis data for shales hydraulic conductivity (steady-state).

Shale	Calibrated Hydraulic Conductivity Values (feet/day)	Manipulated Hydraulic Condutivity Values (feet/day)	% Change in Hydraulic Conductivity Values (feet/day)	Mean error (feet)
	1.1	0.6	-45.5	12.6
	1.1	0.8	-27.3	12.6
Shale 1	1.1	1.1	0.0	12.6
	1.1	1.4	27.3	12.6
	1.1	1.6	45.5	12.6
	10.0	6.0	-40.0	14.5
	10.0	8.0	-20.0	14.7
Shale 2	10.0	10.0	0.0	12.6
	10.0	12.0	20.0	12.8
	10.0	14.0	40.0	13.1
	1.0	0.5	-50.0	12.7
	1.0	0.7	-30.0	12.6
Shale 3	1.0	1.0	0.0	12.6
	1.0	1.2	20.0	12.6
	1.0	1.5	50.0	12.6
	12.0	8.0	-33.3	12.8
	12.0	10.0	-16.7	12.7
Shale 4	12.0	12.0	0.0	12.6
	12.0	14.0	16.7	14.9
	12.0	16.0	33.3	14.8
	22.0	18.0	-18.2	14.7
	22.0	20.0	-9.1	13.6
Shale 5	22.0	22.0	0.0	12.6
	22.0	24.0	9.1	14.4
	22.0	26.0	18.2	13.9

Table C.4 Sensitivity analysis data for shales hydraulic conductivity (transient-state).

Shale	Calibrated hydraulic conductivity values (feet/day)	Manipulated hydraulic conductivity values (feet/day)	% change in hydraulic conductivity values (feet/day)	Absolute error (feet)
	1.1	1.3	18.18181818	8.583749
	1.1	1.2	9.090909091	8.583749
	1.1	1.1	0	8.556977
	1.1	1	-9.090909091	8.583749
Shale 1	1.1	0.9	-18.18181818	8.583749
	0.04	0.06	50	8.5838
	0.04	0.05	25	8.5838
	0.04	0.04	0	8.556977
	0.04	0.03	-25	8.583799
Shale 2	0.04	0.02	-50	8.583799
	0.8	1	25	8.584947
	0.8	0.9	12.5	8.585001
	0.8	0.8	0	8.556977
	0.8	0.7	-12.5	8.583805
Shale 3	0.8	0.6	-25	8.584452
	0.00009	0.00011	22.22222222	8.980972
	0.00009	0.0001	11.11111111	8.751208
	0.00009	0.00009	0	8.556977
	0.00009	0.00008	-11.11111111	8.557578
Shale 4A	0.00009	0.00007	-22.22222222	8.86088
	0.0005	0.0007	40	8.825546
	0.0005	0.0006	20	8.762738
	0.0005	0.0005	0	8.556977
	0.0005	0.0004	-20	8.728022
Shale 4B	0.0005	0.0003	-40	9.307297
	0.02	0.031	55	10.20788
	0.02	0.03	50	9.94838
	0.02	0.02	0	8.556977
	0.02	0.01	-50	13.0191
Shale 5	0.02	0.009	-55	13.83633

Table C.5 Sensitivity analysis data for recharge (transient-state)

Recharge	Calibrated Recharge values (Inches/year)	Manipulated recharge values (inches/year)	% change in recharge values (inches/year)	Absolute error (feet)
R1	0.1	0.12	20	8.59
	0.1	0.11	10	8.585
	0.1	0.1	0	8.556977
	0.1	0.09	-10	8.583366
	0.1	0.08	-20	8.582967
R2	1.5	1.7	13.33333333	8.585
	1.5	1.6	6.666666667	8.584
	1.5	1.5	0	8.556977
	1.5	1.4	-6.666666667	8.584
	1.5	1.3	-13.33333333	8.585
R3	1.4	1.6	14.28571429	8.587
	1.4	1.5	7.142857143	8.583749
	1.4	1.4	0	8.556977
	1.4	1.3	-7.142857143	8.583749
	1.4	1.2	-14.28571429	8.5845
R4	0.01	0.012	20	8.583736
	0.01	0.011	10	8.583736
	0.01	0.01	0	8.556977
	0.01	0.009	-10	8.583756
	0.01	0.008	-20	8.583751

Table C.6 Sensitivity analysis data for the aquifers hydraulic conductivity (transient-state).

Aquifer	Calibrated hydraulic conductivity values (feet/day)	Manipulated hydraulic conductivity values (feet/day)	% change in hydraulic conductivity values (feet/day)	Absolute error (feet)
	6.50	6.70	3.08	8.584
	6.50	6.60	1.54	8.584
	6.50	6.50	0.00	8.557
	6.50	6.40	-1.54	8.584
A	6.50	6.30	-3.08	8.584
	0.10	0.12	20.00	8.584
	0.10	0.11	10.00	8.584
	0.10	0.10	0.00	8.557
	0.10	0.09	-10.00	8.585
B	0.10	0.08	-20.00	8.585
	14.00	16.00	14.29	8.592
	14.00	15.00	7.14	8.584
	14.00	14.00	0.00	8.557
	14.00	13.00	-7.14	8.565
C	14.00	12.00	-14.29	8.558

Table C.7 Sensitivity analysis data for coal hydraulic conductivity (transient-state).

	Calibrated hydraulic conductivity values (feet/day)	Manipulated hydraulic conductivity values (feet/day)	% change in hydraulic conductivity values (feet/day)	Absolute error (feet)
Coal	0.00004	0.00006	50.00	8.58
	0.00004	0.00005	25.00	8.57
	0.00004	0.00004	0.00	8.56
	0.00004	0.00003	-25.00	8.63
	0.00004	0.00002	-50.00	8.77
Voids	45	55	22.22	8.59
	45	50	11.11	8.59
	45	45	0.00	8.56
	45	40	-11.11	8.59
	45	35	-22.22	8.59

Table C.8 Sensitivity analysis for shales specific storage (transient-state).

Shale	Calibrated Specific storage values.	Manipulated Specific storage values.	% change in specific storage values.	Absolute error (feet)
Shale 1	0.0001	0.00014	40	8.712372
	0.0001	0.00012	20	8.591931
	0.0001	0.0001	0	8.583749
	0.0001	0.00008	-20	8.858704
	0.0001	0.00006	-40	9.492711
Shale2	0.0001	0.00014	40	8.583749
	0.0001	0.00012	20	8.583749
	0.0001	0.0001	0	8.583749
	0.0001	0.00008	-20	8.583749
	0.0001	0.00006	-40	8.583749
Shale 3	0.0001	0.00014	40	8.583749
	0.0001	0.00012	20	8.583749
	0.0001	0.0001	0	8.583749
	0.0001	0.00008	-20	8.583749
	0.0001	0.00006	-40	8.583749
Shale 4A	0.001	0.0014	40	8.583749
	0.001	0.0012	20	8.583749
	0.001	0.001	0	8.583749
	0.001	0.0008	-20	8.583749
	0.001	0.0006	-40	8.583749
Shale 4B	0.0001	0.00014	40	8.583749
	0.0001	0.00012	20	8.583749
	0.0001	0.0001	0	8.583749
	0.0001	0.00008	-20	8.583749
	0.0001	0.00006	-40	8.583749
Shale 5	0.0001	0.00014	40	8.583749
	0.0001	0.00012	20	8.583749
	0.0001	0.0001	0	8.583749
	0.0001	0.00008	-20	8.583749
	0.0001	0.00006	-40	8.583749

Table C.9 Sensitivity analysis for aquifers specific storage (transient-state).

Aquifers	Calibrated Specific storage values	Manipulated Specific storage values	% change in specific storage	Absolute error (feet)
	0.001	0.00140	40	8.583749
	0.001	0.00120	20	8.583749
	0.001	0.00100	0	8.583749
	0.001	0.00080	-20	8.583749
A	0.001	0.00060	-40	8.583749
	0.001	0.0014	40	8.583749
	0.001	0.0012	20	8.583749
	0.001	0.001	0	8.583749
	0.001	0.0008	-20	8.583749
B	0.001	0.0006	-40	8.583749
	0.001	0.0014	40	8.703749
	0.001	0.0012	20	8.653749
	0.001	0.001	0	8.583749
	0.001	0.0008	-20	8.643749
C	0.001	0.0006	-40	8.693749

Table C.10 Sensitivity analysis for aquifers specific yield (transient-state).

Aquifers	Calibrated Specific yield values	Manipulated Specific yield values	% change in specific yield	Absolute error (feet)
	0.27	0.29	7.407407407	8.586
	0.27	0.28	3.703703704	8.585
	0.27	0.27	0	8.583749
	0.27	0.26	-3.703703704	8.585
A	0.27	0.25	-7.407407407	8.586
	0.27	0.29	7.407407407	8.586
	0.27	0.28	3.703703704	8.585
	0.27	0.27	0	8.583749
	0.27	0.26	-3.703703704	8.585
B	0.27	0.25	-7.407407407	8.586
	0.27	0.29	7.407407407	8.586
	0.27	0.28	3.703703704	8.585
	0.27	0.27	0	8.583749
	0.27	0.26	-3.703703704	8.585
C	0.27	0.25	-7.407407407	8.586

Table C.11 Sensitivity analysis for shales specific yields (transient-state).

Shale	Calibrated Specific yield values	Manipulated Specific yield values	% change in hydraulic conductivity values	Absolute error (feet)
	0.11	0.13	18.18	9.806268
	0.11	0.12	9.09	9.10582
	0.11	0.11	0.00	8.583749
	0.11	0.1	-9.09	8.833981
shale 1	0.11	0.09	-18.18	10.00552
	0.12	0.14	16.67	8.583749
	0.12	0.13	8.33	8.583749
	0.12	0.12	0.00	8.583749
	0.12	0.11	-8.33	8.583749
Shale 2	0.12	0.1	-16.67	8.583749
	0.12	0.14	16.67	8.583749
	0.12	0.13	8.33	8.583749
	0.12	0.12	0.00	8.583749
	0.12	0.11	-8.33	8.583749
Shale 3	0.12	0.1	-16.67	8.583749
	0.12	0.14	16.67	8.583749
	0.12	0.13	8.33	8.583749
	0.12	0.12	0.00	8.583749
	0.12	0.11	-8.33	8.583749
Shale 4A	0.12	0.1	-16.67	8.583749
	0.12	0.14	16.67	8.583749
	0.12	0.13	8.33	8.583749
	0.12	0.12	0.00	8.583749
	0.12	0.11	-8.33	8.583749
Shale 4B	0.12	0.1	-16.67	8.583749
	0.12	0.14	16.67	8.583749
	0.12	0.13	8.33	8.583749
	0.12	0.12	0.00	8.583749
	0.12	0.11	-8.33	8.583749
Shale 5	0.12	0.1	-16.67	8.583749

APPENDIX D: ARTIFICIAL NEURAL NETWORK

Table D.1 Second degree polynomial equation and significant variables for maximum heads in wells for the data set with water withdraw.

Best formula:	Y=0.65*X1-0.12*X11-0.28-5.6E-002*X10+2.9E-002*X5+0.36*X2+0.26*X1^2+0.15*X2^2-0.43*X1*X2+0.48*X10^2-0.15*X11^2+3.3E-002*X9^2+4.3E-002*X6^2
Legend:	X1=2.*(Surface Elevation for Sampling Station (msl)-602.)/738.-1.
	X2=2.*(Bottom of well elevation (msl)-244.04)/1053.96-1.
	X3=2.*(Overburden thickness (ft)-65.)/475.4-1.
	X4=2.*(Thickness of mined coal seam (ft)-2.25)/9.51-1.
	X5=2.*(Thickness Shale + Clay (ft)-13.9)/333.16-1.
	X6=2.*Thickness Sandstone (ft)/258.71-1.
	X7=2.*Thickness Limestone (ft)/187.04-1.
	X8=2.*Thickness Coal (ft)/26.19-1.
	X9=2.*(Accumulative Coal Volume (Mm^3)-.07)/146.11-1.
	X10=2.*(Underground Mine Area 4mi (acres)-617.98)/110430.52-1.
	X11=2.*(Average Annual Precipitation (in)-38.)/3.-1.
	X12=2.*W/D (MGD / ft)/.-1.
	Y=2.*(Maximum Head (msl)-475.45)/822.98-1.
Most significant variables:	Surface Elevation for Sampling Station (msl)
	Bottom of well elevation (msl)
	Thickness Shale + Clay (ft)
	Thickness Sandstone (ft)
	Accumulative Coal Volume (Mm^3)
	Underground Mine Area 4mi (acres)
	Average Annual Precipitation (in)

Table D.2 Second degree polynomial equation and significant variables for minimum heads in wells for the data set with water withdraw

Best formula:	$Y=-4.4E-002*X10-0.23-3.8E-002*X6-0.13*X11+0.56*X1+0.39*X2+0.16*X1^2-0.27*X1*X2+0.46*X10^2-0.18*X11^2+3.7E-002*X9^2+9.E-002*X2^2-3.7E-002*X3^2+2.9E-002*X8^2$
Legend:	X1=2.*(Surface Elevation for Sampling Station (msl)-602.)/738.-1.
	X2=2.*(Bottom of well elevation (msl)-244.04)/1053.96-1.
	X3=2.*(Overburden thickness (ft)-65.)/475.4-1.
	X4=2.*(Thickness of mined coal seam (ft)-2.25)/9.51-1.
	X5=2.*(Thickness Shale + Clay (ft)-13.9)/333.16-1.
	X6=2.*Thickness Sandstone (ft)/258.71-1.
	X7=2.*Thickness Limestone (ft)/187.04-1.
	X8=2.*Thickness Coal (ft)/26.19-1.
	X9=2.*(Accumulative Coal Volume (Mm^3)-.07)/146.11-1.
	X10=2.*(Underground Mine Area 4mi (acres)-617.98)/110430.52-1.
	X11=2.*(Average Annual Precipitation (in)-38.)/3.-1.
	X12=2.*W/D (MGD / ft)/.-1.
	Y=2.*(Minimum Head (msl)-430.49)/867.94-1.
Most significant variables:	Surface Elevation for Sampling Station (msl)
	Bottom of well elevation (msl)
	Overburden thickness (ft)
	Thickness Sandstone (ft)
	Thickness Coal (ft)
	Accumulative Coal Volume (Mm^3)
	Underground Mine Area 4mi (acres)
	Average Annual Precipitation (in)
Less significant variables:	Thickness of mined coal seam (ft)

Figure D.1 Correlation between observed and calculated heads for the maximum head for mine data with water withdraw.
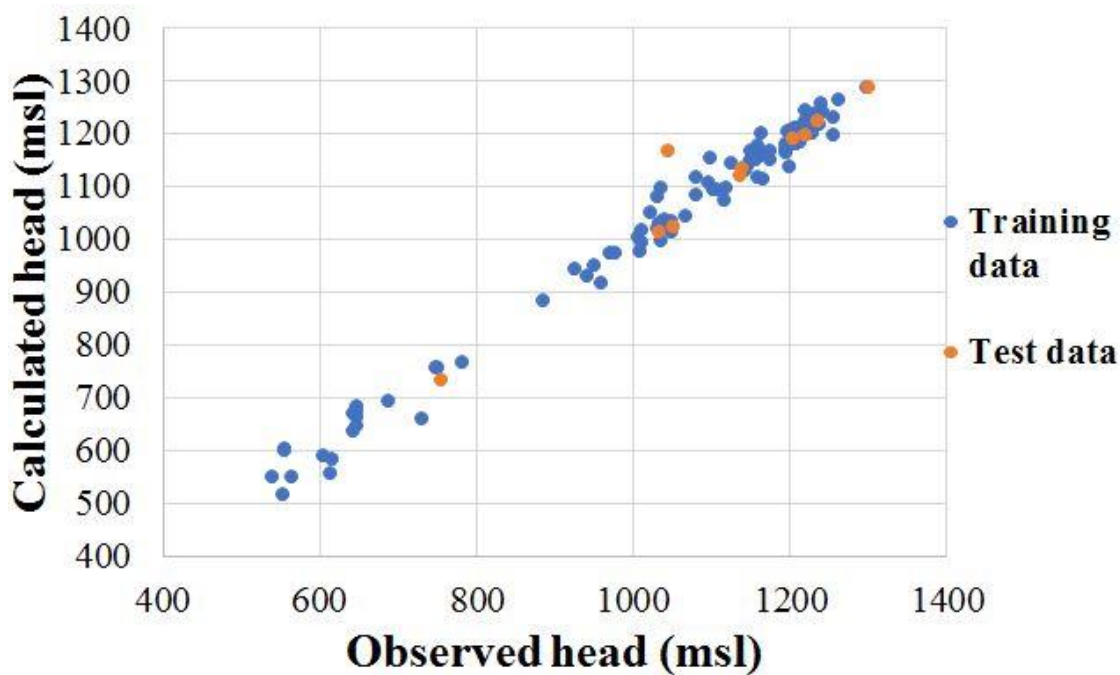
Figure D.2 Correlation between observed and calculated heads for the minimum head for mine data with water withdraw.

Table D.3. Second degree polynomial equation and most significant variables for the maximum head for the mine data set without water withdraw.

Best formula:	Y=-4.1E-003*X7-4.4E-002*X10-3.8E-002*X11-0.19+1.1E-002*X5-1.E-002*X6+0.73*X1+0.31*X2+0.19*X1^2+0.21*X2^2-0.45*X1*X2+0.34*X10^2-0.11*X11^2
Legend:	X1=2.*(Surface Elevation for Sampling Station (msl)-545.)/835.-1.
	X2=2.*(Bottom of well elevation (msl)-80.)/1220.-1.
	X3=2.*(Overburden thickness (ft)-56.)/506.6-1.
	X4=2.*(Thickness of mined coal seam (ft)-1.17)/10.59-1.
	X5=2.*(Thickness Shale + Clay (ft)-13.9)/452.53-1.
	X6=2.*Thickness Sandstone (ft)/258.71-1.
	X7=2.*Thickness Limestone (ft)/204.97-1.
	X8=2.*Thickness Coal (ft)/33.23-1.
	X9=2.*Accumulative Coal Volume (Mm^3)/146.18-1.
	X10=2.*(Underground Mine Area 4mi (acres)-617.98)/110430.52-1.
	X11=2.*(Average Annual Precipitation (in)-37.)/4.-1.
	Y=2.*(Maximum Head (msl)-400.)/932.-1.
Most significant variables:	Surface Elevation for Sampling Station (msl)
	Bottom of well elevation (msl)
	Thickness Shale + Clay (ft)
	Thickness Sandstone (ft)
	Thickness Limestone (ft)
	Underground Mine Area 4mi (acres)
	Average Annual Precipitation (in)
Less significant variables:	Accumulative Coal Volume (Mm^3)

Table D.4 Second degree polynomial equation and most significant variables for the minimum head for the mine data set without water withdraw.

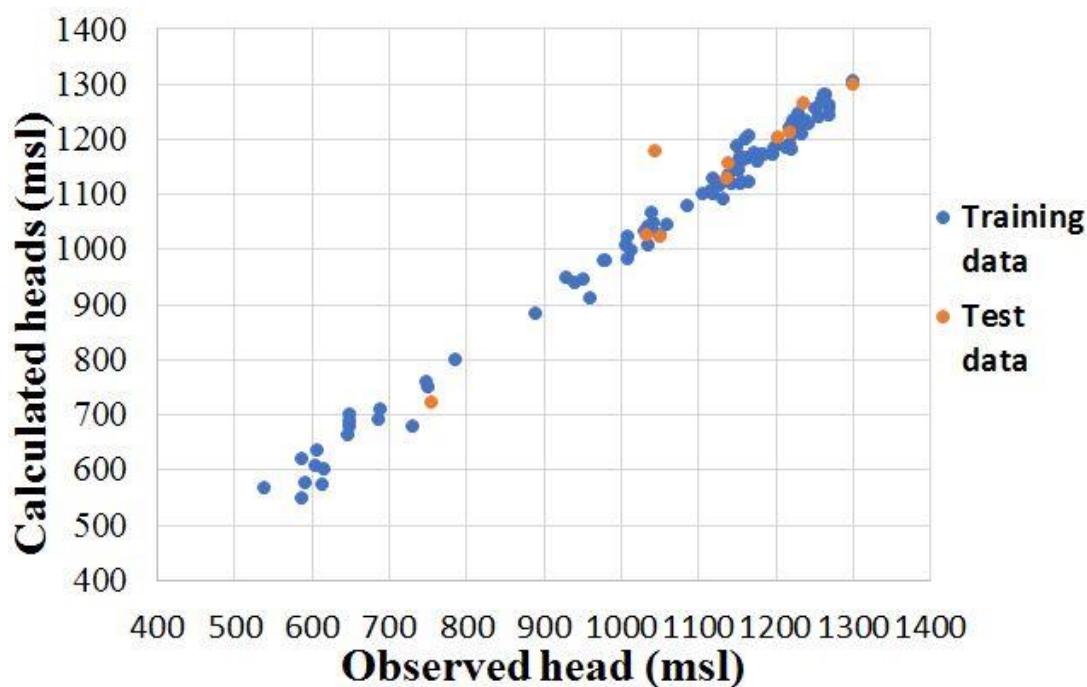|	
Best formula:	Y=3.5E-002*X5-0.17-2.6E-002*X11+1.5E-002*X10-4.4E-002*X4+0.68*X1+0.41*X2+0.21*X1^2+0.28*X2^2-0.57*X1*X2-3.1E-002*X5^2-4.1E-002*X7-3.5E-002*X7^2-5.6E-002*X9+4.3E-002*X1*X9+2.6E-002*X2*X9+1.5E-002*X1^2*X9+1.8E-002*X2^2*X9-3.6E-002*X1*X2*X9+0.18*X10^2-1.8E-003*X4^2-4.9E-002*X11^2
Legend:	X1=2.*(Surface Elevation for Sampling Station (msl)-545.)/835.-1.
	X2=2.*(Bottom of well elevation (msl)-80.)/1220.-1.
	X3=2.*(Overburden thickness (ft)-56.)/506.6-1.
	X4=2.*(Thickness of mined coal seam (ft)-1.17)/10.59-1.
	X5=2.*(Thickness Shale + Clay (ft)-13.9)/452.53-1.
	X6=2.*Thickness Sandstone (ft)/258.71-1.
	X7=2.*Thickness Limestone (ft)/204.97-1.
	X8=2.*Thickness Coal (ft)/33.23-1.
	X9=2.*Accumulative Coal Volume (Mm^3)/146.18-1.
	X10=2.*(Underground Mine Area 4mi (acres)-617.98)/110430.52-1.
	X11=2.*(Average Annual Precipitation (in)-37.)/4.-1.
	Y=2.*(Minimum Head (msl)-400.)/930.-1.
Most significant variables:	Surface Elevation for Sampling Station (msl)
	Bottom of well elevation (msl)
	Thickness of mined coal seam (ft)
	Thickness Shale + Clay (ft)
	Thickness Limestone (ft)
	Accumulative Coal Volume (Mm^3)
	Underground Mine Area 4mi (acres)
	Average Annual Precipitation (in)
Less significant variables:	Overburden thickness (ft)
	Thickness Sandstone (ft)

Figure D.3 Correlation between maximum observed and calculated heads for the data set without water withdraw.
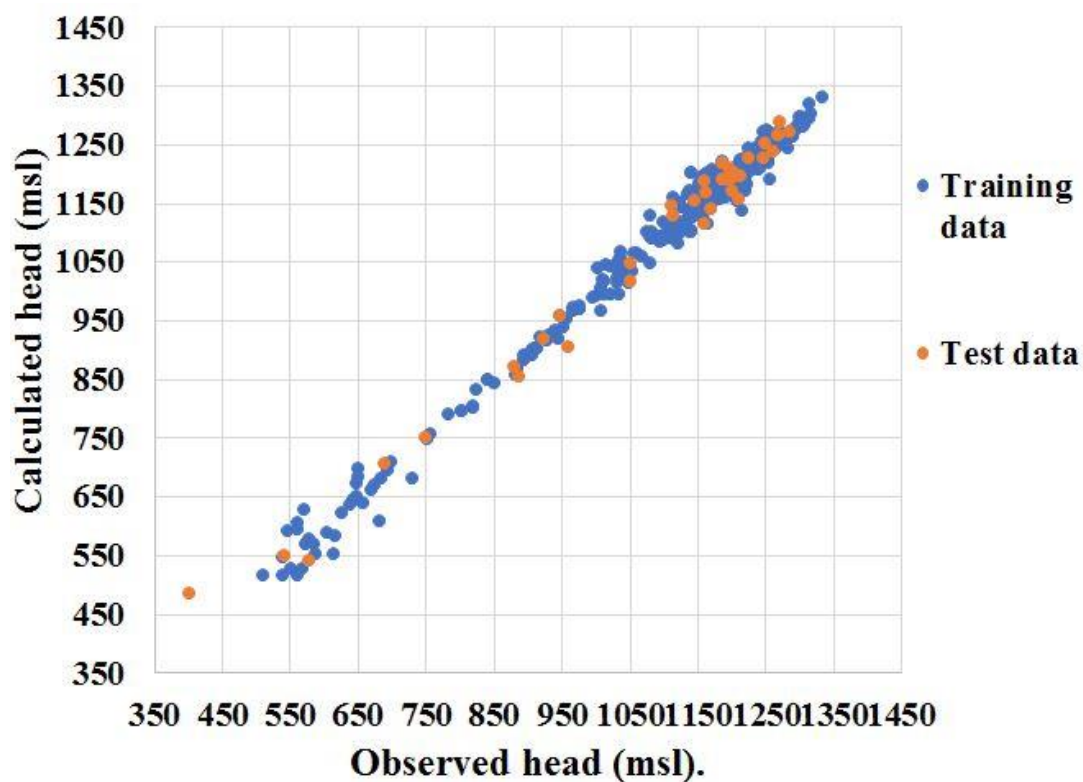
Figure D.4 Correlation between minimum observed and calculated heads for the data set without water withdraw.

Table D.5 Average observed and calculated heads for datasets containing water withdrawal and datasets without water withdrawal.

Well	Observed Average Head	Multi-mine without water withdrawal	Multi-mine with water withdrawal	Delta Multi-mine without water withdrawal	Delta Multi-mine with water withdrawal
South Meins Shaft	457.17	425.55	580.86	-31.62	123.69
Roving Crew	457.72	630.76	600.29	173.05	142.57
Danville Shaft	460.08	601.59	551.43	141.51	91.35
South Bleeder	557.90	564.40	598.26	6.51	40.37
North East Intake	566.73	622.39	513.47	55.67	-53.25
Grange	557.92	525.18	1288.70	-32.74	730.78
NW Shaft	557.51	1274.47	1281.70	716.95	724.19
DW-118	1288.17	1272.13	1290.84	-16.03	2.67
DW-122	1286.67	1281.36	1283.42	-5.30	-3.25
DW-126	1289.00	1273.13	1272.14	-15.88	-16.86
DW-129	1284.17	1255.30	1278.55	-28.86	-5.61
DW-161	1273.00	1263.88	1095.39	-9.12	-177.61
DW-162	1270.17	1083.44	1204.41	-186.73	-65.76
DW-169	1081.17	1193.48	1077.14	112.31	-4.03
DW-178	1194.67	1057.90	1224.14	-136.77	29.47
DW-180	1065.83	1215.39	1218.27	149.56	152.44
DW-196	1231.50	1213.99	1235.96	-17.51	4.46
DW21-156.00	1222.00	1230.92	1115.95	8.92	-106.05
DW21-190.00	1237.98	1104.22	1269.74	-133.76	31.75
DW-22.004.00	1117.00	1257.78	1282.72	140.78	165.72
DW-22.008.05	1261.33	1265.50	1003.14	4.17	-258.20
DW-318	1283.70	990.60	966.35	-293.10	-317.35
DW-324	998.00	952.32	946.72	-45.68	-51.28
DW-330	955.67	921.51	942.87	-34.15	-12.80
DW-331	927.00	916.89	1100.40	-10.11	173.40
DW-354	916.33	1080.15	1007.02	163.81	90.69
DW-356	1092.17	984.23	1230.22	-107.94	138.05
DW-362	993.17	1224.13	1243.73	230.97	250.56
DW-376	1244.83	1234.06	1108.10	-10.78	-136.73
DW-387	1241.00	1097.18	1311.95	-143.82	70.95
DW-391	1097.67	1302.15	1298.72	204.48	201.05
DW-393	1315.00	1288.26	1306.69	-26.74	-8.31
DW-399	1294.17	1296.80	1228.60	2.64	-65.57
DW-406	1298.95	1219.96	1241.82	-78.99	-57.13
DW-420	1222.67	1219.06	1256.52	-3.61	33.85
DW-427	1229.50	1248.55	1062.12	19.05	-167.38

Cont'd

DW-430	1252.00	1050.78	1147.51	-201.23	-104.49
DW-457	1049.50	1142.52	1218.53	93.02	169.03
DW-481	1148.00	1202.30	1226.88	54.30	78.88
DW502-338.08	1219.23	1215.37	1178.26	-3.86	-40.97
DW-679	1220.75	1174.82	1264.88	-45.93	44.13
DW-702	1167.50	1261.54	1169.13	94.04	1.63
DW-717	1275.17	1164.64	1275.91	-110.53	0.74
DW-719	1174.42	1254.28	1267.59	79.87	93.17
W-114	1264.17	1252.21	1279.43	-11.96	15.26
W-125	1279.33	1262.93	1245.43	-16.40	-33.91
W-140	1265.00	1228.39	1254.34	-36.61	-10.66
W-153	1240.33	1238.75	1267.05	-1.59	26.71
W-157	1259.33	1249.62	1117.48	-9.72	-141.85
W-159	1251.80	1103.98	1078.38	-147.82	-173.43
W-165	1107.50	1053.81	1086.21	-53.69	-21.29
W-166	1034.17	1063.73	1091.00	29.57	56.83
W-170	1054.00	1066.76	1111.22	12.76	57.22
W-174	1033.67	1087.37	1182.00	53.71	148.33
W-175	1117.50	1157.74	848.12	40.24	-269.38
W-199	1183.08	827.23	1189.24	-355.85	6.15
W-2	822.20	1164.03	1182.70	341.83	360.50
W-202	1161.67	1158.71	1259.32	-2.96	97.65
W-204	1187.58	1241.88	1220.58	54.30	33.00
W21-029.00	1233.33	1205.75	1317.87	-27.58	84.54
W21-043.00	1201.20	1301.44	1230.74	100.24	29.54
W21-045.01	1296.97	1212.44	1227.53	-84.53	-69.44
W21-057.00	1224.43	1210.03	1234.03	-14.40	9.60
W21-059.00	1216.17	1217.07	1142.00	0.91	-74.16
W21-064.00	1205.67	1124.96	1038.71	-80.70	-166.96
W21-066.00	1162.83	1030.12	1050.14	-132.71	-112.70
W21-080.00	1030.40	1042.09	1061.24	11.69	30.84
W21-083.00	1037.10	1052.91	1058.18	15.81	21.08
W21-087.00	1039.10	1049.06	1078.74	9.96	39.64
W21-087.01	1050.97	1066.97	1041.63	16.01	-9.34
W21-095.00	1030.83	1029.46	1046.81	-1.37	15.98
W21-106.00	1047.33	1039.11	1023.48	-8.22	-23.85
W21-110.01	1029.60	1012.56	1055.15	-17.04	25.55
W21-111.00	1032.63	1047.19	1204.35	14.56	171.71
W21-112.00	1032.07	1184.20	1280.22	152.13	248.15

Cont'd

W21-138.00	1207.30	1269.65	1189.58	62.35	-17.72
W21-155.08	1259.97	1162.96	1201.26	-97.01	-58.71
W21-160.00	1160.17	1166.90	1196.67	6.73	36.51
W21-165.04	1042.07	1172.61	1209.24	130.54	167.17
W21-171.00	1176.93	1190.43	1196.11	13.50	19.18
W21-173.01	1207.83	1171.83	1199.59	-36.00	-8.24
W21-180.01	1193.63	1190.57	1216.77	-3.06	23.14
W21-183.01	1194.20	1206.57	1257.56	12.37	63.36
W21-187.00	1219.23	1247.47	1165.04	28.24	-54.19
W21-195.00	1223.37	1152.67	1162.70	-70.70	-60.66
W21-260.00	1142.47	1149.47	1175.61	7.00	33.14
W21-265.00	1148.03	1160.55	1173.45	12.51	25.42
W21-452.00	1155.50	1154.02	1156.49	-1.48	0.99
W21-481.00	1149.13	1143.17	1229.76	-5.96	80.63
W21-502.00	1142.85	1209.23	1135.90	66.38	-6.95
W-22.007.00	1209.92	1123.90	1072.50	-86.02	-137.41
W-225	1139.33	1061.14	1280.39	-78.20	141.06
W-226	1058.00	1251.43	1230.11	193.43	172.11
W-229A	1262.33	1207.57	1248.85	-54.76	-13.49
W231.356.00	1196.65	1237.08	1275.85	40.43	79.20
W231.356.04	1246.36	1264.64	1259.80	18.27	13.44
W-289	1267.33	1245.92	1282.75	-21.41	15.41
W-291	1271.83	1252.21	1110.50	-19.63	-161.34
W-292	1242.40	1095.29	1247.79	-147.11	5.39
W-294	1080.50	1224.67	1294.97	144.17	214.47
W-295	1232.80	1271.90	1283.31	39.10	50.51
W-299	1249.40	1258.39	1234.12	8.99	-15.28
W-312A	1254.67	1211.45	1182.45	-43.22	-72.22
W-314A	1218.00	1163.50	1106.98	-54.50	-111.02
W-316	1159.67	1087.10	945.59	-72.57	-214.08
W-323	1077.50	915.57	916.82	-161.93	-160.68
W-325	943.17	889.31	917.47	-53.86	-25.69
W-327	903.17	890.31	926.06	-12.86	22.89
W-333	904.33	899.83	926.03	-4.50	21.69
W-334	907.17	899.16	924.25	-8.00	17.09
W-335	907.50	897.08	900.65	-10.43	-6.85
W-336	903.17	881.72	965.54	-21.45	62.38
W336.367.00	885.20	945.25	929.66	60.05	44.46

Cont'd

W336.375.00	925.35	904.21	919.78	-21.14	-5.57
W-340	910.17	892.63	889.23	-17.53	-20.94
W-341	892.17	860.91	1163.31	-31.26	271.14
W-342	879.00	1151.90	1239.44	272.90	360.44
W-344	1164.33	1223.75	940.69	59.42	-223.64
W-345	1238.83	914.99	1146.72	-323.84	-92.11
W-346	919.83	1128.16	1192.19	208.33	272.36
W-347	1078.50	1165.20	1186.71	86.70	108.21
W-350	1141.33	1170.62	1213.69	29.28	72.36
W-353	1136.67	1192.42	1115.72	55.75	-20.95
W-358	1196.50	1095.22	1058.65	-101.28	-137.85
W-359	1106.50	1040.47	1214.01	-66.03	107.51
W-363	1000.17	1186.81	1163.09	186.65	162.92
W-365	1182.50	1137.40	1268.42	-45.10	85.92
W-368	1132.33	1255.76	1249.80	123.43	117.47
W-374	1247.67	1237.49	1295.83	-10.18	48.16
W-377	1245.17	1283.92	1288.63	38.75	43.46
W-378	1297.33	1270.14	1310.34	-27.20	13.00
W-379	1244.00	1287.86	1232.37	43.86	-11.63
W-382	1268.67	1219.68	1281.17	-48.99	12.50
W-394	1231.33	1266.64	1291.05	35.31	59.72
W-396	1267.67	1276.28	1286.01	8.62	18.34
W-400	1267.83	1269.06	1292.01	1.23	24.18
W-401	1277.83	1274.32	1309.46	-3.51	31.63
W-402	1252.67	1280.97	1114.50	28.30	-138.16
W-403	1301.83	1105.96	1285.45	-195.88	-16.39
W-404	1112.50	1262.73	1283.10	150.23	170.60
W-407	1248.83	1268.89	1261.01	20.06	12.17
W-410	1250.54	1251.30	1259.37	0.76	8.83
W-413	1244.58	1248.84	1114.09	4.26	-130.49
W-414	1249.27	1103.96	1138.83	-145.31	-110.44
W-415	1108.67	1127.14	1165.43	18.48	56.77
W-417	1111.33	1157.66	1170.54	46.33	59.21
W-418	1167.83	1142.50	1245.41	-25.34	77.58
W-423	1123.83	1232.06	1134.00	108.23	10.16
W-425	1226.25	1109.36	1247.22	-116.89	20.97
W-426	1118.50	1219.70	1177.28	101.20	58.78
W-428	1211.64	1165.30	1232.42	-46.34	20.78

Cont'd

W-432	1185.83	1098.89	1146.42	-86.95	-39.41
W-438	1089.50	1136.06	1058.69	46.56	-30.81
W-452	1151.75	1044.08	1177.87	-107.67	26.12
W-455	1020.00	1162.90	1132.82	142.90	112.82
W501.077.00	1141.78	1115.01	1131.64	-26.77	-10.14
W501.077.01	1072.70	1120.50	1006.50	47.79	-66.21
W501.343000	1116.63	988.13	1189.12	-128.50	72.49
W-53.01	1004.23	1169.88	1202.02	165.64	197.79
W-568	1171.33	1182.41	1212.65	11.08	41.32
W-576	1148.00	1191.17	1225.15	43.17	77.15
W-583	1158.00	1210.17	1137.34	52.17	-20.66
W-587	1238.20	1128.71	1164.25	-109.49	-73.95
W-609	1123.87	1159.58	1230.66	35.71	106.79
W-620	1146.64	1214.60	1150.63	67.96	4.00
W6-6	1229.54	1133.16	1047.82	-96.38	-181.72
W-660	1135.25	1039.77	1149.49	-95.48	14.24
W-666	1049.08	1133.81	1281.68	84.73	232.60
W-671	1097.50	1265.03	1021.83	167.53	-75.67
W-681	1258.50	1000.19	1343.56	-258.32	85.06
W-683	1020.67	1317.91	1253.41	297.24	232.74
W-690	1312.67	1243.41	1237.92	-69.26	-74.74
W-691	1260.67	1216.33	1230.80	-44.34	-29.87
W-694	1227.62	1213.34	1291.69	-14.27	64.08
W-696	1193.50	1274.57	1242.27	81.07	48.77
W-701	1269.33	1227.24	1261.30	-42.10	-8.03
W-705	1222.93	1245.15	1209.34	22.21	-13.60
W-706	1238.30	1190.29	1059.05	-48.01	-179.25
W-707	1220.00	1034.79	1295.59	-185.22	75.59
W-709	1010.77	1286.49	1355.89	275.72	345.12
W-716	1305.00	1328.26	1148.26	23.26	-156.74
W-722	1330.67	1128.03	1122.12	-202.63	-208.54
W-723	1131.00	1105.90	1193.24	-25.11	62.24
W-728	1115.67	1184.96	1247.54	69.30	131.87
W-734	1187.67	1232.04	1237.88	44.37	50.21
WL-113	1225.00	1221.79	1274.05	-3.21	49.05
WL-116	1244.80	1254.79	1141.64	9.99	-103.16
WL21-041.01	1255.37	1116.04	1279.01	-139.33	23.65
WL231.362.00	1116.65	1259.60	1294.38	142.96	177.73

Cont'd

WL-301	1253.40	1269.53	1085.22	16.13	-168.18
WL-319	1265.17	1064.80	900.09	-200.37	-365.08
WL336.373.00	1076.71	872.96	1178.91	-203.75	102.20
WL-338	881.00	1160.26	1162.41	279.26	281.41
WL-348	1110.83	1145.23	1205.07	34.40	94.24
WL-349	1108.00	1180.22	1287.93	72.22	179.93
WL-351	1198.17	1271.90	1231.42	73.74	33.25
WL-381	1283.17	1215.11	1190.68	-68.06	-92.48
WL-419	1238.33	1171.28	1117.94	-67.06	-120.39
WL-567	1151.67	1100.76	1321.91	-50.90	170.24
WL-674	1098.00	1290.92	1202.06	192.92	104.06
WL-692	1311.00	1189.89	1139.46	-121.12	-171.54
WL-721	1149.20	1123.29	1104.54	-25.91	-44.66
WL-729	1127.67	1091.63	1297.40	-36.04	169.73
WL-736	1118.74	1261.74	1235.27	143.00	116.53
WL-739	1257.00	1215.93	1173.49	-41.07	-83.51
WL-747	1217.67	1153.28	1112.38	-64.38	-105.29
W-100	1169.00	1163.04	1204.40	-5.96	35.40
W-14	1066.93	1176.37	1254.82	109.44	187.89
W-201	1202.74	1236.62	1148.67	33.88	-54.06
W-202	1223.25	1124.51	1223.85	-98.74	0.60
W-242	1138.00	1196.40	1207.00	58.40	69.00
WL-13	1253.67	1191.89	980.31	-61.78	-273.35
WL-14	1064.75	959.66	1201.23	-105.09	136.48
WL-18	973.91	1173.89	1230.98	199.98	257.07
WL-201	1217.14	1199.36	1162.66	-17.78	-54.49
WL-3	1198.57	1138.72	795.33	-59.85	-403.24
WL-39A	1212.56	788.88	1092.37	-423.68	-120.20
W-10	801.00	1097.51	1122.83	296.51	321.83
W-100	1079.38	1144.80	1095.03	65.41	15.64
W-101	1141.93	1105.14	1126.46	-36.79	-15.47
W-102	1134.57	1143.01	1161.50	8.43	26.93
W-23	1155.06	1170.30	1178.80	15.23	23.73
W-256	1134.40	1190.04	1213.07	55.64	78.67
W-277	1186.20	1230.21	1179.51	44.01	-6.69
W-278	1182.77	1189.67	1160.04	6.90	-22.73
W-279	1171.00	1172.23	1138.00	1.23	-33.01
W-285	1201.20	1154.26	1106.86	-46.94	-94.35

Cont'd

W-299	1120.67	1120.17	1180.78	-0.50	60.12
W-3	1158.00	1210.36	1128.59	52.36	-29.41
W-30	1137.86	1143.73	1136.11	5.87	-1.75
W-300	1166.33	1152.73	1131.40	-13.60	-34.93
W-305	1157.78	1148.75	1173.29	-9.03	15.51
W-309	1142.53	1190.99	1147.70	48.46	5.16
W-311	1164.87	1162.27	1145.67	-2.60	-19.19
W-312	1206.93	1160.28	1129.52	-46.65	-77.41
W-312A	1204.60	1144.36	1188.71	-60.24	-15.89
W-315	1159.13	1202.01	1128.16	42.87	-30.98
W-351	1154.97	1143.19	1204.71	-11.78	49.74
W-352	1135.07	1215.21	1183.97	80.14	48.91
W-353	1192.07	1195.08	1185.49	3.01	-6.58
W-358	1188.00	1197.85	1173.62	9.85	-14.38
W-360	1183.20	1185.01	1167.12	1.81	-16.09
W-361	1187.17	1183.74	1159.30	-3.43	-27.87
W-363	1202.27	1175.94	1143.06	-26.33	-59.20
W-5	1160.00	1161.54	1192.42	1.54	32.42
W-6	1179.66	1204.79	1127.34	25.13	-52.33
W-9	1192.82	1146.54	1091.02	-46.28	-101.79
WL-101	1165.30	1103.45	961.90	-61.86	-203.40
WL-102	1137.80	971.90	785.95	-165.90	-351.85
WL-2	964.30	797.79	1222.19	-166.51	257.89
WL-200	816.32	1236.63	1183.44	420.30	367.12
WL-273	1250.60	1195.26	1120.77	-55.34	-129.83
WL-284	1177.00	1136.06	1198.71	-40.94	21.71
WL-295	1156.00	1215.50	1167.12	59.50	11.12
WL-362	1168.45	1183.74	1135.80	15.29	-32.65
WL-364	1193.40	1151.45	1093.00	-41.95	-100.41
WL-365	1160.80	1107.76	1123.25	-53.04	-37.55
WL-368	1119.20	1142.15	1184.71	22.95	65.51
WL-4	1159.07	1203.19	795.33	44.13	-363.74
WL-8	1184.00	791.24	1092.37	-392.76	-91.64
W-10	801.00	1097.51	1122.83	296.51	321.83
W-100	1079.38	1145.11	1095.03	65.73	15.64
W-101	1141.93	1105.48	1126.46	-36.45	-15.47
W-102	1134.57	1143.26	1161.50	8.69	26.93
W-23	1155.06	1170.30	1178.49	15.23	23.43
W-256	1134.40	1189.55	1212.76	55.15	78.36

Cont'd

W-277	1186.20	1229.68	1179.20	43.48	-7.00
W-278	1182.77	1189.16	1159.73	6.40	-23.03
W-279	1171.00	1171.79	1137.69	0.79	-33.31
W-285	1201.20	1153.92	1106.86	-47.28	-94.35
W-299	1120.67	1120.43	1180.78	-0.24	60.12
W-3	1158.00	1210.48	1128.29	52.48	-29.71
W-30	1137.86	1143.40	1135.80	5.54	-2.06
W-300	1166.33	1152.39	1131.09	-13.94	-35.24
W-305	1157.78	1148.43	1172.98	-9.35	15.21
W-309	1142.53	1190.57	1147.39	48.03	4.86
W-311	1164.87	1161.88	1145.37	-2.98	-19.50
W-312	1206.93	1159.90	1129.22	-47.03	-77.72
W-312A	1204.60	1144.03	1188.40	-60.58	-16.20
W-315	1159.13	1201.51	1127.85	42.38	-31.28
W-351	1154.97	1142.86	1204.40	-12.11	49.43
W-352	1135.07	1214.65	1183.67	79.58	48.60
W-353	1192.07	1194.57	1185.18	2.50	-6.88
W-358	1188.00	1197.36	1173.32	9.36	-14.68
W-360	1183.20	1184.53	1166.81	1.33	-16.39
W-361	1187.17	1183.32	1159.30	-3.85	-27.87
W-363	1202.27	1176.08	1143.06	-26.19	-59.20
W-5	1160.00	1161.74	1192.42	1.74	32.42
W-6	1179.66	1204.72	1127.03	25.06	-52.63
W-9	1192.82	1146.25	1090.72	-46.57	-102.10
WL-101	1165.30	1103.17	961.90	-62.13	-203.40
WL-102	1137.80	973.09	785.65	-164.71	-352.15
WL-2	964.30	798.45	1221.89	-165.85	257.59
WL-200	816.32	1236.06	1183.14	419.73	366.81
WL-273	1250.60	1194.76	1120.46	-55.84	-130.14
WL-284	1177.00	1135.75	1198.40	-41.25	21.40
WL-295	1156.00	1215.00	1166.81	59.00	10.81
WL-362	1168.45	1183.32	1135.50	14.87	-32.96
WL-364	1193.40	1151.11	1092.69	-42.29	-100.71
WL-365	1160.80	1107.51	1123.25	-53.29	-37.55
WL-368	1119.20	1142.45	1180.83	23.25	61.63
WL-4	1159.07	1197.49	1005.29	38.43	-153.78
WL-8	1184.00	992.64	1020.27	-191.36	-163.73
MW-8	1004.41	1007.92	1062.79	3.51	58.38
MW-9	1007.80	1031.49	1190.19	23.69	182.39

Cont'd

W-10	1012.50	1170.39	1240.61	157.89	228.11
W-201	1142.00	1230.96	1162.70	88.96	20.70
W-202	1216.28	1137.55	1005.10	-78.72	-211.18
W-26	1160.44	975.65	936.46	-184.79	-223.98
W-624	1010.50	916.63	953.12	-93.87	-57.38
W-625	938.50	927.14	921.25	-11.36	-17.25
W-626	949.25	892.44	1167.95	-56.81	218.70
W-628	956.87	1152.96	978.17	196.09	21.30
WL-113	1170.00	960.24	851.77	-209.76	-318.23
WL-18	975.00	841.37	956.02	-133.63	-18.98
DW-6	838.67	948.17	1194.83	109.50	356.16
MW1	945.22	1190.62	1211.68	245.40	266.46
W-2	1217.33	1202.04	1066.95	-15.29	-150.38
W-3	1210.00	1175.15	1226.34	-34.85	16.34
W-303	1177.80	1223.11	1094.29	45.31	-83.51
W-352	1251.50	1212.37	1224.57	-39.14	-26.93
W-370	1207.61	1209.94	979.75	2.33	-227.87
W-5	1162.00	1087.67	1219.65	-74.33	57.65
W-8	1109.63	1205.20	1172.90	95.58	63.27
WL-3	1213.53	1172.06	851.77	-41.46	-361.76
WL-318	1198.50	843.22	955.98	-355.28	-242.52
DW-6	838.67	949.62	1194.83	110.96	356.16
MW1	945.22	1190.53	1211.64	245.31	266.42
W-2	1217.33	1201.85	1066.91	-15.49	-150.42
W-3	1210.00	1175.18	1226.34	-34.82	16.34
W-303	1177.80	1222.71	1094.25	44.91	-83.55
W-352	1251.50	1212.28	1216.55	-39.22	-34.95
W-370	1207.61	1206.62	979.75	-0.99	-227.87
W-5	1162.00	1086.70	1211.64	-75.30	49.64
W-8	1109.63	1201.85	1172.90	92.22	63.27
WL-3	1213.53	1172.28	762.21	-41.25	-451.32
WL-318	1198.50	753.99	755.23	-444.51	-443.27
DW-7	753.00	746.32	767.86	-6.68	14.86
W-13	749.00	751.99	592.24	2.99	-156.76
WL-936	746.00	586.64	781.35	-159.36	35.35
DW-11A	575.00	801.20	670.95	226.20	95.95
DW-13	781.30	659.44	646.13	-121.86	-135.17
DW-21	666.33	645.52	821.65	-20.81	155.32
DW-22	643.50	839.91	861.21	196.41	217.71

Cont'd

DW-22A	847.50	882.42	630.80	34.92	-216.70
DW-22B	892.00	627.85	648.95	-264.15	-243.05
DW-23	624.20	660.66	686.15	36.46	61.95
DW-24	640.67	695.81	589.21	55.14	-51.46
DW-406	691.27	571.45	848.86	-119.81	157.59
DW-414	571.50	869.65	679.42	298.15	107.92
DW-42	876.63	683.89	643.97	-192.74	-232.66
DW-46	682.83	642.20	695.11	-40.63	12.28
DW-602	635.09	700.84	704.49	65.75	69.40
M1A	647.00	710.47	673.20	63.47	26.20
M1B	685.67	677.05	682.90	-8.61	-2.77
M2A	645.83	687.04	654.72	41.20	8.88
M2B	646.83	655.43	565.09	8.59	-81.74
M3B	645.00	560.22	561.34	-84.78	-83.66
W-10	540.00	548.03	600.06	8.03	60.06
W-125	584.50	598.28	600.08	13.78	15.58
W-134	601.80	591.28	592.56	-10.52	-9.24
W-18	545.00	588.78	564.52	43.78	19.52
W3	613.00	560.87	582.94	-52.13	-30.06
W3.01	612.00	578.81	596.73	-33.19	-15.27
W-41	581.80	627.43	673.93	45.63	92.13
W41.01	737.89	684.43	633.61	-53.46	-104.28
W41.02	728.43	635.53	661.42	-92.89	-67.01
W-600	654.70	671.37	527.90	16.67	-126.80
W-604	671.40	554.70	542.38	-116.70	-129.02
WL-1	665.00	538.13	564.62	-126.87	-100.38
WL-12	548.00	548.02	608.24	0.02	60.24
WL-154	537.00	616.99	560.25	79.99	23.25
WL-16	680.00	549.00	530.79	-131.00	-149.22
WL-21	575.00	512.57	535.32	-62.43	-39.68
WL-24C	507.00	528.93	498.37	21.93	-8.63
WL-3	538.00	494.93	701.71	-43.07	163.71
WL-4	400.00	711.78	640.87	311.78	240.87
WL-5	695.00	639.18	627.38	-55.82	-67.62